# 浙江大学

# 博士学位论文

**中文论文题目**：绿木霉及其纳米制剂对园艺作物三种重要土传病原物的拮抗效果和机制

**英文论文题目**：Antagonistic effects and mechanisms of *Trichoderma virens* and its nano-fungicide against three main soil-borne phytopathogens of horticultural crops

申请人姓名： **ALI ATHAFAH TOMAH**

指导教师： 李斌 教授

专业名称： 植物病理学

研究方向： 植物病害生物防治

所在学院： 农业与生物技术学院

论文提交日期： 2023 年 5 月

# Antagonistic effects and mechanisms of *Trichoderma virens* and its nano-fungicide against three main soil-borne phytopathogens of horticultural crops

A Dissertation Presented in Partial Fulfillment of Requirement

For the Award of a Doctor of Philosophy (PhD) Degree in

Plant Pathology

By

## ALI ATHAFAH TOMAH

Supervised by
Professor Li Bin,
PhD

## Institute of Biotechnology,

### College of Agriculture and Biotechnology,

Zhejiang University, Hangzhou, P. R. China

**May, 2023**

# 绿木霉及其纳米制剂对园艺作物三种重要土传病原物的拮抗效果和机制

论文作者签名：

指导教师签名：

论文评阅人 1: <u>隐名评阅</u>

评阅人 2: <u>隐名评阅</u>

评阅人 3: <u>隐名评阅</u>

评阅人 4: <u>隐名评阅</u>

评阅人 5: <u>隐名评阅</u>

**答辩委员会主席: <u>张修国 教授</u>**

委员 1: <u>季鹏飞 教授</u>

委员 2: <u>姚燕来 研究员</u>

委员 3: <u>冯国忠 研究员</u>

委员 4: <u>王道泽 研究员</u>

答辩日期：<u>2023 年 5 月 27 日</u>

# Antagonistic effects and mechanisms of *Trichoderma virens* and its nano-fungicide against three main soil-borne phytopathogens of horticultural crops

Author's signature: _____

Supervisor's signature: _____

External Reviewer 1: _____Anonymity_____

External Reviewer 2: _____Anonymity_____

External Reviewer 3: _____Anonymity_____

External Reviewer 4: _____Anonymity_____

External Reviewer 5: _____Anonymity_____

**Examining Committee Chairperson:**

_____Zhang Xiuguo_____

**Examining Committee Members:**

Committee member 1: _____Ji Pengfei_____

Committee member 2: _____Yao Yanlai_____

Committee member 3: _____Feng Guozhong_____

Committee member 4: _____Wang Daoze_____

Date of oral defence：_____2023.05.27_____

# 浙江大学研究生学位论文独创性声明

本人声明所呈交的学位论文是本人在导师指导下进行的研究工作及取得的研究成果。除了文中特别加以标注和致谢的地方外，论文中不包含其他人已经发表或撰写过的研究成果，也不包含为获得 浙江大学 或其他教育机构的学位或证书而使用过的材料。与我一同工作的同志对本研究所做的任何贡献均已在论文中作了明确的说明并表示谢意。

学位论文作者签名：　　　　　　　　　　　　　签字日期: 2023 年 05 月 27 日

# 学位论文版权使用授权书

本学位论文作者完全了解 浙江大学 有权保留并向国家有关部门或机构送交本论文的复印件和磁盘，允许论文被查阅和借阅。本人授权 浙江大学 可以将学位论文的全部或部分内容编入有关数据库进行检索和传播，可以采用影印、缩印或扫描等复制手段保存、汇编学位论文。

（保密的学位论文在解密后适用本授权书）

学位论文作者签名：　　　　　　　　　　　导师签名：

签字日期: 2023 年 05 月 27 日　　　　　　签字日期: 2023 年 05 月 27 日

# Thesis Release Certificate

The author has agreed that the library, Zhejiang University, Hangzhou, China, can make this thesis freely available for inspection. Moreover, the author has agreed that permission for extensive copying of this thesis for scholarly purposes may be granted by the professor who has supervised the thesis work herein or, in their absence, by the Head of department, or the Dean of faculty in which this work was done. It is understood that the recognition will be given to the author of this thesis and the Zhejiang University, Hangzhou in any use of the material in this thesis. Copying or publication or any other use of the thesis for financial gain without the prior approval by the Zhejiang University, Hangzhou and the author's written permission is prohibited.

Request for permission to copy or to make any other use of material in this thesis in whole or in part should be addressed to:

Institute of Biotechnology,

College of Agriculture and Biotechnology,

Zhejiang University,

Hangzhou 310058,

P. R. China.

# Certification

This is to certify that the work presented herein title "**Antagonistic effects and mechanisms of *Trichoderma virens* and its nano-fungicide against three main soil-borne phytopathogens of horticultural crops**" was carried out by Mr. Ali Athafah Tomah, candidate for the doctor of philosophy (PhD) degree in Plant Pathology, College of Agriculture and Biotechnology, Zhejiang University, under my supervision and has not been presented earlier for the award of any other degree in any university.


Supervisor

Professor Li Bin, PhD

Institute of Biotechnology,

College of Agriculture and Biotechnology,

Zhejiang University, Hangzhou 310058,

P. R. China

# Acknowledgments

To My Mother that died during my study in China. I was hoping that you would share the happy graduating me. Also, I would like to extend my great profound thanks and heartiest gratitude to my father, who are always supporting and encouraging me in all of my life.

I am grateful to my family initially my angel and sweetheart wife and my road companion, we have climbed the ladder of success together and we will stay together forever. My Sons Moamel and Mohammed Ridha, I thank you for your long-lasting emotional support and unconditional love.

My brothers and sisters, thank you from my heart to your prays to me

I would like to sincerely thank my supervisor, Professor Li Bin, for giving me the opportunity to be his PhD student and finishing my thesis. His optimism, encouragement, and tactical advice have been very helpful for my research and my future career.

I also wish to express my deepest appreciation to my supervisor, Dr. Zhang, not only for his guidance, patience, and encouragement but also for the opportunity to work in his laboratory, glasshouses and experimental farm at the Department of Plant Pathology. In what was a technically demanding research program for me, I learnt many new techniques and had to think through many issues and loopholes. Your expertise guided me through all of this, for which I thank you.

Thank you to all Chinese friends for joyful activities during my study in China, it made my life in China truly unforgettable.

I really don't have adequate words to express my thanks to my wonderful Iraqi-mates Mustafa Khalid, Thaair Ameen, Abbas Fadhil and Amjed and Ali for their kind helps and supports me.

Thank you to all my international friends from Egypt, Pakistan, Bangladesh and Sudan.

I also wish to acknowledge the Chinese Scholarship Council (CSC) for the financial assistance to complete my PhD program in Plant Pathology.

There are many people I wish to thank for their help and encouragement during my PhD study. This list probably isn't exhaustive, but them in my heart.

Ali Athafah Tomah

Zijin Port, Zhejiang University, may 2023

# Abstract

The *Phytophthora* blight, *Verticillium* wilt, and white mold are serious diseases that occur every year, which are caused by the soil-borne phytopathogens *Phytophthora capsici*, *Verticillium dahliae*, and *Sclerotinia sclerotium*, respectively, leading to severe economic loss in production of the horticulture crops worldwide. Control of these diseases is often difficult due to formation and long-term survival of their dormant structures such as oospores, microsclerotia and sclerotia in soil. To control these diseases, huge quantities of synthetic chemical fungicides are used. However, the extensive usage of chemicals causes environmental and food safety problems. By comparison, biological control has been considered as one of the most promising and environmentally friendly methods to protect plant production by constructing an integrated pest management scheme. Among biocontrol agents, *Trichoderma* species, which are widely distributed in soil, are now often used as biocontrol agents for the control of a large number of plant diseases. Therefore, the objective of this research was to isolate, characterize, and identify *Trichoderma* isolates, reveal the mechanisms of their interaction with pathogens, and produce silver nanoparticles as new approaches to their application in the control of three important soil-borne plant pathogens. The main results are outlined below:

1. This study identified 15 *Trichoderma* strains with antagonistic activity, one of which is a new species. A total of 77 isolates of *Trichoderma* spp. were obtained from the rhizosphere soil of bell or chilli pepper plants in the heavily infested fields by *P. capsici*. Among them, 15 isolates showed the highest antagonistic activity with antagonism class 1 against *P. capsici*. Furthmore, 15 candidate isolates were identified as eight species, including *T. brevicompactum*, *T. atroviride*, *T. afroharzianum*, *T. koningiopsis*, *T. citrinoviride*, *T. virens*, *T. asperellum*, and *T. harzianum*. Among them, a new species isolated was described as *T. dorothopsis* by a combination of the morphological characteristics and phylogenetic analysis using sequences of the rDNA internal transcribed spacers (*ITS*), translation elongation factor 1-α (*TEF1*) and RNA polymerase II subunit B (*RPB2*) gene.

2. This study identified the antagonistic active substances of *T. virens* and its mechanism to control chili pepper blight. The antagonistic activity of *T. virens* HZA14 against *P. capsici* HZ07 was investigated by the dual culture technique. The antagonistic component produced by *T. virens* HZA14 was analyzed by Reversed-Phase High-Performance Liquid Chromatography. The *in vitro* antagonistic assay and analysis of metabolite fractions indicate that *T. virens* HZA14 could cause colony collapse and hypha degradation of *P. capsici*, and a high activity compound was identified as gliotoxin by spectrometric analysis. The biocontrol tests demonstrated that the *T. virens* HZA14 significantly delayed the occurrence of chili pepper blight and caused a 62.64% and 64.20% reduction in disease incidence and severity, respectively. Thus, isolate HZA14 could be considered for developing potential biocontrol agent for management of *P. capsici* in pepper.

3. This study identified the microsclerotial degradation mechanism of *T. virens* against *Verticillium* wilt disease. The mechanism of *T. virens* HZA14 degrading microsclerotia of *V. dahliae* was determined by using the dual culture method and pot experiment, in combination with transcriptome data analysis. Among 15 isolates, isolate HZA14 exhibited the greatest potential for microsclerotial degradation after 15 days. The disease control tests showed that *T. virens* HZA14 decreased *Verticillium* wilt disease severity for 2.77% in eggplant seedlings 30 days after inoculation. When hyphae of *T. virens* HZA14 interacting with microsclerotia of *V. dahliae* for 6, 9, 12, and 15 days, transcriptome analysis indicated that compared with the control, genes of *T. virens* HZA14 were differentially expressed in mycoparasitism process, while the numbers of up-regulated genes were 1197, 1758, 1936, and 1914 and the numbers of down-regulated genes were 1191, 1963, 2050, and 2114 for 6, 9, 12, and 15 days, respectively. Among these genes, enzymes associated with the degradation of microsclerotia, such as Endochitinase A1, Endochitinase 3, Endo-1,3-beta-glucanase, Alpha-N-acetylglucosaminidase, Laccase-1, and Peroxidase were predicted based on bioinformatics analysis. The expression of several genes encoding enzymes being related to the degradation of microsclerotia were confirmed by the real-time quantitative PCR (qPCR) analysis as well, being similar to the results of gene expression in the transcriptomes.

4. This study biosynthesized nanoparticles with antifungal activity using *T. virens* HZA14 metabolites and revealed their antifungal mechanism. The 15 isolates of the *Trichoderma* species was screened for the biosynthesis of silver nanoparticles (AgNPs).

Among them, the highest yield occurred in the synthesis of AgNPs using an aqueous cell-free filtrate of *T. virens* HZA14 producing gliotoxin. The synthetic AgNPs were charactered by SEM, EDS, TEM, XRD, and FTIR. Electron microscopic observation showed that AgNPs with size ranging from 5 nm to 50 nm had spherical or oval shapes with smooth surfaces. FTIR analysis revealed the interaction of AgNPs with carbohydrate, protein and heterocyclic compound molecules, and especially, interaction patterns of AgNPs with the gliotoxin molecule were proposed. The antifungal activity assays demonstrated that percentage inhibition of the biosynthesized AgNPs was 100% against hyphal growth, 93.8% against sclerotial formation and 100% against myceliogenic germination of sclerotia at a concentration of 200 µg/ml, respectively. The direct interaction between this biosynthesized AgNPs and *Trichoderma* cells revealed by SEM and EDS, includes contact with nanoparticles, accumulation and production of lamellar fragment as well as micropore or fissure formation on cell walls. These findings will greatly enriched our understanding of the action mechanisms of AgNPs for controlling diversified fungal disease.

Keywords: *Trichoderma virens*, Gliotoxin, *Phytophthora capsici*, Mycoparasitism, Transcriptome, *Verticillium dahliae*, AgNPs, Antifungal mechanism, *Sclerotinia sclerotium*.

# 摘要

辣椒疫病、茄子黄萎病和菌核病分别由土传病原菌辣椒疫霉菌(*Phytophthora capsici*)、大丽轮枝菌(*Verticillium dahliae*)和核盘菌(*Sclerotinia sclerotium*)引起，给园艺作物生产造成了巨大的经济损失。这些土传病原菌因能形成卵孢子、微菌核和菌核等休眠结构，可以在土壤中长期存活。防治这些土传病害通常十分困难，当前主要是通过化学杀菌剂来阻止病害的爆发和保护植物的健康。然而，大量化学农药的使用会导致环境污染和食品安全问题，极大地限制了其更广泛的应用。相比较，生物防治是众所周知的环境友好型有害生物防治方法，被认为是降低植物病害损失最有希望的途径之一。在生物防治中，广泛分布于土壤中的木霉菌经常被用于制备生防制剂，目前已应用于多种植物病害的防治。因此，本研究目标是分离、鉴定木霉分离株，揭示木霉与病原菌的互作机制，并探索木霉菌在防治三种重要植物土传病害中的应用新途径。

取得的主要结果概述如下：

1. 鉴定出 15 株具有拮抗活性的木霉，其中一个是新种：从辣椒疫病严重侵染地区的甜椒或辣椒植物根际土壤中分离出 77 株木霉，其中，15 株具有显著的拮抗活性，拮抗级别为 1 级。依据形态特征，并结合 rDNA 内部转录间隔子(*ITS*)、转录延伸因子 1-α (*TEF1*)和 RNA 聚合酶 II 亚基 B (*RPB2*)基因序列进行系统发育分析，15 株候选分离株被鉴定为 8 个种，包括 *Trichoderma brevicompactum*、*T. atroviride*、*T. afroharzianum*、*T. koningiopsis*、*T. citrinoviride*、*T. virens*、*T. asperellum* 和 *T. harzianum*。其中，一个分离系被鉴定为一个新种——拟桃乐茜木霉菌(*T. dorothopsis*)。

2. 绿木霉的拮抗活性物质鉴定及其防治辣椒疫病的机制探究：采用对峙培养技术研究了绿木霉株系 HZA14 对辣椒疫霉菌株系 HZ07 的拮抗活性，并用反相高效液相色谱法分析了绿木霉株系 HZA14 产生的拮抗组分。体外拮抗试验和代谢产物组分分析表明，绿木霉株系 HZA14 可引起辣椒疫霉菌菌落塌陷和菌丝降解。通过色谱分析，一种高活性化合物被鉴定为胶霉菌素。生物防治试验显示，绿木霉株系 HZA14 延缓了辣椒疫病的发生，辣椒疫病发病率和病害严重度分别降低 62.64%和 64.20%。因此，绿木霉株系 HZA14 可作为防治辣椒疫病的潜在生防菌株。

3. 绿木霉降解大丽轮枝菌微菌核的机制探究：采用对峙培养法和盆栽实验以及转录组数据，研究了绿木霉株系 HZA14 降解大丽轮枝菌微菌核的作用机制。在 15 株木霉分离系中，仅绿木霉株系 HZA14 在 15 天后显示其有最降解微菌核的潜力。病害防治试验结果表明，在接种 30 天后，绿木霉菌株 HZA14 可使茄子幼苗上的黄萎病严重度降低至 2.77%。当绿木霉株系 HZA14 菌丝与大丽花微菌核互作 6、9、12 和 15 天后，转录组分析表明，绿木霉株系 HZA14 在重寄生过程中的基因表达与对照具有显著差异。在接种 6、9、12 和 15 天后，上调表达的基因数量分别为 1197、1758、1936 和 1914，下调表达的基因数量分别为 1191、1963、2050 和 2114。在这些基因中，通过生物信息学分析和预测，与微菌核降解相关的酶包括内切几丁质酶 A1、内切几丁质酶 3、内切-1、3-葡聚糖酶、α-N-乙酰氨基葡萄糖苷酶、漆酶-1 和过氧化物酶。实时定量 PCR (real-time quantitative PCR) 分析也证实了几个编码与微菌核降解相关酶基因的表达，其结果与转录组中的基因表达结果相似。

4. 利用绿木霉代谢物生物合成了具有抗真菌活性的纳米制剂并揭示了其抗菌机制：15 个木霉株系被用于银纳米粒子（AgNPs）生物合成的筛选，其中，产胶霉菌素的绿木霉株系 HZA14 的无细胞滤液合成 AgNPs 产量最高。通过 SEM、EDS、TEM、XRD 和 FTIR 对合成的 AgNPs 进行了表征，扫描电镜研究表明，合成 AgNPs 的大小在 5~50 nm 之间，呈球形和椭圆形，表面光滑。FTIR 分析阐明了合成 AgNPs 与蛋白质、碳水化合物和杂环化合物分子相互作用的机理，提出了 AgNPs 与胶霉菌素分子的潜在互作模式。抗菌活性试验表明，在 200 μg/ml 浓度下，AgNPs 对核盘菌菌丝生长、菌核形成和菌丝萌发的抑制率分别为 100%、93.8% 和 100%。SEM 和 EDS 揭示了 AgNPs 与真菌细胞的直接作用机理，包括 AgNPs 的接触、积累、层状片段的产生以及真菌细胞壁上微孔或裂隙的形成。这些抑菌机制的明确将有助于我们更好地利用合成 AgNPs 来防治多样性的真菌病害。

关键词：绿木霉，胶霉菌素，辣椒疫霉菌，重寄生，转录组，大丽轮枝菌，银纳米粒子，抗真菌机制，核盘菌

# List of Contents

# List of Tables

# List of Figures

# List of abbreviations

| Abbreviations | Full spelling |
|---|---|
| AgNO$_3$ | Silver nitrate |
| AgNPs | Silver nanoparticles |
| cDNA | Complementary DNA |
| CFCL | Cell-free culture liquid |
| CMD | Cornmeal dextrose |
| CWDEs | Cell wall-degrading enzymes |
| DEGs | Differentially expressed genes |
| DMSO | Dimethyl Sulfoxide |
| DNA | Deoxyribonucleic acid |
| EDS | Energy dispersive spectroscopy |
| EST | Expressed-sequence-tag |
| EtOAc | Ethyl acetate |
| FPKM | Fragments per Kilobase Million |
| GO | Gene ontology |
| HZA(x) | Hangzhou Zhejiang Ali, (x) number of isolate |
| IP | Inhibition percentage |
| KEGG | Kyoto Encyclopedia of Genes and Genomes |
| ML | Maximum likelihood |
| PGP | Plant growth promotion |
| qRT-PCR | Quantitative reverse transcription polymerase chin reaction |
| RPB2 | RNA polymerase II subunit B |
| RP-HPLC | Reversed-Phase High-Performance Liquid Chromatography |
| SNA | Synthetic low nutrient agar |
| TEF1 | Translation elongation factor 1 α |
| TEM | Transmission electron microscope |
| TLC | Thin Layer Chromatography |
| TSM | Trichoderma selective medium |

# Chapter 1

# Introduction and literature review

## 1.1 Introduction

Agricultural production contributes to providing and improving food, both in quantity and quality, to ensure food needs are met, chiefly in countries with projected rates of slower growth in agricultural production compared to strong population growth (Pawlak and Kołodziejczak, 2020). Managing agricultural production and increasing yields face various challenges, one of which is the risk of plant diseases. where plant diseases are considered a major factor affecting food production and thus negatively reflected in the standard of living of human society (Palmgren et al., 2015). Over the past years, soil-borne plant pathogens have caused significant economic losses to global agricultural production in terms of lower yield and higher production costs (Mihajlović et al., 2017). Overall, soil-borne plant pathogens caused huge economic losses, reaching 50–75% of the total yield of many crops (Mokhtar and El-Mougy, 2014). *Capsicum annuum* (Chili) and *Solanum melongena* L. (eggplant) are horticultural crops with nutritional and economic value that are cultivated throughout the world. Chili pepper is used as a fresh vegetable, food colorant, seasoning, and for medicinal purposes, which has led to a 40-fold increase in consumption (Rehrig et al., 2014). China occupies the lead in terms of cultivated area for this crop, as it produces no less than 28 tons yearly, divided between domestic consumption and export (Li et al., 2009). Eggplant fruits are rich in fiber with a variety of alkaloids, anthocyanins, polyphenols, and chlorogenic acid; they help protect the human body from cancer, protect cells from damage caused by free radicals, and lower the level of lipids in the blood. Annual eggplant production in China is approximately 36.6 million tons, while global eggplant production is approximately 56.3 million tons (Acciarri et al., 2002; Ai et al., 2020; Alam and Salimullah, 2021; FAOSTAT., 2011). Chili and eggplant in the initial stages of growth are fundamentally grown inside the plastic and greenhouses, where they are susceptible to infection with many soil-borne pathogens at all stages of their growth, whether in the soil of the nursery or greenhouse (Ali et al., 2022).

The *Phytophthora capsici* belongs to the class Oomycetes and is one of the phytopathogens that spread in soil and are most destructive to chili pepper (Barchenger et al., 2018). The wide-scale hosts of a fungal-like pathogen are indexed in more than 50 plant species belonging to different families, such as Cucurbitaceae and Solanaceae, including many fruits and vegetables important for health human (Hausbeck and Lamour, 2004). While the chili pepper is considered one of the more susceptible vegetables to root rot disease caused by *P. capsici*, substantial yield damages are caused (Song et al., 2020). The losses caused by this plant pathogen are estimated in the chili pepper amounting to about 100 million dollars annually worldwide (Bosland, 2008). In China, pepper *Phytophthora* blight (PPB), caused by the pathogen, was recorded as constituting a complex problem to the profitable fabrication of bell pepper (Yun and Daohuai, 1988). *P. capsici* is classified as a hazard dispersed globally and the infection by it leads the root and crown of the rot. Also, it infects the aerial parts of bell peppers, causing a blight on the leaves, stems, and fruits, leading to huge economic losses in pepper production, especially in high-temperature, and moist environments over a wide range of different geographical regions in China (Hartman and Wang, 1992; Larkin et al., 1995). This pathogen is economically important and infects susceptible chili peppers during the growth and development stages, resulting in yield casualties of up to 100% (Lee et al., 2001).

The soil-borne *Verticillium dahliae* is a devastating fungus, causing several diseases in over 400 plant species that are in direct contact with human food and industry (Song et al., 2020). The *V. dahliae* could complete its lifecycle via microsclerotia formation, which may dormancy several years in agricultural soil (Menzies and Griebel, 1967). The economic loss on annual yield produced by wilt diseases caused by *V. dahliae* is very significant and at the worldwide level may reach 10 to 35% in the cotton crop (Song et al., 2020). *Sclerotinia sclerotiorum* belongs to the class Discomycetes (Bolton et al., 2006). *S. sclerotiorum* is a widespread pathogen agent that does not have a specific host and causes symptoms of disease in different plant species, the majority being dicotyledonous and monocotyledonous species such as onion and tulip, which is threatening the economic production of crops (Boland and Hall, 1994). China, with its cool and humid weather, was not spared from this plant disease. *Sclerotinia* stem rot disease is considered a major disease that reduces the yield of rapeseed in Mainland China and Australia (Li et al., 2009; Ma et al., 2009).

*S. sclerotiorum* was spread to infect more than 6 million hectares annually in *Brassica napus* cultivation regions in Mainland China (Ni et al., 2014). Also, it infects peanut (*Arachis hypogaea*) trees in northeastern China (Yan et al., 2014), medicinal plant (*Andrographis paniculata*) trees in Changing County, Beijing City, China (Shi et al., 2016), and sweet potato (*Ipomoea batatas*) plantations in Hangzhou, Zhejiang Province, East China (Ojaghian, 2020; Xiong et al., 2021). Rape seed yield damages caused by *S. sclerotiorum* ranged from 10-20 percent and could reach 80% during serious pathogenic epidemic periods (Mei et al., 2011).

The increased risk of agricultural epidemics with the high demand for complete, safe, and varied food is an important challenge. Current phytopathogens administration aims to preserve economic plants to improve food production and provide stability to human society by using ecosystems (He et al., 2016). Plant diseases have caused severe economic losses to farmers throughout the world. Agricultural, chemical, and physical measures were used for the protection of plants and the control of pests. The control procedures prosperity depends on the stability of the efficacy of the biocontrol agent used for plant protection at the required place and time against different kinds of plant pathogens and on the mechanism used in the attack of the pathogens (Bardin et al., 2015).

## 1.2 Biological control

The biocontrol term means to use bio methods in the management of the pest (Daintith and Martin, 2005). In plant pathology, the biological control refers to the harnessing of microbial communities or one of their antagonists to suppress plant disease pathogens (Pal and Gardener, 2006). Some rhizospheric plant microorganisms are exploited as promising natural sources and eco-friendly ways to manage serious plant pathogens (Gerbore et al., 2014). For the successful application of biocontrol of plant diseases, microbial biological control agents are added to the soil by different methods. Biocontrol agents are appearing many mechanisms, including interactions with plants by inducing systemic resistance, nutrient competition, and antagonistic actions through hyperparasitism and antibiosis, often combining different modes of action (Köhl et al., 2019). The biological control method occupies advanced positions in field application because it has many advantages, such as being environmentally harmonious, granting the possibility of plant disease control in a long-term and sustainable form, increasing the workers' safety, and decreasing the resistance of pests (Alabouvette et al., 2006; Mathre et al., 1999).

And this is what the chemical methods are missing through the development of resistance in the target species upon repeated exposure to industrial pesticides (McDonald and Linde, 2002). On this basis, biological control systems were assumed to be more evolutionarily stable than chemical control systems (Holt and Hochberg, 1997). An issue of an increased number of pathogens resistant to chemical pesticides, in addition to the hazardous effects on human and environmental health resulting from excessive usage of pesticides, led to scientists being strongly stimulated to explore alternate eco-friendly administration artifices. The use of *Trichoderma* species or one of its secondary metabolites as a modern biocontrol approach is recognized internationally (Khan et al., 2020). *Trichoderma* spp. is a widespread soil-borne saprophytic and normally reproduces inside soil; it was recently given special attention as a biological resistance factor against soilborne plant pathogenic fungi (Nega, 2014). Some *Trichoderma* species are mycoparasitic on or in plant pathogenic fungi in their biosphere and kill them via the release of cell wall degrading enzymes. Some other species produce antibiotics or exploit the nutrients and location of their surroundings, while another species improves plant development through the release of some useful hormones (Vinale et al., 2008). Some species of *Trichoderma* are producing bioactive compounds that prohibit the development of pathogens such as gliotoxin (Roberts and Lumsden, 1990). Species and strains of *Trichoderma* differ in reducing and killing target plant pathogens species depending on the means of suppress which it have, so the search for compounds that are bioactive in controlling plant pathogens is a basic and sustainable strategy in biological control.

## 1.3 *Trichoderma* spp.

The lifestyle of *Trichoderma* is passing two stages: the sexual first stage (teleomorphic) is named Hypocrea, and the asexual second stage (anamorphic) is called *Trichoderma* (Druzhinina et al., 2011). Genus *Trichoderma* has generally been defined  at the sexual stage (telomorphic) as Fungi Imperfect based on its ability to form asexual spores, i.e., conidia, and variation in morphology to the under Deuteromycotina, Hyphomycetes, Phialasporace, Pyphales, and Dematiaceae (Singh et al., 2006). *Trichoderma* spp. is a filamentous fungus of saprophytic nature, present in nearly all soils, and reproduces on decaying woody and the roots system (Schuster and Schmoll, 2010). The advantages of some of its species include their abundance of propagules in soil and their production of several enzymes, which make them the most used

biological control agents; furthermore, they are environment-friendly and simple to cultivate and apply (Srivastava et al., 2015). The year 1794 is considered the beginning of the description of the fungus called *Trichoderma* by Persoon, whereas the Tulasne brothers in 1865 suggested that the Hypocrea species is teleomorphic to the sexual status of *Trichoderma* spp. (Gams and Bissett, 2002a). The sexual morph of *Trichoderma* of *H. cornu-damae* was first recorded in 1895 from decaying woody samples in Sichuan Province, China (Patouillard, 1895). Over the last few years, the species have increased due to the discovery of teleomorphs such as *T. virens = H. virens* and *T. harzianum = H. lixii*. However, not all species of teleomorphs have been revealed, such as *T. asperellum* (Samuels, 2006). In 1969, *Trichoderma* is a critical reexamined which included nine aggregate (Rifai, 1969). In 1991, after revising all species, Bissett found that distinguishing among *Trichoderma* species is not easy. Bissett had determined the species of Rifai's groups only according to the form and number of branches in conidiophores. After that, Bissett subdivided the *Trichoderma* genra into 5 departments, including; section *Longibrachiatum*, *Trichoderma* section, *Pachybasium* section, *Saturnisporum* section, and *Hypocreanum* section (Bissett, 1991).

## 1.4 Morphological taxonomy of *Trichoderma* spp.

Taxonomy and correct identification of *Trichoderma* species are very required due to its ecological and economic significance. By macroscopic characters, *Trichoderma* species possess rapid growth; hence, the morphological characterization is dependent on the rate of growth on the substrate (Nirengerg, 1976). Some culture media synthesized from potatoes, cornmeal, and synthetic low nutrient had been used to measure colonies radius and characteristics (Samuels, 2006). Also, temperature and pH are among the factors that show some important characteristics between the species (Yu et al., 2007).

Furthermore, a half day of cool green fluorescent light alternated with a half day without light was used to assay colony characters that can be used as distinctive characteristics of *Trichoderma* species such as increased ratio, pigmentation, pustules types, and smell (Chaverri et al., 2011). To distinguish biologically similar species, it was noted that 30°C and pH 7-8 are the optimum conditions for the growth and development of *T. harzianum*, but 20°C and pH 4 are the best conditions for the growth and development of *T. aureoviride* (Kamala et al., 2015).

After the emergence of conidia, spreading yellowish or greenish pustules are seen. Most of the time, circles with green-yellow dye appeared (Shah et al., 2012). Some species produce pigments and odors distinctively; for example, brown pigmentation is formed by diffusing on the agar, with an odor like that of slightly fruity in *T. amazonicum* (Chaverri et al., 2011). While cultures of *T. viride* and *T. atroviride* are spread with an aromatic compound like coconut smell (Gams and Bissett, 2002a). Either by microscopic features or key morphological characteristics, the body of the genus *Trichoderma* consists of key morphological characteristics, which include a fungus with septate hyphae and several divaricated conical or pyramidal conidiophores (Rifai, 1969). The structures that look like flasks are emerging from conidiophores called phialides that produce the phialospores, also known as conidia, which arrange to fabricate a conidial vertex (Gams et al., 1998). The conidiophores contain the main organ ramified, and modified side branches arise, which may be single or paired, and sometimes they may be re-branching (Singh et al., 2014). The conidiophores bear a few numbers of phialides, which may be flask-shaped, cylindrical, or nearly subglobose (Samuels et al., 2002). Conidia are formed from one cell, which may be globose, semi-globose, ellipsoidal, colorless, yellowish, or greenish. The conidia typically are surface-smooth or surface-roughened (Samuels et al., 1999). The many species produce one-celled Chlamydospores. They are thick-walled, smooth, globose or ellipsoidal, and colorless, yellowish, or greenish (Lin and Heitman, 2005).

## 1.5 Molecular taxonomy of *Trichoderma* spp.

Due to its abundance of variability, the discovery and the correct classification of the species have required the deep integration of multiple information from molecular, morphological, physiological and life-cycle studies (Bissett, 1991). On the other hand, basic techniques and morphology-based features are insufficient to split among their species (Druzhinina et al., 2005; Druzhinina and Kubicek, 2005). Molecular tools used to describe species have advanced with the increasing number of species and the complexity of their characteristics (Lieckfeldt et al., 2002). The evolutionary relationships among species of *Trichoderma* are beginning to expand with the prosperity of means for analysing DNA sequence polymorphisms and their growing use. Whereas several polymerase chain reaction (PCR) assays have been developed through amplifying DNA based on specific primers (Jaklitsch, 2009).

*ITS* region sequence analysis is a known molecular approach that uses to disclose relationships among species. This is because the *ITS* region is one of the better-developing regions, and its characteristics may change within a genre (Schoch et al., 2012; White et al., 1990). Several genes such as *tef1, rpb2*, *ech42*, and *cal* have all been introduced for separating among *Trichoderma* spp. (Bissett et al., 2003; Chaverri and Samuels, 2003; Kim et al., 2013; Kubicek et al., 2003; Wang et al., 2009). The gene *tef1* is regarded as the preferred marker for the identification of *Trichoderma*. In addition, the coding portions of (*ech42*) and *(rpb2)* have significantly high intra- and interspecific variability compared with the *ITS* gene and ssu-mDNA (Devi et al., 2017). Also, the sequence-based technique on two or more genes is more accurate in identifying the species. Where, using three gene regions (*ITS*, *TEF1*, and *RPB2)*, have the best results been obtained for identifying new species within the clade of Harzianum (Gu et al., 2020). Nowadays, the strategy of *Trichoderma* species delimitation depends on the union of multi-sequences with a phylogenetic tree supported by phenotypic characteristics (du Plessis et al., 2018; Innocenti et al., 2019; Qiao et al., 2018).

### 1.6 *Trichoderma* spp. as biological control agent

*Trichoderma* strains were applied worldwide in the management of a great number of plant diseases. Nowadays, a variety of mechanisms including direct and indirect mechanisms have been reported to be involved in biological control of *Trichoderma* strains against various plant pathogens. The exploiting of resources and area by competition or antibiosis has been regardes as one of the main indirect mechanisms, while mycoparasitism has been proposed to be the main direct mechanisms (Harman, 2006).

### 1.6.1 Mechanism of competition

The ability to vie for nutriments and place with pathogenic organisms is a key mechanism that makes antagonistic organisms successful biocontrol agents. Exploitation of nutrients and place is an indirect action the *Trichoderma* strains naturally exert in biocontrol against fungal phytopathogens (Benítez et al., 2004). Competition law in microorganisms has two main elements: places or sources of nutriments, such as competition on siderophores with other filamentous fungi. For instance, a plant pathogen such as *Pythium* needs iron for survival but, under iron starvation, it will die (Benítez et al., 2004).

Also, *T. asperellum* strain T34 favorably competes for sources of iron with *Fusarium* spp., causing the elimination of the *Fusarium* wilt disease on tomato crops (Segarra et al., 2010). Where conidia germinate and the mycelial growth of a pathogen is dependent on nutrient concentrations in the habitat, thus reduced nutrient levels lead to fewer infection locations and symposis advancement (Nassr and Barakat, 2013). Under an iron deficiency condition, some of the *Trichoderma* strains will produce iron and inhibit the growth of many microorganisms (Chet and Inbar, 1994). Siderophore production is beneficial because enemy fungi can inhibit the reproduction and development of pathogens by prohibiting the supply of iron in the biosystem (Mukherjee et al., 2012b). Many species of *Trichoderma* colonize the surface of the root system and cause what is known as *Trichoderma*-plant interaction (Harman et al., 2004). The onion rhizosphere colonization by the biocontrol agent *T. atroviride* showed high efficiency in controlling the plant pathogen *Sclerotium cepivorum* via competition for position and/or alimentary in the rhizosphere (McLean et al., 2005).

### 1.6.2 Mechanism of antibiosis

Antibiosis is an influential mechanism of bio-agents used in control that considers compounds with low-weight molecular weight or antibiotics released by some *Trichoderma* strains that suppress various plant pathogens, including bacteria and fungi. Antibiotics that release from *Trichoderma* spp. can be divided into two types: volatiles and non-volatiles (Dennis and Webster, 1971). Antibiotics generated by *Trichoderma* can be divided into three groups: volatile substances such as several isocyanide derivatives and 6-pentyl-pyrone; a second group of water-soluble substances such as koningic acid and heptelidic acid; and the last group, peptaibols such as peptide antibiotics (Ghisalberti and Sivasithamparam, 1991). Antibiotics that *Trichoderma* produced inhibited the growth of pathogens during interaction with their cell wall (Benítez et al., 2004). Numerous strains from different *Trichoderma* species have produced a large variety of antibiosis that have a role in biological control mechanisms (Reino et al., 2008).

Previously, *T. virens* produced the antibiotic gliotoxin that had an restrained impact toward the *Pythium ultimum* and *Rhizoctonia solani* (Lumsden et al., 1992). Compound gliotoxin is listed under the class of toxins (epipolythiodioxopiperazine), which consist of disulfide-bridg specifically (Howell et al., 1993). A bioactive compound called gliovirin was released by *T. virens* in the specific medium, and it was classified as an antibiotic (Howell, 1998).

Trichokonins of types VI, VII, and VIII had been extracted from *T. koningii* and identified as antibiotics. They belong to the peptaibols group with high activity in inhibition of both *Rhizoctonia* spp., *Fusarium* spp., *V. dahliae*, and *B. cinerea* (Xiao-Yan et al., 2006).

Harzianopyridone is a bioactive compound first isolated from *T. harzianum*. Its chemical structure contains a 2,3-Dimethoxypyridine pattern, which makes it an antibiotic with powerful activity against pathogens such as *Gaeumannomyces* sp. and *Pythium* spp. (Vinale et al., 2006). Also, two antifungal butenolide compounds, harzianolide and T39 butenolide, had been extracted from *T. harzianum* isolates and reported high inhibitory activity toward three serious pathogens infecting plants (Vinale et al., 2009). Trichothecenes are highly bioactive antibiotics against dangerous plant diseases such as *Rhizoctonia* spp., *B. cinerea*, and *Colletotrichum lindemuthianum*, which are extracted from *T. brevicompactum* (Shentu et al., 2014b). Four antibiotics (1,8-dihydroxy-3-methylanthraquinones, 1-hydroxy-3-methylanthraquinones, and 6-methyl-1,3,8 trihydroxyanthraquinones) had been extracted from *Trichoderma* strains that exhibited great potential in the repression of *Sclerotia* sp., *Macrophomina* sp., *R. solani*, and *Fusarium* spp. (Ahluwalia et al., 2015). An antifungal named cremenolide (1) was obtained from *T. cremeum* and showcased striking results against many dangerous plant diseases (Vinale et al., 2016). In another study, *T. koningiopsis* YIM PH30002 produced two secondary metabolites called koninginins R-S (1 and 2), which inhibited the development of both *F. flocciferum* and *F. oxysporum* in culture media (Hu et al., 2017).

Gliotoxin is one of the toxins that belong to epipolythiodioxopiperazine class (Kwon-Chung and Sugui, 2009; Scharf et al., 2016). The gliotoxin was separated for the first from the fungus *T. lignorum* in 1936 (Weindling and Emerson, 1936). Further, in 1944 the gliotoxin was separated from *T. viride* and described as moderately toxic to a great variety of actinomycetes, molds, bacteria, and yeasts (Brian and Hemming, 1945). In 1975, this compound also separated from *T. hamatum* (Hussain et al., 1975). Especially, this compound was separated from the "Q' strain of *T. virens* which exhibited important effects in curtailing the growth and multiplication of plant pathogens (Howell et al., 1993). Using a gene disruption strategy, it has been clarified that the gene cluster (*gliP*) is the pathway responsible for the gliotoxin biosynthesis of *T. virens* by noting the weakness of mutants in offense on the sclerotia after removing the *gliP* locu (Vargas et al., 2014).

Some researchers have reported on the important role that gliotoxins play in the support performance of *T. virens* toward many microorganisms that are plant pathogenic (Scharf et al., 2016; Vey et al., 2001).

For example, the gliotoxin extracted from *T. virens* at two or four ppm achieved great effectiveness with anastomosis groups of *Rhizoctonia* spp. (Jones and Pettit, 1987). Using low concentrations, gliotoxin separated from strain *T. virens* (ITC-4777) showed inhibitory activity against each of *R. bataticola*, *M. phaseolina*, *P. deharyanum*, *P. aphanidermatum*, *S. rolfsii*, and *R. solani*, using ED50 concentration rates of 0.03, 1.76, 29.38, 12.02, 2.11, and 3.18 µg/ml (Singh et al., 2005). Overall, the disulfide bridge in a gliotoxin's chemical composition plays an effect role in their toxicity toward microbes, resulting in the inactivation of proteins and/or the production of reactive oxygen species (Gardiner et al., 2005). Even though the effect mechanism of gliotoxin on the pathogens of plants is not clear, some researchers described it as an antibiotic and a leakage factor that caused seepage of carbs and bicarbonates, which led to a reduction in mycelial weight in *Rhizoctonia* sp. (Lewis et al., 1991). Also, this toxin (gliotoxin) is an important compound in the discouragement of the reproductive parts of *P. ultimum* (Roberts and Lumsden, 1990), and the capacity to degrade the sclerotia that are produced by *S. sclerotium* (Vargas et al., 2014). Transmission electron microscopy revealed distinguished changes-cells, including a decrease in the amount and sizes of mitochondrial cristae, striking plasmolysis, and ultrastructural changes in the *S. rolfsii* mycelial that were treated for 12 hours with 30 μg/ml of gliotoxin extracted from *T. virens* T23 (Hua et al., 2021). Strains of *T. virens* have been reported to be able to produce gliotoxin in rhizosphere soil, but can secrete this toxin at large scales in liquid culture on agar or in natural substrates like sugarcane bagasse fermentation (Anitha and Murugesan, 2005; Scharf et al., 2016).

### 1.6.3 Mechanism of mycoparasitism

Mycoparasitism is a feeding style that occurs when an organism is parasitic on another organism, especially when a plant pathogen is a host. Recently, many biocontrol agents have been studied in species that belong to the genera *Hypocrea* (Kubicek et al., 2011). Steps of the mycoparasitism mechanism of most strains of *Trichoderma* are clearly explained by Harman et al. (2004). First, *Trichoderma* grows toward the target fungus after their identification through the connecting of carbs in the wall of *Trichoderma* cells with lectins in the cell wall of the target

fungus. Secondly, the connection between *Trichoderma* hyphae and the host hyphae is occurring, and the hyphae attach to it and can coil about it, beginning formulation of the appressoria. After appressoria penetration, *Trichoderma* is beginning to generate numerous fungi-toxic enzymes that degrade the walls of the cell organisms, like chitinases, glucanases, and proteases (Baek et al., 1999; Djonović et al., 2007; Pozo et al., 2004). The accumulative activity of these enzymes causes the degradation of the cell walls of the host, which finally results in killing the target host. Gene analysis revealed several genes that expressed CWDEs, such as the alkaline proteinase associated with gene *Prb1* in *T. harzianum* (Flores et al., 1997), the β-1,4-Endoglucanase associated with *Egl1* gene in *T. longibrachiatum* (Migheli et al., 1998), the Chitinase associated with *Chit33* gene present in *T. harzianum* (Limón et al., 1999), the β -1,3-glucanase enzyme associated with the *Chit33* gene and the β-1,6-glucanase enzyme associated with the *TvBgn3* gene both present in *T. virens* (Djonović et al., 2007). Genome-wide expression study is considered one of the new approaches followed to identify genes associated with the mycoparasitism operation (Reithner et al., 2011). The technique of transcriptome analysis using expressed sequence tags (ESTs) has been exploited significantly to reveal mycoparasitism-related genes for different *Trichoderma* strains before, during, and after the confrontation with host fungi (Steindorff et al., 2012; Vizcaíno et al., 2007). In recent times, the quantitative real-time PCR approaches and data presented of RNA-seq had facilitated the explanation of gene patterns of the whole genome sketch of *Trichoderma* and revealed clearly advanced in interpreting the mechanism of mycoparasitic for *Trichoderma* with plant pathogenic fungi (Steindorff et al., 2014). Usually, gene ontology analysis indicates that code genes during mycoparasitism are fundamentally engaged in the metabolism of biological regulation, cellular processes, and catalysis of molecular function (Sun et al., 2015). Functionality representations of transcriptome analysis afforded a clear notion of the way of mycoparasitism  was practiced by some strains of *Trichoderma* and their effective aspect in the suppression of several pathogens of plants (Morán-Diez et al., 2019).

The 402 bio-control genes for one species of *Trichoderma* (*T. harzianum*) had determined, including genes related to competition, genes related to mycoparasitism, genes associated with antibiosis, and one gene involved in eliciting plant response (Guo et al., 2020). The gene expression regulation differs between *Trichoderma* species.

Based on RNA-seq results analysis, the different genes related to mycoparasitism in three different species of *Trichoderma* have been expressed (Atanasova et al., 2013).

On the other hand, the genes expressed for *Trichoderma* species during maize root colonization stimulated the biosynthesis of some compounds of phytohormone-like (Malinich et al., 2019). Also, the genes of the cryptic IPKS-containing cluster responsible for synthesizing tricholignan A in *T. harzianum* strain T-22 have been determined and described, which work to decrease $Fe^{+3}$ and lead to promoting growth in plants in deficient iron (Chen et al., 2019).

### 1.7 *Trichoderma* spp. as plant growth promotion agent

The fungi that improve growth in plants are soil-borne filamentous fungi that are linked in or on the root hairs symbiotically and have positive responses through root colonization and production of the various plant growth-improving metabolites, with supporting the inauguration of resistance in plants against phytopathogens (Hyakumachi, 1994). The growth promotion trait is not species-specific, but rather isolate-specific, where individual isolates of the same species exhibit varying degrees of plant growth enhancement. Several PGPF isolates have been evidenced to be positive in root colonization and enhance plant growth apart from the induction of resistance against phytopathogens such as species from the genus of *Penicillium*, *Aspergillus*, *Trichoderma*, and *Talaromyces* (Naziya et al., 2019). *Trichoderma* attracted a lot of interest as a species group concerned in promoting plant growth and increase their biomass (Tyśkiewicz et al., 2022). Some of it positively affected seed germination through the induced creation and deposit of reactive species of oxygen, which mainly work as an indicator to induce seed emergence. Also, most species of *Trichoderma* exploit root systems and stretch them with the number of nutrients they need (Tančić-Živanov et al., 2020).

An affirmative connection was found between chemical indicators like superoxide dismutase enzyme activity, catalase activity, and emergence percentage in seeds treated with Trichoderma isolates (Tančić-Živanov et al., 2020). *Trichoderma* spp. are able to improve plant development directly by incrementing the average of germination, totalling both biomass and length of roots, root diameter, the average of the tips of the roots, and the number of branches, stimulating flowering, and incrementing vigor; or improving plant development indirectly by increasing the plant's resistance to diverse stresses (Halifu et al., 2019; Stewart and Hill, 2014).

*Trichoderma* isolates are capable of enhancing plant biomass production through increased nutrient availability such as auxins, nutrient solubilization, and the conversion of iron through the production of a wide variety of siderophores (Contreras-Cornejo et al., 2009). Several *Trichoderma* strains are capable of producing the auxin plant hormone 3-indoleacetic acid (IAA). This hormone is one of the common classes of auxin traded in plants and is responsible for regulating and stabilizing various parts of the plant (Nieto-Jacobo et al., 2017). *Trichoderma* isolates produced in the IAA *in vitro* are usually detected in the presence of tryptophan using Salkowski's reagent (Abdenaceur et al., 2022). IAA plays a prime role in improving the quantity of plant production through the multiplication of the hairs of roots, the formation of lateral branches, and leaf and flower morphogenesis (Ferguson and Beveridge, 2009; Overvoorde et al., 2010).

Siderophores are produced by some *Trichoderma* strains as compounds with a high affinity for iron ($Fe^{3+}$), a molecular weight less than 10 KDa chelator, able to improve plant growth in medium without iron or with present iron but insoluble (Zhao et al., 2020). The isolates of *Trichoderma* produced in the siderophore *in vitro* are usually detected on both media (CAS and 8-hydroxyquinoline) (López et al., 2019). Several reports had proven that the *Trichoderma* strains producing siderophore and 3-indoleacetic acid in soil improved all germination and growth indices in tested plants, in addition to exhibiting the highest biomass quality (Chen et al., 2021; López et al., 2019). Most positive results of isolates of *Trichoderma* in improving the production of vegetables and crops are achieved in a safe and sustainable way. Also, formulations such as green biofertilizers are considered attractive for future field applications.

## 1.8 Mycosynthesis of nanoparticles

Mycosynthesis is the term released onto nanoparticles when using biomass or fungi derivatives to synthesize them. The term "mycosynthesis" was first used when silver nanoparticles were synthesized and described by mediating a *Fusarium acuminatum* (Ingle et al., 2008). After that, the term "Myconanotechnology" was proposed to include scientific research that has produced nanoscale bodies by fungi (Rai et al., 2009). The methods based on biological sources are more advantageous when compared with the methods based on physics and chemistry in synthesizing nanoparticles due to the ability to modify the morphology and size of the nanoproduct (Ukkund et al., 2019).

13

Among microorganisms, fungi can be mass-produced in the laboratory, without causing environmental problems and demonstrate easy downstream processing for nanoparticles (Banerjee and Rai, 2018).Whereas, fungi are now taking center stage in researches on the biological routes of mineral nanoparticle synthesis due to their tolerance to high-toxic levels and their role in metallic bioaccumulation (Sastry et al., 2003). The methods based on mold and yeast in the synthesis of nanoprodacts have many important features, such as the rapid increase in growth, metallic ion reduction capacity, and NP settlement (Castro-Longoria et al., 2011). Compared with other microorganisms, fungi used in nanoparticle synthesis have several advantages (Figure 1-1). For example, it is relatively easy for fungal isolation, while fungal cultures can secrete large amounts of metabolites (Kaur, 2018).
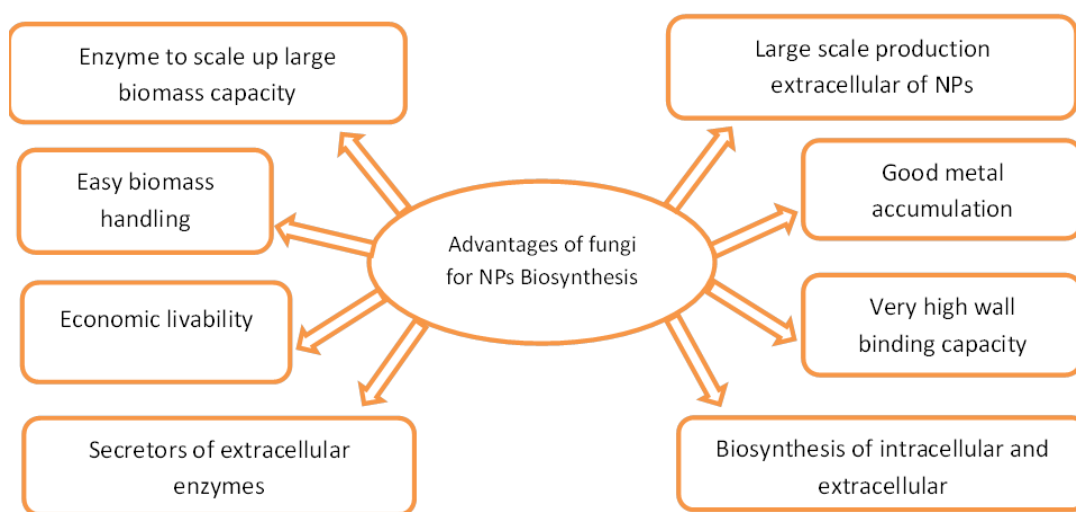


**Figure 1-1. The advantages of using fungi in myco-synthesis for NPs production (Salem and Fouda, 2021).**

Also, fungi based advantageous because of their ability to secrete many enzymes and compounds, many of which can be applied in different scientific fields. Where, the filamentous fungi (ascomycetes and imperfect fungi) had produced around 6,400 known bioactive substances (Berdy, 2005). Some fungi can create and format nanostructures through the release of intra- or extracellularly reducing enzymes (Alghuthaymi et al., 2015).

### 1.8.1 Mycosynthesis of nanoparticles using *Trichoderma* spp.

The species of *Trichoderma* was recently applied for the synthesis of nanoparticles due to their unique advantages, such as being eco-friendly and significantly free of hazards associated with toxic chemicals or organic solvents like in the chemical synthesis nanoparticle process

(Arya et al., 2020), fast growth, simplicity of handling, and release of a huge number of enzymes (Gemishev et al., 2019), and the possibility of controlling the size and shape of nanoparticles as presented in Figure 1-2 (Maliszewska et al., 2009).

Mycosynthesis of nanoparticles employing *Trichoderma* species offered advantages that made it a success agent as a biological control agent for resolving problems related to various phytopathogens through the contribution of biomolecules that engaged in inhibiting plant pathogenic enzymes and bioactive compounds in the reducing metallic process (Mukherjee et al., 2008). Also, the antimycotic action of AgNPs biofabricated from the culture supernatant of *Trichoderma* is revealed as a better antimycotic agent than their chemical compounds in the inhibition of fungal pathogens (Kumari et al., 2019).
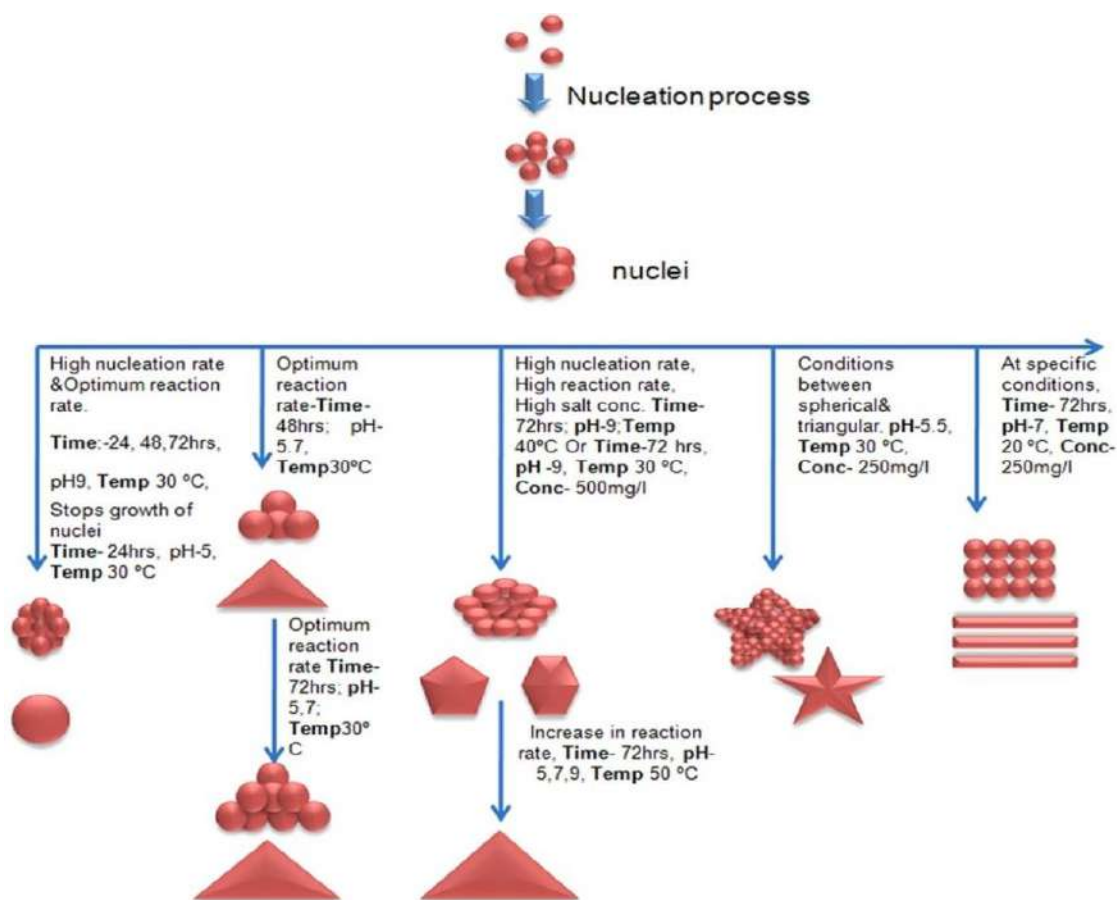


**Figure 1-2. Schematic diagram representing the mechanism of control by sizes and shapes of the AuNPs was biosynthesized by *T. harzianum* under different reaction conditions (Kumari et al., 2019).**

**1.8.2 Role of NPS synthesized using *Trichoderma* spp. in management of phytopathogenic infections**

Recently, the NPs synthesized by *Trichoderma* have been widely applied in the management of phytopathogenic infections. Reliable and low-cost silver nanoparticles were developed utilizing the SYA.F4 strain supernatant of *T. harzianum*, which showed high antifungal activity in the agar-well diffusion method against plant pathogens that cause leaf spot diseases (El-Moslamy et al., 2017). The nanoproduct of gold and silver that are formed by culture filtrates of *T. atroviride* have been used in the control on disease of *Phomopsis* canker, which is resulted by the fungal pathogen *Phomopsis theae* in tea plants (Gnanamangai et al., 2017). Also, the culture filtrate of six different species of *Trichoderma* had success in the synthesis of selenium nanoparticles (SeNPs), which showed biological activities in suppressing each of mycelial growth, sporulation and zoospore viability of *S. graminicola* (Nandini et al., 2017). The pure supernatant of the non-pathogenic fungal *T. harzianum* had succeeded in the synthesis of silver nanoparticles and displayed high inhibition against both mycelial growth and killing conidia of *Fusarium* (Al-Abboud, 2018). The AgNPs biosynthesis was achieved using cell filtrate of *T. longibrachiatum* when using 10 g fungal biomass, without shaking and 72-hour incubation at 28°C, which it showed the possibility inhibits the formation of colonies of some important plant pathogens on rice (Elamawi et al., 2018). The silicon and titanium nanoparticles developed using *T. harzianum* (ThFT1) had shown good management to reduce powdery mildew disease on wheat seedlings caused by *Blumeria graminis* under special growth conditions (Farhat et al., 2018). In another hand, the SeNPs synthesized by selenium and the supernatant of *T. atroviride* had shown an antibiotic action towards *P. grisea* and unincreased the infection on the leaves of tomato crops by *C. capsici* and *A. solani* (Joshi et al., 2019). The AgNPs manufactured by the filtrate of the antagonist fungus *T. harzianum* proved their high ability to inhibit the bacteria *Clavibacter michiganensis* subsp. *michiganensis* that cause tomato canker disease at low concentrations using the disc diffusion method *in vitro* (Noshad et al., 2019). Hydrolytic enzymes of *T. harzianum* were determined in the filtrates that contributed to silver nanoparticle synthesis, where the AgNP-TS exhibited inhibitory activity towards sclerotia development and mycelial growth of *S. sclerotiorum* (Guilger-Casagrande and Lima, 2019).

Mycosynthesis of ZnONPs was achieved by mixing ZnO3 with *Trichoderma* secondary metabolites of three different strains (PGT4, PGT5, and PGT13), which showed antibacterial activity against *Xanthomonas* sp., the pathogen of bacterial leaf blight of rice (Shobha et al., 2020). The extract supernatant of *T. harzianum* was used to reduce and stabilize three types of minerals, which are silver, gold, and copper, as a simple, abundant, and sustainable method, but just the Ag and Cu nanoparticles reduced the mycelial growth of plant pathogenic fungi such as *A. alternata* and *P. oryzae*, in addition to inhibiting the formation of sclerotia in media at differing doses (Consolo et al., 2020). The AgNPs trustworthy and sustainable formation had been developed by *T. viride* cell filtrate as a nano-fungicide agent against soil-borne root rot diseases like *Fusarium* sp. and *Rhizoctonia* sp. in rice crops (Manikandaselvi et al., 2020). In the near period, the bio- synthesized iron nanoparticles (FeNPs) using the biological control agent *T. harzianum* has been used as a bio-source contributed to the inhibition of *S. sclerotiorum* mycelium in PDA medium (Bilesky-Jose et al., 2021). Also, the nano-fungicide synthesized by the extract of *T. harzianum* had prevented the growth of fungal hyphae at a rate of 63% for each of the pathogens that infect the groundnut, including *A. niger*, which causes collar rot; *S. rolfsii*, which causes stem rot and *Sclerotium* wilt; and *M. phaseolina*, which causes dry root rot and dry wilt disease (Raja et al., 2021).

### 1.8.3 Action mechanisms of NPs derived from *Trichoderma* spp. against phytopathogens

The nanoparticles synthesized by *Trichoderma* species had been tested widely in the management of human and plant pathogens *in vitro* and *in vivo*, but without explaining the mechanical action of these particles precisely. In general, several theories have been proposed about the action mechanism, such as the inhibition of expression of the ribosomal subunit proteins and certain cellular enzymes and proteins essential to adenosine triphosphate manufacture (Yamanaka et al., 2005). Some of the mechanisms of AgNPs were explained based on their effects on microbes, including surface connection, penetration, and spread inside cells. The true impacts of nano-compounds begin on the cells from outside to inside, such as through perforation of the cell wall and rupture of the cellular membrane, spreadation of free toxic metal ions from NPs, adhesion with the cellular organelles, and super-oxidative stress by generating reactive oxygen species (Dakal et al., 2016).

In the case of the nanoparticles derived from species of *Trichoderma*, the free radicals produced by the Ag-NPs derived from *T. interfusant* (Fu21) had induced fungal cell membrane damages and enhanced protein and sugar leakage by elevating the permeability of the membrane of the hyphal cell, as well as the effect on the enzymatic activity and respiration in the phytopathogenic *S. rolfsii* (Hirpara and Gajera, 2020).

Selenium nanoparticles (TSNP) derived from the strain of *T. harzianum* JF309 had led to the collapsed structure of the mycelium and the hyphae shrinking that were seen dry and deformed in *A. alternata* XJa1, in addition to showing more oxidative stress in *F. verticillioide* BJ6 (Hu et al., 2019). While the major mechanism of Silver-nanoproduct created by the supernatant of *Trichoderma* strain MTCC 5661 is revealed, the nitroblue tetrazolium assay and scanning electron microscopy confirmed that oxygen-containing reactive species generation, down-regulation of stress enzymes, disruption of endogenic antioxidant machinery, disruption of cell walls, and osmotic imbalance are the main effects resulted by BSNP that lead to the fungal cell death of *A. brassicicola* (Kumari et al., 2019).

**1.9 Research objectives**

    *Trichoderma* spp. are common rhizosphere inhabitants, and some species of this genus have many mechanisms that make them competent biological control agents because of their complex interactions with plant pathogens, such as mycoparasitism , secretion of antibiotics, and competition for space and nutrients. This study was conducted to illustrate the safety strategies produced from a biological basis in plant protection and control of plant pathogens transmitted in soil. The specific objectives of this study are the following.

1- To isolate *Trichoderma* species and test their antagonism against agronomical important soil-borne phytopathogens infecting economic vegetable crops.

2- To characterize the phenotypic and molecular profiles of antifungal *Trichoderma* isolates and explore the new species.

3- To detect and identify active secondary metabolites and discover their mode of action in antagonism against *Phytophthora capsisi* which causes *Phytophthora* blight disease.

4- To investigate and mycoparasitism-related genes through the mechanisms of gene expression and assess their effect in biological control against *Verticillium* wilt caused by the soilborne fungus *Verticillium dahliae*.

5- To biosynthesize silver nanoparticles using metabolites of *Trichoderma*, and evaluate their antifungal activity and mechanism against *Sclerotinia sclerotiorum* which causes white mold disease *in vitro*.

# Chapter 2

## Screening of *Trichoderma* and identification of new species: A novel observation in enhancing biological management efficiency toward *Phytophthora capsici* in *in vitro*

### 2.1 Introduction

The ubiquitous species of the *Trichoderma* genus belong to the Ascomycota, which are one of the most useful groups of fungi in many aspects and important applications that humans have invested in their lives in recent years (Saravanakumar and Wang, 2020; Zhang et al., 2022). *Trichoderma* spp. are widely distributed in soil and interact in a variety of ways with other microorganisms in the rhizosphere. Many of *Trichoderma* spp. are employed in agriculture to promote plant development and manage various diseases that harm crops, serving as helpful instruments for the production of sustainable foods (Ferreira and Musumeci, 2021). The ability of some *Trichoderma* strains to suppress soil-borne pathogens directly by either lowering pathogen populations or disrupting their pathogenic pathways, such as mycotoxins, has been supported (Amira et al., 2017; Modrzewska et al., 2022). Selecting *Trichoderma* strains as a good biological control agent involves following the direct mechanisms that use it in suppressing plant pathogens such as antibiosis, competition, and mycoparasitism, but excluding *Trichoderma* strains involving secondary mechanisms (Ferreira and Musumeci, 2021). That the screening process for the best *Trichoderma* strains is very necessary, and this includes looking at all isolated strains in the biocontrol environment. Whereas many *Trichoderma* species are weak or do not have antagonistic mechanisms, Therefore, the careful selection of suitable strains is important for agricultural systems success (Pedrero-Méndez et al., 2021). In light of this fact, the identification of *Trichoderma* species with high biocontrol interest will give a deeper understanding to the early screening of potential antagonists against soil-borne pathogens (Schmoll et al., 2014). Morphological characteristics are used as approaches for *Trichoderma* species identification, but recently, the results of this approach have become uncertain due to the instability of most characteristics or their overlap among some species (Gams and Bissett, 2002b; Samuels, 2006). The introduction of DNA sequence analysis allowed for more accurate identification of *Trichoderma* species (Druzhinina and Kopchinski, 2006).

The phylogeny of *Trichoderma* and the evolutionary relationships among differnet species were determined by both maximum parsimony analysis and distance analysis of DNA sequences from several genetic loci (Kullnig-Gradinger et al., 2002). Though the multiple *ITS* rRNA sequences were widely used in species identification, currently they are considered insufficient for *Trichoderma* species identification (Druzhinina and Kopchinski, 2006; Raja et al., 2017). Recently, the identity of *Trichoderma* spp. could be determined when the *ITS* sequence of the target fungus reaches ≥ 76% similarity value to the sequences in the dataset according to the protocol of Cai and Druzhinina (2021). The sequence analyses of genes encoding both RNA polymerase II subunit B and translation elongation factor 1-α facilitate in species identifications reliable where, they used in the phylogenetic analysis and identification of new *Trichoderma* species (Bissett et al., 2015; Jaklitsch and Voglmayr, 2015; Cai and Druzhinina, 2021).

The study aim at: (1) Isolation of *Trichoderma* spp. from farmer soil near Hangzhou city; (2) Assessment of the antagonistic properties of isolates against the soil-borne plant pathogen *P. capsici*; (3) Identification of the *Trichoderma* isolates using morphological characteristics and phylogenetic analysis based on (*ITS rRNA*, *tef1*, and *rpb2*) to identify native *Trichoderma* species or detect new species.

## 2.2 Materials and methods

### 2.2.1 Pathogen isolate

The *P. capsici* HZ07 was a highly aggressive isolate and it was isolated previously from the infected roots of *Capsicum annuum* cv. *Hangxian* No. 3 and identified as the A2 mating types (Jiang et al., 2016a). It was deposited at 11–12°C in the Culture Collection of Institute of Biotechnology, Zhejiang University, Hangzhou, Zhejiang Province, China.

### 2.2.2 Isolation of *Trichoderma* spp.

Forty soil samples were collected from the rhizosphere of bell or chili pepper plants in the heavily infested fields by *P. capsici* from eight different farms near to Hangzhou city, China. All soil samples were stored at 4°C in a refrigerator in the laboratory. Serial dilutions were made with each soil sample. For this, 1 g of soil was added into 9 ml of sterile distilled water, the suspension was shaken and then a series of dilutions were carried out.

An aliquot of 1 ml of each diluted soil suspension was uniformly spreaded on the surface of a *Trichoderma* selective medium (TSM: $MgSO_4·7H_2O$ 0.2 g; $K_2HPO_4$ 0.9 g; KC1 0.15 g; $NH_4NO_3$ 1.0 g; glucose 3.0 g; chloramphenicol 0.25 g; rose-bengal 0.15 g; agar 20 g with 1 L water) (Elad et al., 1981) and the plates were incubated at 27±1°C for four days. Colonies growing on TSM were transferred to the potato dextrose agar (PDA) for their single spore isolation. The single spore isolates were stored at 4°C for use in this study.

## 2.2.3 Screening of antagonistic isolates

The dual culture technique was adopted to screen the isolates with highest antagonistic activity against *P. capsici* HZ07. For this, a disc (5-mm diameter) from the margin of a three-day-old colony of a *Trichoderma* isolate was put on one side on a PDA plate (9-cm diameter), with another 5-mm diameter of five days old mycelia of *P. capsici* was placed on the opposite side. Each treatment contained three replicates. The plates were incubated at 25±1°C. Degree of antagonism was assessed for each isolates on a scale of classes 1–5 (1: *Trichoderma* sp. grew well on the fungal pathogen until finally covered the whole surface of the culture medium; 2: *Trichoderma* sp. grew on at least 2/3 of the culture medium; 3: *Trichoderma* sp. and the fungal pathogen colonized nearly 1/2 of the culture medium and no organism dominated the other; 4: at least 2/3 of the culture medium was colonized by the fungal pathogen and the fungal pathogen resisted encroachment of the antagonist; 5: the fungal pathogen grew well on the *Trichoderma* sp. and finally colonized the whole surface of the culture medium) (Zhang et al., 2015).

## 2.2.4 Detection of activity metabolites

The active metabolites produced by 15 isolates of *Trichoderma* against *P. capsici* were evaluated. A mycelia-disc (5 mm) obtained from the isolate cultured on PDA was transferred into a 250 ml flask containing 100 ml PDB and the flasks were incubated in a ZWY-211B rotary shaker at 25°C for 14 days. After filtering mycelium from the culture liquid with cheesecloth, the used culture medium was centrifuged and 50% (v/v) and 20% culture liquids were prepared by dilution and then sterilized by filtration through millipore membrane with 0.22 μm pore size. One ml of each culture liquid was added into a 9-cm-diameter plate containing 10 ml molten PDA, and then a mycelia-disc (0.5 cm) of five days old *P. capsici* was placed into the centre of a plate.

Plates with PDA but without culture liquid were used as the controls. Each treatment was replicated five times. The plates were kept at 25°C, and the diameter of the colonies was measured when the diameter of control colonies reached the plate edge. Inhibition percentage of mycelial growth was calculated using the following formula: IP (%) = [(C−T)/C)] × 100, where IP is the inhibition percentage, C is hyphal growth diameter of the control; T is the hyphal growth diameter in the culture liquid-treated plates.

### 2.2.5 Molecular identification

The fungal isolates were cultured in a 250 ml flask containing 100 ml potato dextrose broth (PDB), shaken at 150 rpm at 27±1°C for four days. The mycelia were filtered and homogenized to a fine powder in liquid nitrogen in a mortar. Extract of genomic DNA was carried out according to the method of Zhang and Li (2009). After re-suspending in 50 µl TE buffer, the obtained genomic DNA was stored at −20°C. Three DNA fragments of various sizes were amplified in the automated thermal cycler (Eppendorf AG, Germany). The primer pairs *ITS5* (5'GGAAGTAAAAGTCGTAACAAGG3') and *ITS4* (5'TCCTCCGCTTATTGATATGC3') were used for amplification of rDNA *ITS* regions (Jiang et al., 2016b), the primers *EF1*-728F (5′-CATCGAGAAGTTCGAGAAGG-3′) (Carbone and Kohn, 1999), and *TEF1*LLErevR (5′-AACTTGCAGGCAATGTG G-3′) (Samuels et al., 2002) for the translation elongation factor 1 α (*TEF1*) gene and primers *RPB2*- 5F (5′-GAYGAYMGWGATCAYTTYGG-3′) and *RPB2*-7cR (5′-CCCATRGCTTGYTTRCCCAT-3′) for the RNA polymerase II subunit B (*RPB2*) gene (Jiang et al., 2016a).

It was a final total volume of 50 µl by fully mixing 2 µl of DNA with 0.5 µM of each of the primers and 25 µl of 2x PCR Master Mix (Sangon Biotech, Shanghai, China). Parameters used in PCR reactions performed in a thermal cycler for three primers were applied as follows: For *ITS* gene were used the parameters (94°C – 3 min 94°C (30 cycles) 1min, 56°C – 30 sec, 72°C – 30 sec, 72°C– 10 min and 4°C on hold). For the *TEF1* gene, parameters were used (94°C – 2 min, 66°C – 56°C (9 cycles), 94°C – 30 sec, 56°C – 1 min, 72°C – 1 min, Repeat 3-6 for 36 cycles, 72°C – 10 min, 4°C on hold), while for *RPB2* primer gene were (94°C – 3 min, 94°C – 20 sec, 55°C – 30 sec, 72°C – 1 min, Repeat 2-4 for 40 cycles, 72°C – 10 min, 4°C on hold).

### 2.2.6 Phylogenetic analysis

The sequences were edited by BioEdit 7.1.3.0 (Hall, 1999) and analyzed by the nucleotide BLAST search in the GenBank database. They were deposited in GenBank and reference sequences were downloaded from GenBank. Phylogenetic tree was constructed by using the three-locus combined *ITS*, *TEF1*, and *RPB2* dataset with 60 in group taxa and two outgroup taxa (*Nectria berolinensis* and *N. eustromatica*).

The sequences of each region or genes were aligned with MAFFT v7.273 (Katoh and Standley, 2013) and edited by the BioEdit. The resulting sequences were assayed by using Gblocks 0.91b for eliminating the poorly aligned positions and divergent regions prior to phylogenetic analyses (Katoh and Standley, 2013). The suitable model of evolution for each alignment was estimated by using jModel Test 2.1.7 (Darriba et al., 2012), and the model was selected based on the Akaike information criterion. The best TrNef + I + G model was chosed for *TEF1* and CTR + I + G for *RPB2* and TrNef + I + G for *ITS*. The molecular phylogenies of *Trichoderma* spp. were analyzed by using both Maximum likelihood (ML) and Bayesian inference (BI). ML analyses were implemented with RaxmlGUI v. 1.5 (Silvestro and Michalak, 2012).

ML bootstrap (ML- BS) analysis of each ML tree completed with a fast 1000 bootstrap frequency with the same parameter settings using the GTR + I + G model of the nucleotide substitution. The 80% values were showed on a tree for significantly supported nodes. BI analyses are conducted with MrBayes v. 3.2.6 (Ronquist et al., 2012). The MCMC (Markov-chain Monte-Carlo) used to seek in four chains; these branches have been run on 10 million generations with 100 tree samples every generation. The remaining trees merged into one tree with 50% majority rule consensus tree. It was found to be significant when BI posterior probability (BI-PP) values equal or above 0.95.

### 2.2.7 Morphological observation

The isolates were cultured on PDA, cornmeal dextrose agar (CMD) (cornmeal agar 20 g, dextrose 20 g, agar 20 g with 1 L distilled water) and synthetic low nutrient agar (SNA) ($KH_2PO_4$ 1.0 g, $KNO_3$ 1.0 g, $MgSO_4 \cdot 7H_2O$ 0.5 g, KCl 0.5 g, glucose 0.2 g, sucrose 0.2 g, agar 15.0 g with 1 L water) and incubated at 20–25°C under an alternating cycle of 12 h light and 12 h darkness (Jaklitsch, 2009).

The fungal asexual structures such as conidiophores, phialides, conidia and chlamydospores were photographed and measured using a Zeiss Axiophot 2 microscopy with Axiocam CCD camera and Axiovision digital imaging software (AxioVision Software Release 3.1., v.3–2002; Carl Zeiss Vision Imaging Systems). The closely related species on phylogenetic tree were morphologically compared by taxonomic characteristics.

### 2.2.8 Statistical Analysis

The analysis was carried out on the data of the inhibition experiment depending on the analysis of variance (ANOVA) using the SAS software version 9.1.3. To compare the means, the LSD test level of significance of 0.05 was used. The experiment had been analyzed using three replicates.

## 2.3 Results

### 2.3.1 Isolation and screening of antagonistic isolates

A total of 77 isolates of *Trichoderma* spp. were obtained from the roots zones of soil. Among them, 19.5% (n = 15) of *Trichoderma* isolates showed the highest antagonistic activity with antagonism class 1, while 80.5% of the isolates had antagonism classes for 2–5. The 15 isolates with antagonism class 1 (Figure 2-3) were chosen as the antagonistic candidates and they were designated as HZA1-HZA15.
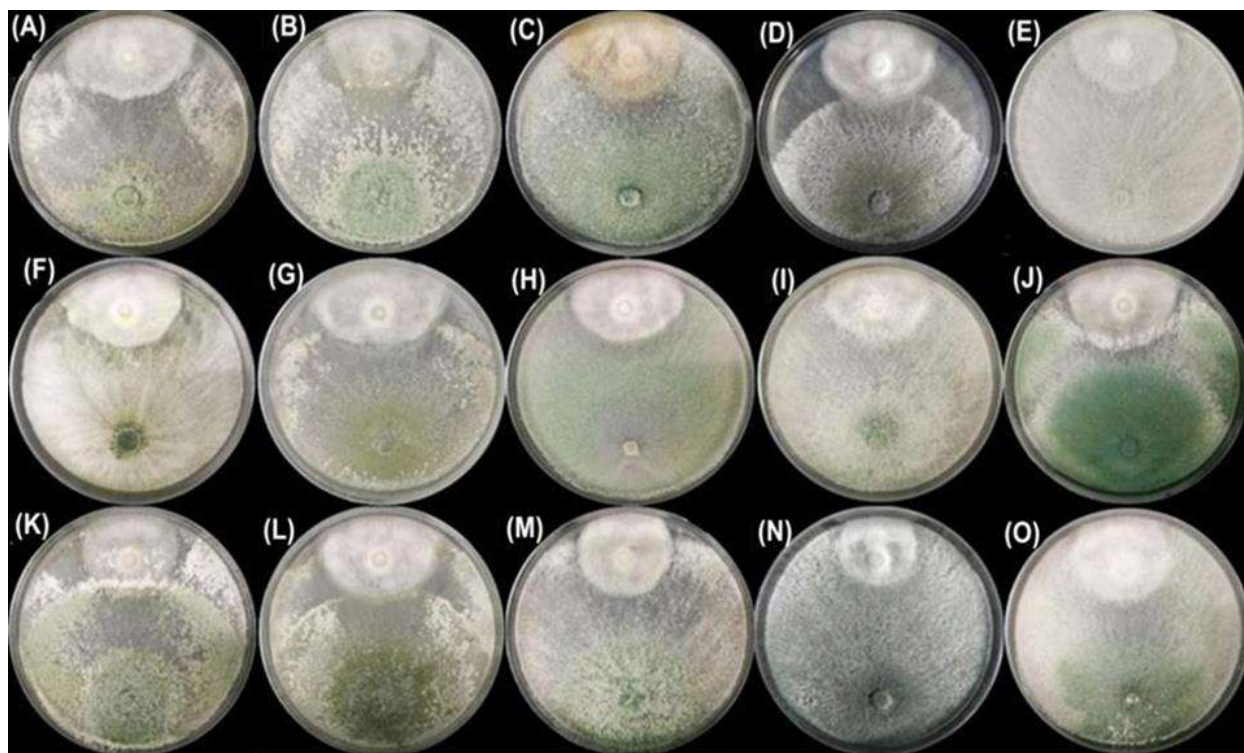


**Figure 2-3. Antagonistic effect of 15 isolates (bottom) with antagonism class for 1 on the hyphae of *P. capsici* (upper parts) on PDA five days after inoculation.** A, HZA1. B, HZA2. C, HZA3. D, HZA4. E, HZA5. F, HZA6. G, HZA7. H, HZA8. I, HZA9. J, HZA10. K, HZA11. L, HZA12. M, HZA13. N, HZA14. O, HZA15.

### 2.3.2 Inhibitory activity of culture liquid against *P. capsici*

The inhibitory activity of 15 isolates metabolites against the hyphae growth of *P. capsici* was assessed. All metabolites from different isolates indicated different levels of inhibitory activity ($p < 0.05$) (Table 2-1). The metabolites produced by *T. virens* HZA14 completely inhibited the hyphae growth after diluted by 20- or 40-folds, showing the highest inhibition percentage (100%), followed by *T. afroharzianum* HZA3 with 44.85% (20-folds) and 78.96% (40-folds) inhibition and *T. citrinoviride* HZA9 with 42.445% (20-folds) and 77.81% (40-folds)

as well as *T. dorothopsis* HZA5, HZA8 and HZA15 with 34.67–39.59% (20-folds) and 71.0–771.33% (40-folds) and *T. koningiopsis* HZA6 with 37.29% (20-folds) and 72.18% (40-folds). While the lowest inhibition percentage was found in *T. atroviride* HZA1, HZA2 and HZA13, *T. asperellum* HZA10 and *T. harzianum* HZA11 with 0.62–1.59% (20-folds) and 5.18%–6.29% inhibition (40-folds).

**Table 2-1. Inhibitory activity of metabolites produced from 15 *Trichoderma* isolates against hyphae growth of *P. capsici*.**

| *Trichoderma* isolates | Inhibition percentage (%) | |
|:---:|:---:|:---:|
| | **40-folds** | **20-folds** |
| HZA1 | 1.11±0.62 [e] | 6.29±0.05 [e] |
| HZA2 | 1.11±0.62 [e] | 6.18±0.02 [e] |
| HZA3 | 44.85±0.44 [b] | 78.96±1.05 [b] |
| HZA4 | 15.93±0.77 [d] | 23.74±0.74 [d] |
| HZA5 | 34.67±0.21 [c] | 71.07±0.64 [c] |
| HZA6 | 37.29±0.50 [c] | 72.18±0.92 [c] |
| HZA7 | 13.51±0.56 [d] | 21.17±0.28 [d] |
| HZA8 | 34.97±0.60 [c] | 70.92±0.19 [c] |
| HZA9 | 42.44±0.20 [b] | 77.81±0.72 [b] |
| HZA10 | 0.62±0.05 [e] | 5.92±0.11 [e] |
| HZA11 | 1.59±0.04 [e] | 07.40±0.16 [e] |
| HZA12 | 16.52±0.22 [d] | 20.70±0.15 [d] |
| HZA13 | 1.11±0.12 [e] | 5.18±0.03 [e] |
| HZA14 | 100.00± 0.00 [a] | 100.00±0.00 [a] |
| HZA15 | 39.59±0.57 [c] | 71.33±0.54 [c] |

Inhibition percentage (%) of diameter growth of *P. capsici* hyphae on PDA containing the diluted culture liquid five days after inoculation. The culture liquid was diluted 40-folds or 20-folds. Value are means ± standard deviations of three replicates, and the different lowercase letters in the same column are significantly different at p <0.05 according to LSD test.

### 2.3.3 Sequencing and phylogenetic analysis

The genomic DNA of 15 isolates amplified by primer pairs *ITS5* F/*ITS4* R, *EF1-*728F/TEF1LLErevR and *RPB2-5*F/*RPB2-7c*R produced the fragments of approximately 630 bp (*ITS*), 1300 bp (*TEF1* region) and 1077 bp (*RPB2*), respectively. Sequences of each *Trichoderma* isolate were aligned, edited, analyzed and deposited in the GenBank database (Table 2-2).

**Table 2-2. Isolates and their GenBank accessions of *Trichoderma* species used for phylogenetic analyses.**

| Species | Isolates | GenBank NO. | | | References |
|---------|----------|------|------|------|------------|
| | | *ITS* | *TEF1* | *RPB2* | |
| *T. atroviride* | HZA1 | MH624136 | MK850823 | MH647791 | This study |
| *T. atroviride* | HZA2 | MH624137 | MK850824 | MH647792 | This study |
| *T. afroharzianum* | HZA3 | MH624138 | MK850825 | MH647793 | This study |
| *T. brevicompactum* | HZA4 | MH624139 | MK850826 | MH647794 | This study |
| *T. dorothopsis* | HZA5 | MH624140 | MK850827 | MH647795 | This study |
| *T. koningiopsis* | HZA6 | MH624141 | MK850828 | MH647796 | This study |
| *T. brevicompactum* | HZA7 | MH624142 | MK850829 | MH647797 | This study |
| *T. dorothopsis* | HZA8 | MH624143 | MK850830 | MH647798 | This study |
| *T. citrinoviride* | HZA9 | MH624144 | MK850831 | MK962804 | This study |
| *T. asperellum* | HZA10 | MH624145 | MK850832 | MH647800 | This study |
| *T. harzianum* | HZA11 | MH624146 | MK850833 | MH647801 | This study |
| *T. brevicompactum* | HZA12 | MH624147 | MK850834 | MH647802 | This study |
| *T. atroviride* | HZA13 | MH624148 | MK850835 | MH647803 | This study |
| *T. virens* | HZA14 | MH624149 | MK850836 | MH647804 | This study |
| *T. dorothopsis* | HZA15 | MH624150 | MK850837 | MH647805 | This study |
| *T. atroviride* | TRS18 | KJ786757.1 | KJ786839.1 | KP009061.1 | (Skoneczny et al., 2015) |
| *T. atroviride* | TRS26 | KJ786751.1 | KJ786832.1 | KP009054.1 | (Skoneczny et al., 2015) |
| *T. atroviride* | TRW | KX538952.1 | KX538956.1 | KX538954.1 | Unpublished |
| *T. atroviride* | SB6 | KX538951.1 | KX538955.1 | KX538953.1 | Unpublished |
| *T. valdunense* | CBS 120923 | FJ860863.1 | FJ860717.1 | FJ860605.1 | (Jaklitsch, 2009) |
| *H. atroviride* | CBS 119499 | FJ860726.1 | FJ860611.1 | FJ860518.1 | (Jaklitsch, 2011) |
| *T. afroharzianum* | TRS835 | KP009351.1 | KP008787.1 | KP009149.1 | (Oskiera et al., 2015) |
| *T. atrobrunneum* | T42 | KX632515.1 | KX632629.1 | KX632572.1 | Unpublished |
| *T. brevicompactum* | TRS859 | KP009365.1 | KP008906.1 | KP009162.1 | (Oskiera et al., 2015) |
| *T. polysporum* | 8232 | KJ783311.1 | KJ634779.1 | KJ634746.1 | (Zhu and Zhuang, 2015) |
| *T. albolutescens* | CBS 119286 | FJ860721.1 | FJ860609.2 | FJ860517.1 | (Jaklitsch, 2011) |
| *T. minutisporum* | CBS 341.93 | MH862411.1 | KJ665612.1 | KJ665314.1 | (Jaklitsch and Voglmayr, 2015) |
| *T. atlanticum* | CBS 120632 | FJ860781.1 | FJ860649.1 | FJ860546.1 | (Jaklitsch, 2011) |
| *T. koningiopsis* | 7745 | KJ783287.1 | KJ634755.1 | KJ634722.1 | (Zhu and Zhuang, 2015) |
| *T. koningii* | 7723 | KJ783285.1 | KJ634753.1 | KJ634720.1 | (Zhu and Zhuang, 2015) |
| *T. auranteffusum* | CBS 119284 | FJ860728.1 | FJ860613.1 | FJ860520.1 | (Jaklitsch, 2011) |

| | | | | |
|---|---|---|---|---|
| *H. rodmanii* | C.P.K. 2852 | FJ860825.1 | FJ860688.1 | FJ860581.1 | (Jaklitsch, 2011) |
| *H. rodmanii* | CBS 121553 | FJ860824.1 | FJ860687.1 | FJ860580.1 | (Jaklitsch, 2011) |
| *T. margaretense* | C.P.K. 3127 | FJ860741.1 | FJ860625.1 | FJ860529.1 | (Jaklitsch, 2011) |
| *T. lixii* | C.P.K. 1934 | EF392746.2 | FJ179573.1 | FJ179608.1 | (Jaklitsch, 2011) |
| *T. bannaense* | HMAS:248865 | KY687948.1 | KY688038.1 | KY688003.1 | (Chen and Zhuang, 2017) |
| *T. zayuense* | HMAS:248836 | KY687919.1 | KY688032.1 | KY687975.1 | (Chen and Zhuang, 2017) |
| *T. citrinoviride* | isolate7987 | KJ783299.1 | KJ634767.1 | KJ634734.1 | (Zhu and Zhuang, 2015) |
| *T. chlamydosporicum* | HMAS:248851 | KY687934.1 | KY688053.1 | KY687990.1 | (Chen and Zhuang, 2017) |
| *T. citrinoviride* | TRS745 | KP009362.1 | KP008894.1 | KP009188.1 | (Oskiera et al., 2015) |
| *T. citrinoviride* | TRS750 | KP009360.1 | KP008889.1 | KP009186.1 | (Oskiera et al., 2015) |
| *T. asperellum* | TRS705 | KP009366.1 | KP009011.1 | KP009068.1 | (Oskiera et al., 2015) |
| *T. rogersonii* | 7795 | KJ783292.1 | KJ634760.1 | KJ634727.1 | (Zhu and Zhuang, 2015) |
| *T. asperellum* | TRS746 | KP009371.1 | KP008926.1 | KP009073.1 | (Oskiera et al., 2015) |
| *T. samuelsii* | S42 | JN715652.1 | JN715593.1 | JN715598.1 | (Jaklitsch et al., 2012) |
| *T. gamsii* | TW20050 | KU523894.1 | KU523895.1 | KU523896.1 | (Chen et al., 2016) |
| *T .valdunense* | CBS 120923 | FJ860863.1 | FJ860717.1 | FJ860605.1 | (Jaklitsch, 2011) |
| *T. aff.harzianum* | TRS861 | KP009233.1 | KP008786.1 | KP009103.1 | (Oskiera et al., 2015) |
| *T. harzianum* | T18 | KX632492.1 | KX632606.1 | KX632549.1 | Unpublished |
| *T. harzianum* | T2 | KX632477.1 | KX632591.1 | KX632534.1 | Unpublished |
| *T. solum* | HMAS:248849 | KY687932.1 | KY688051.1 | KY687988.1 | (Chen and Zhuang, 2017) |
| *T. linzhiense* | TC982 | KY687957.1 | KY688048.1 | KY688011.1 | (Chen and Zhuang, 2017) |
| *T. virens* | TRS106 | KP009291.1 | KP008854.1 | KP009093.1 | (Oskiera et al., 2015) |
| *T. virens* | TRS112 | KP009296.1 | KP008860.1 | KP009098.1 | (Oskiera et al., 2015) |
| *T. spinulosum* | CBS 311.50 | FJ860844.1 | FJ860701.1 | FJ860591.1 | (Jaklitsch, 2011) |
| *T. orientale* | IsolateS187 | JQ685873.1 | JQ685868.1 | JQ685884.1 | (Jaklitsch and Voglmayr, 2012) |
| *T. applanatum* | Isolate7781 | KJ783289.1 | KJ634757.1 | KJ634724.1 | (Zhu and Zhuang, 2015) |
| *T. minutisporum* | Isolate7828 | KJ783294.1 | KJ634762.1 | KJ634729.1 | (Zhu and Zhuang, 2015) |
| *Trichoderma alni* | CBS120633 | EU518651.1 | EU498312.1 | EU498349.1 | (Jaklitsch et al., 2008) |
| *T. austriacum* | CBS 122494 | FJ860735.1 | FJ860619.1 | FJ860525.1 | (Jaklitsch, 2009) |
| *Nectria berolinensis* | CBS 127382 | HM534893.1 | HM534872.1 | HM534883.1 | (Jaklitsch and Voglmayr, 2012) |
| *Nectria eustromatica* | CBS 121896 | HM534896.1 | HM534875.1 | HM534886.1 | (Jaklitsch and Voglmayr, 2011) |

To delineate species boundaries, phylogenetic analysis was carried out by utilizing the combined three-locus dataset of *ITS*, *TEF1* and *RPB2*. After removing the poor aligned regions, the alignments were 2034 characters, of which 609 were phylogenetically informative.

The parsimony informative characters were 243 in *TEF1* alignment, 277 in *RPB2* and 89 in *ITS*, respectively. The phylogenetic tree exhibited that all tested isolates in this study were separated into different clades (Figure 2-4).

29

The topology of the best scoring ML tree analysis was consistent with the BI tree for the concatenated three-locus dataset. The relationship of all reference isolates could be clearly differentiated on the species level.

The isolates HZA13, HZA1 and HZA2 clustered with *T. atroviride* SB6, *T. atroviride* TRW, *H. atroviride* CBS 119499 and *T. atroviride* TRS 26 as a clade with high ML-BS (100%) and high BI-PP (1.00) support.

The isolates HZA8, HZA5 and HZA15 clustered as a distinct clade with high ML-BS (100%) and high BI-PP (1.00) support, forming a sister clade with tested isolate HZA6 and *T. koningiopsis* 7745 to the well-supported clade with higher ML-BS (84%) and higher BI-PP (0.98) support. The phylogenetic analysis indicated that isolates HZA8, HZA5 and HZA15 have a close relationship, and *T. koningiopsis* being more closely related to the HZA6.

Similarly, HZA4, HZA7 and HZA12 clustered as a distinct clade with high ML-BS (100%) and high BI-PP (1.00) support, forming a sister clade with *T. brevicompactum* TRS859 with high ML-BS (100%) and high BI-PP (1.00) support.

In addition, HZA10, HZA9, HZA14, HZA11 and HZA3 clustered with *T. asperellum* TRS705 and TRS746, *T. citrinoviride* TRS745 and TRS750, *T. virens* TRS106 and TRS112, *T. aff. harzianum* TRS861, *T. harzianum* T5 and *T. harzianum* T18, and *T. afroharzianum* TRS835 as a distinct clade with high ML-BS (100%) and high BI-PP (1.00) support, respectively.

**Figure 2-4. Maximum likelihood (ML) tree generated from the linked of *ITS*, *TEF1* and *RPB2* sequences of 62 taxa of *Trichoderma*.** Both of *Nectria berolinensis* and *N. euchromatica* had used for tree rooted. thick black lines represented of Clades with 100% ML bootstrap branch support and 1.00 (BPP). Clades with>80% ML-BS (left) and 0.95 BPP (right) are showed by the corresponding support values. Dashes show support values lower than 80% ML-BS and 0.95 BPP. Species isolated from the rhizosphere of pepper plants are presented in bold.

## 2.3.4 Taxonomy

### 2.3.4.1 *Trichoderma dorothopsis*

A.A. Tomah & J.Z. Zhang, sp. nov. MycoBank: MB 831,879 Figure 2-5.

**Holotype:** CHINA, ZHEJIANG PROVINCE: Shaoxin, from Soil, 30°18′3"N, 120°51′3"E, 5.7 M, 2 Jun. 2017, A.A. Tomah and J.Z. Zhang (HOLOTYPE dry culture HMAS 248251 and ex-type living culture CGMCC3.19672 = HZA5).

**Etymology:** "dorothopsis" in reference to the similarity to *T. dorotheae* with phialides tending to proliferate percurrently to form new phialides.

**Description:** The optimum temperature for growth on PDA and SNA is 27–30°C. Colonies grown on PDA producing conidia within 96 h, with abundant aerial mycelium without the concentric rings (Figure 2-5A); on CMD abundant yellowish conidia in the aerial mycelium forming differentiated concentric rings (Figure 2-5B); on SNA conidia beginning to form small pustules in a ring around the original inoculum in marked concentric rings (Figure 2-5C). No diffusing pigment or distinctive odour detected on any medium. On SNA, conidial masses green to deep green. Conidial production nearly continuous with a tendency to form highly compact to cottony, 1–2 mm diam pustules (Figure 2-5D and 2-5E). Often long, entirely fertile branches visible in the pustules (Figure 2-5F). Conidiophores comprising a recognizable main axis; fertile branches arising along the length of the main axis, more or less paired with longer or shorter internodes (Figure 2-5G).

The longer branches near the base and short branches or solitary phialides are arising near the tip (Figure 2-5H); branches rebranching or producing directly phialides (Figure 2-5I); sometimes several phialides arising from the same point and crowded (Figure 2-5K). Phialides, (9.76-) 9.69–11.43 (-11.92) × (2.54-) 3.06–3.89 (-4.36) μm, narrowly lageniform, straight, only slightly swollen in the middle. In some cases, phialides tending to proliferate percurrently to form new phialides (Figure 2-5I and 2-5J). Conidia, (3.19-) 3.34–3.91 (-4.18) (avr. 3.63) × (2.86-) 3.07 × 3.48 (-3.56) (avr. 3.28) μm, globose to subglobose, occasionally ellipsoidal, smooth (Figure 2-5L). Chlamydospores, abundant, terminal to intercalary, globose to subglobose (Figure 2-5M).

**Specimens examined:** CHINA, ZHEJIANG PROVINCE: Hangzhou, from Soil, 30°3′36″N, 120°49′22″E, 5.7 M, 2 Jun. 2017, J.Z. Zhang (living culture CGMCC3.19673 = HZA8,

CGMCC3.19674 = HZA15). The living cultures HZA5, HZA15, and HZA8 were deposited in the Culture Collection of Institute of Biotechnology, Zhejiang University, Hangzhou, Zhejiang Province, China.

**Comments:** *Trichoderma dorothopsis* is characterized by main axis branched conidiophores, lush aerial mycelium production on CMD, narrowly lageniform phialides tending to proliferate percurrently to form new phialides, smooth, globose to subglobose conidia but with yellow coloration on CMD. It has a nearest phylogenetic relationship with *T. koningiopsis* and *T. koningii* and clusters with *T. koningiopsis* (Figure 2-4), which is morphologically distinct. *T. dorothopsis* producing lush aerial mycelium on CMD, being different from *T. koningii* and *T. koningiopsis* with very little aerial mycelium (Samuels, 2006). It has narrowly lageniform phialides but lacks intercalary phialides comparing with *T. koningiopsis*. Unlike *T. koningii* with oblong conidia and *T. koningiopsis* with ellipsoidal conidia, *T. dorothopsis* has globose to subglobose conidia. In addition, *T. dorothopsis* produces phialides tending to proliferate percurrently to form new phialides, being similar to *T. dorotheae* (Samuels, 2006).

### 2.3.4.2 Identification of other species.

The isolates HZA4, HZA7 and HZA12 grown on CMD or SNA, conidiophores pyramidally verticillately branched in the Pachybasium-type patterns (Bissett, 1991). Phialides mostly broadly ampulliform with a short slender neck. Conidia, 2.6–3.1 × 2.1–2.9 μm, subglobose to short ellipsoidal. Based on morphological characteristics, they were identified as *T. brevicompactum* described by Degenkolb et al. (2008), and Kraus et al. (2004). Isolates HZA1, HZA2 and HZA13 grown on CMD had similarly morphological characteristics. Conidiophores typically unilateral although paired branches. Phialides straight or sinuous, wide at the base, typically flask-shaped and enlarged in the middle, constricted to the tip. Conidia, 2.5–3.5 × 2.4–3.2 μm, subglobose to ovoidal. They were identified as *T. atroviride*, being identical with description by Dodd et al. (2003). Similarly, based on morphological characteristics, isolate HZA3 was identified as *T. afroharzianum* (Chaverri et al., 2015), HZA6 as *T. koningiopsis* (Samuels, 2006), HZA9 as *T. citrinoviride* (Bissett, 1984), HZA10 as *T. asperellum* (Samuels et al., 1999), HZA11 as *T. harzianum* (Samuels et al., 2002), and HZA14 as *T. virens* (Chaverri et al., 2011).
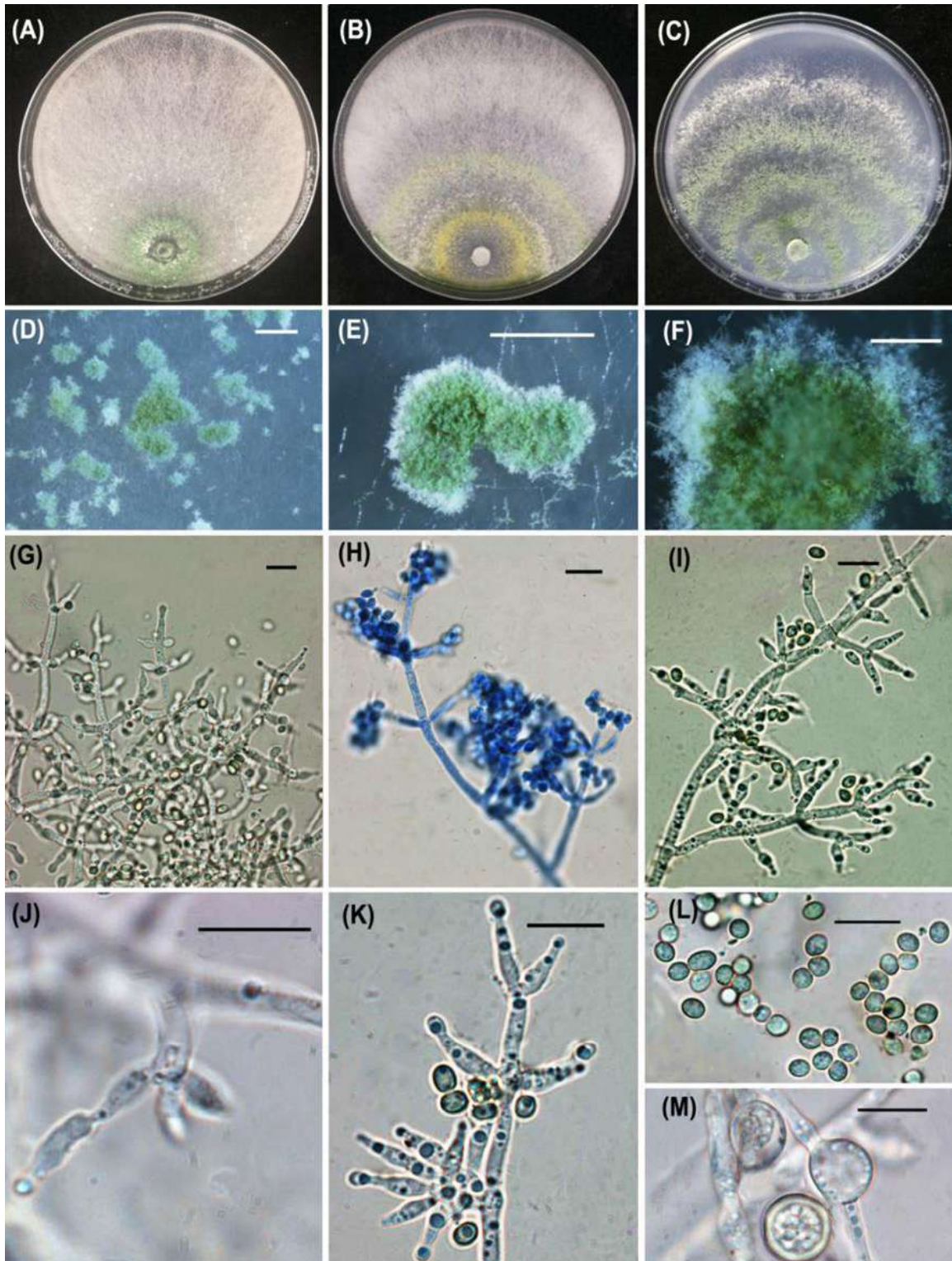
**Figure 2-5.** *Trichoderma dorothopsis* **grown on PDA or CMD or SNA in 9-cm-diam petri dishes under 12 h darkness/12 h light for four days.** A, On PDA. B, On CMD. C, On SNA. D-M, On CMD. D-F, Conidial pustules. Individual plumose conidiophores can be seen in the pustule (F). G-K, Conidiophores and phialides. The percurrently proliferated phialides can be seen in (I and J) (arrows). L, Conidia. M, Chlamydospores. Scale bars: D and E = 1 mm; F = 500 μm; G–M = 10 μm.

**2.4 Discussion**

*Trichoderma* species have a cosmopolitan distribution and inhabit diverse ecological niches, frequently finding on dead wood and bark, on other fungi, in soil and living within healthy plant roots, stems and leaves (du Plessis et al., 2018; Mukherjee et al., 2013). In recent years, the number of *Trichoderma* species has dramatically increased. Until now, more than 290 species of *Trichoderma* have been described (Bissett et al., 2015; Zhu et al., 2017; du Plessis et al., 2018). Phylogenetic analyses currently detect new species or separate closely related and morphologically similar species based on the use of three phylogenetic markers: *ITS* rRNA, translation elongation factor 1-alpha (*TEF1*), and RNA polymerase subunit 2 (*RPB2*) (Dou et al., 2020). Phylogenetic analyses are tools for species identification. With MEGA-X software, cured sequences were used for maximum parsimony analysis with 1,000 bootstrap replicates (Jaklitsch and Voglmayr, 2013; Zhu et al., 2017). We found that several species had a larger base variation range in their gene sequences. In the isolate HZA4, HZA7, and HZA12, phylogenetic analysis displayed that they clustered as a clade, which formed a sister clade with *T. brevicompactum* TRS859 (Figure 2-4). Although they had more than 20-base difference comparing with the isolate TRS859 only in *TEF1* gene sequences, morphological data did not support to separate them from *T. brevicompactum* as a distinct species, showing that *T. brevicompactum* had a larger variation range in its gene sequences (Degenkolb et al., 2008). Similarly, five reference isolates and test isolates (HZA1, HZA2 and HZA13) in *T. atroviride* indicated a larger base variation rang in tree-loci sequences as well. So our study provides demarcation information about *Trichoderma* species. So our study provides demarcation information about *Trichoderma* species, based on the similarities analysis of sequence and significant morphological differences between the test strains and the reference strains, (Jaklitsch and Voglmayr, 2013). In addition, HZA10, HZA9, HZA14, HZA11 and HZA3 clustered with *T. asperellum* TRS705 and TRS746, *T. citrinoviride* TRS745 and TRS750, *T. virens* TRS106 and TRS112, *T. aff. harzianum* TRS861, *T. harzianum* T5 and *T. harzianum* T18, and *T. afroharzianum* TRS835 as a distinct clade with high ML-BS (100%) and high BI-PP (1.00) support, respectively (Chaverri et al., 2015; Samuels, 2006; Chaverri et al., 2011).

In this study, a new species *T. dorothopsis* from soil was found. However, the number of *Trichoderma* species will still probably increase since soil fungal communities have not been widely investigated from many parts of the country.

In phylogenetic analysis, *T. dorothopsis* has a closest phylogenetic relationship with *T. koningiopsis* to form a well-supported branch that separated it from its relatives, while in morphology, it can be distinguished clearly from *T. koningiopsis* by globose conidia and percurrently proliferated phialides. The molecular and morphological analysis all confirms that *T. dorothopsis* is an unreported new species.

Antagonistic compounds produced by *T. virens* HZA14 may play a key role in antagonistic mechanisms. Subsequently, *in vitro* test confirmed that its culture liquid had high inhibitory activity (Table 2-3). Several species of *Trichoderma* have been reported to have a great effect in controlling pepper blight (Ezziyyani et al., 2007; Osorio-Hernández et al., 2011; Sid Ahmed et al., 1999).

## 2.5 Conclusions

As it is known, agricultural soils contain a large number of *Trichoderma* species, but the discovery of an anti-plant pathogen requires more laboratory tests. The study concludes that the soil of farms near Hangzhou, China, contains a large population of diverse *Trichoderma*. Out of the 77 *Trichoderma* spp. isolates evaluated, fifteen isolates displayed the relative capability to control *Phytophthora capsici in vitro* using the dual culture method and free culture filtrate at different dilutions. A molecular approach using three genes (*ITS*, *TEF1*, and *RPB2*) and phylogenetic analysis allowed us to identify 15 isolates belonging to eight species of *Trichoderma*; among them, we found a new species of *Trichoderma* we called *T. dorothopsis* and recorded it in GeneBank.

# Chapter 3

# Gliotoxin produced by *Trichoderma virens* HZA14: an important secondary metabolite in the suppression of pepper blight disease caused by *Phytophthora capsici*

## 3.1 Introduction

Phytophthora disease caused by *P. capsici* is the most destructive disease on pepper plants grown in greenhouses and fields (Granke et al., 2012). The disease usually occurs in the underground parts of a plant, leading to root and crown rot of pepper. During a serious disease epidemic, pathogen dispersal causes aerial blight on leaves, stems and fruit (Callaghan et al., 2016). The white mycelia with zoosporangia often produce on the water-soaked lesions under the humid conditions (Foster and Hausbeck, 2010). Irreversible pepper blight generally develops quickly, resulting in the plant death. Pepper blight is one of important diseases on chilli and bell pepper in Zhejiang province and it occurs severely each year (Jiang et al., 2016a).

For management of the diseases, agricultural and chemical approaches, such as rotation of various crops, resistant varieties and the use of fungicides are widely applied. However, among these strategies, the crop rotation is not widely chosen due to the limitation of agricultural areas and long-term survival of pathogen oospores that can withstand desiccation, heat and cold temperatures, as well as other extreme environmental conditions in soil (Quesada-Ocampo et al., 2009; Roberts et al., 2008). In relation to genetic resistance, the availability of resistant varieties is not common (Foster and Hausbeck, 2010). Moreover, highly resistant pepper cultivars showed susceptibility or moderate resistance when the plants were inoculated with *P. capsici* (Dunn and Smart, 2015).

Management of *P. capsici* relies on use of common-use fungicides metalaxyl and mefenoxam, resulting in the development of fungicide resistance in the *P. capsici* (Barchenger et al., 2018; Parra and Ristaino, 2001) and environmental or human health problems (Hausbeck and Lamour, 2004). Biological control is a promising green approach for the efficient management of phytopathogenic fungi.

*Trichoderma* species, such as *T. asperellum* (Jiang et al., 2016a), *T. harzianum* (Ezziyyani et al., 2007; Sid Ahmed et al., 1999), *T. koningiopsis* (Ramírez-Delgado et al., 2018), have been reported to be greatly effective in management of *P. capsici*. However, the introduction of new strains of *Trichoderma* in the soils has had limited success, probability due to the poor competition and adaptation ability, and the complexity of the soil environment (Hyakumachi et al., 2012; Savazzini et al., 2009).

*Trichoderma* spp. possesses a variety of antagonistic mechanisms against plant pathogens, such as production of lytic enzymes, mycoparasitism, competition of space and nutrients and so on, for their successful colonization (Harman, 2006; Mukherjee et al., 2012b). For example, (Jiang et al., 2016a) revealed that the hyphae of *T. asperellum* isolate CGMCC 6422 could penetrate the hyphae and oospores of *P. capsici* by mycoparasitism, leading to the degradation of hyphal cells. Mycoparasitism involves cell wall degrading enzymes (CWDEs), which allow mycoparasitic fungi to extract nutrients by boring holes from other fungi for their own growth (Cao et al., 2009).

Also, *Trichoderma* strains produce antibiotics or low-molecular-weight compounds, which inhibit the growth of plant pathogens such as 6-pentyl-pyrone (Jeleń et al., 2014), viridiofungin (El-Hasan et al., 2009), gliotoxin (Roberts and Lumsden, 1990), etc. However, the antagonistic mechanisms of the *Trichoderma* spp. against different types of pathogens depend on species and strains. Indeed, the ability to produce the antibiotics vary between isolates of the same species as well as between isolates of different species (Dennis and Webster, 1971).

So for different pathogens, screening the isolates of *Trichoderma* spp. with highest antagonistic activity and characterizing their antagonistic mechanisms are becoming more and more common for their application as biocontrol agents (Vinale et al., 2008).

In this study, we screened a native isolate of *T. virens* HZA14 for antagonistic activity against *P. capsici* and evaluated the underlying mechanisms, such as the production of antagonistic compounds. This will provide isolates resources for developing the effective biological control agents against pepper blight by *P. capsici* that will work in the region.

## 3.2 Materials and methods

### 3.2.1 Assessment of antagonistic mechanism for *T. virens* HZA14

The dual culture technique was used to confirm the antagonistic activity of *T. virens* HZA14 against the *P. capsici* HZ07. For this, a 5-mm-diameter disc from the margin of a 3-day-old colony of a HZA14 isolate was put on one side of a PDA plate (9-cm diameter), and another 5-mm-diameter disc of 5-day-old mycelia of *P. capsici* placed on the opposite side. Each treatment was replicated three times. The plates were incubated at 25±1°C for 5 days. Microscopic observations were performed by using glass slides with the covers sterilized to observe the hyphal disappearance of *P. capsici*, which was detected in the interaction zone between *P. capsici* and *T. virens* HZA14 isolate.

### 3.2.2 Identification of active fractions

Based on the results of the previous experiments in (3.2.1), the highest active fractions produced by the *T. virens* HZA14 isolate were purified and their chemical structures were identified. The isolate HZA14 was inoculated into a flasks containing PDB and incubated in a ZWY-211B rotary shaker at 25°C for 14 days. Two litres of culture liquid were obtained and the metabolites were extracted using equal volume of ethyl acetate. The solvent was evaporated under reduced pressure and low temperature about 35°C. The residue was purified by silica gel column chromatography (particle size 200–300 mesh) and different fractions were purified by preparative silica gel TLC (GF254). A small amount of each fraction was dissolved in DMSO (Dimethyl Sulfoxide, Sangon Biotech, Shanghai China) for bioactive determination using the agar well diffusion method. Aliquots of 10 µl of each fraction (by a ratio of 100 µg/ml) were added into four wells of 0.3 cm size in solidified PDA on three plates, and then a mycelial disc (5-mm) of *P. capsici* was placed in the center PDA plate.

The active fractions were determined by observing the amount of pathogen growth on the plates (absence or presence of an inhibition zone) after incubation at 25°C for four days. For purification of the fraction that showed anti-phytophthora activity further, Reversed-Phase High-Performance Liquid Chromatography with an inert sustain C18 column (µm, 250 × 20 mm) was carried out using Waters Quaternary Gradient Module 2545, Waters UV/visible Detector Module 2489, and Waters Fraction Collector III (made in Japan).

### 3.2.3 Analysis of active fraction

The active fractions were purified further with a Waters 600 HPLC instrument fitted with a Shimpack Prep ODS column (20×250 mm) to identify chemical structures. The eluent was monitored with a Waters 2487 Dual λ absorbance detector at 254 nm. Good semipreparative separation of the active fraction peaks was obtained with a flow rate 6 μl/min by isocratic elution with the mixture of methanol and distilled water (1:1, v/v). The mass spectrum of active fraction was analyzed with a VG Autospec-3000 mass spectrometer (VG, Manchester, UK) and API QSTAR Pulsar 1 (Applied Bio-systems, Foster City, USA).

### 3.2.4 Assay of bioactive fraction

The purified compound was dissolved in DMSO, and different mother solutions were obtained for bioactive determination. For this, they were mixed with a molten V8 medium and seeded onto plates at final concentration of 0.5, 1.0, 5.0, 10.0 and 15.0 μg/ml. Mycelial discs (5 mm) of 5-days old *P. capsici* were placed into the centre of V8 media plate. Each treatment was replicated five times. The plates were kept at 25°C for four days and colony diameters were measured when the diameter of control colonies reached the plate edge. Inhibition percentage of mycelial growth was calculated using the formula: IP (%) = [(C−G)/C)] ×100, where IP is the inhibition percentage, C is hyphal growth diameter of the control; G is the hyphal growth diameter in the purified compound-treated plates.

### 3.2.5 Transmission electron microscopic observation

The JEM-1010 transmission electron microscope (TEM) (JEOL USA Inc., Peabody, MA, USA) was used to detect the impact of gliotoxin on the *P. capsici* hyphae. The 5 cm disc of *P. capsici* was grown on PDA plates covered by cellophane membrane at 28°C. After five days of incubation, the mycelia were transferred to a 2 ml tube containing DMSO with *Trichoderma*-gliotoxin at a final concentration of 5.0 μg/ml. The mycelia were transferred to a 2-ml tube containing DMSO without *Trichoderma*-gliotoxin as a negative control. The tubes were incubated at 28°C for two periods of 6 and 12 h. The mycelia of both the treated with and without gliotoxin were fixed with glutaraldehyde (2.5% v/v) in 0.1 M sodium phosphate buffer (pH 7.0) at 4°C for 18 h and fixed with (1% w/v, osmium tetroxide) at room temperature for 1 h.

It was dehydrated with a sequence of ethanol solutions with increasing concentrations (50%, 70%, 80%, 90%, 95%, and 100%). Then, the specimen was embedded in a Spurr resin and cut with an LKB 8800 Ultra tome, stained in 2% (w/v) lead citrate and 2% (w/v) uranyl acetate, and analyzed using an electron microscope (TEM) at an operating voltage of 80 kV.

**3.2.6 Effect of antagonistic isolates against chili pepper blight**

Based on previous experiment results, the *Trichoderma* isolates were used for *in vitro* tests of biocontrol against chilli pepper blight. Seeds of chili pepper (*Capsicum annuum* L. cv *Jizua*) were sterilized with 2% sodium hypochlorite solution, placed into the surfaces of the wet sterilized filter papers that were in a plate, and the plates were incubated at 25°C for 5–6 days. The germinated seeds were sowed into the pots (11 × 11 × 11 cm) containing the soil mixture (peat: vermiculite: farmyard soil in a 2:1:1 ratio) and incubated at 28–30°C and relative humidity level of 80–90%. *Trichoderma* isolates were cultured in the flasks containing wheat grains autoclaved and incubated at 25°C with a 12 h photoperiod for 15 days for fungal conidial production. One hundred of ml of sterile water was poured into each conical flask and vortexed vigorously to dislodge the spores. Spore suspensions were collected in a container. Spores were counted using a hemocytometer. For soil inoculation, the 10-ml conidial suspension (about $1 \times 10^7$ spores/mL) was applied around the root zone of each seedling with six to eight leaf stage. One week after inoculation, each pot was inoculated with 5 ml of zoospores suspension (about $2 \times 10^3$ zoospores/ml) of *P. capsici* (Bosland and Lindsey, 1991). For preparation of pathogen inocula, the five mycelia discs of *P. capsici* were put into a plate with 10 ml of sterile distilled water and incubated at 25°C under light condition for three days for zoosporangial production. The zoospores suspension was prepared by incubating plates at 4°C for 30 min for zoospore release, filtration with cheesecloth and quantification with a hemocytometer, as described by Ristaino (1990). Seedlings inoculated only with zoospores suspension were used as control. Each treatment (with 25 plants) was repeated three times. The plants were observed daily and disease incidence (DI%) and disease severity (DS%) were recorded after 15 days from inoculation. Disease severity was assessed using a scale of classes 0–4, where 0 = no symptoms; 1 = wilting of the plant; without a stem lesion; 2 = wilting and stem lesion without girdling; 3 = girdled plant stem; 4 = dead plant (Ristaino, 1990).

**3.2.7 Statistical Analysis**

The analysis was carried out on the data of the inhibition experiment depending on the analysis of variance (ANOVA) using the SAS software version 9.1.3. To compare the means, the LSD test level of significance of 0.05 was used. The experiment had been analyzed using three replicates.

**3.3 Results**

**3.3.1 *T. virens* HZA14 antagonism against *P. capsici***

To confirm the antagonistic activity of *T. virens* HZA14 against *P. capsici* HZ07 *in vitro* the dual culture technique in PDA plates was used. The results in Figure 3-6 showed a distinct interaction zone of hypha disappearance of *P. capsici* HZ07 in the interaction between *P. capsici* and *T. virens* HZA14 was observed. For confirming this phenomenon, the repeated test showed that colonization of the HZA14 was able to lead to a clear interaction zone of hypha disappearance of *P. capsici* HZ07 (Figure 3-6). Microscopic observation showed that near margin of a interaction zone of *P. capsici* hyphal disappearance, the hyphae of *P. capsici* were penetrated and encircled by hyphae of *T. virens*, leading to its hyphal degradation (Figure 3-7B and 3-7C). Especially, it was found that the part of a hyphal of *P. capsici* was killed but it's another part was normal yet (Figure 3-7A). In addition, complete disintegration of *P. capsici* hyphae was common in the interaction zone (Figure 3-7D).



**Figure 3-6. The isolate *T. virens* HZA14 causing the interaction zone (\*) of hyphal disappearance of *P. capsici*.**
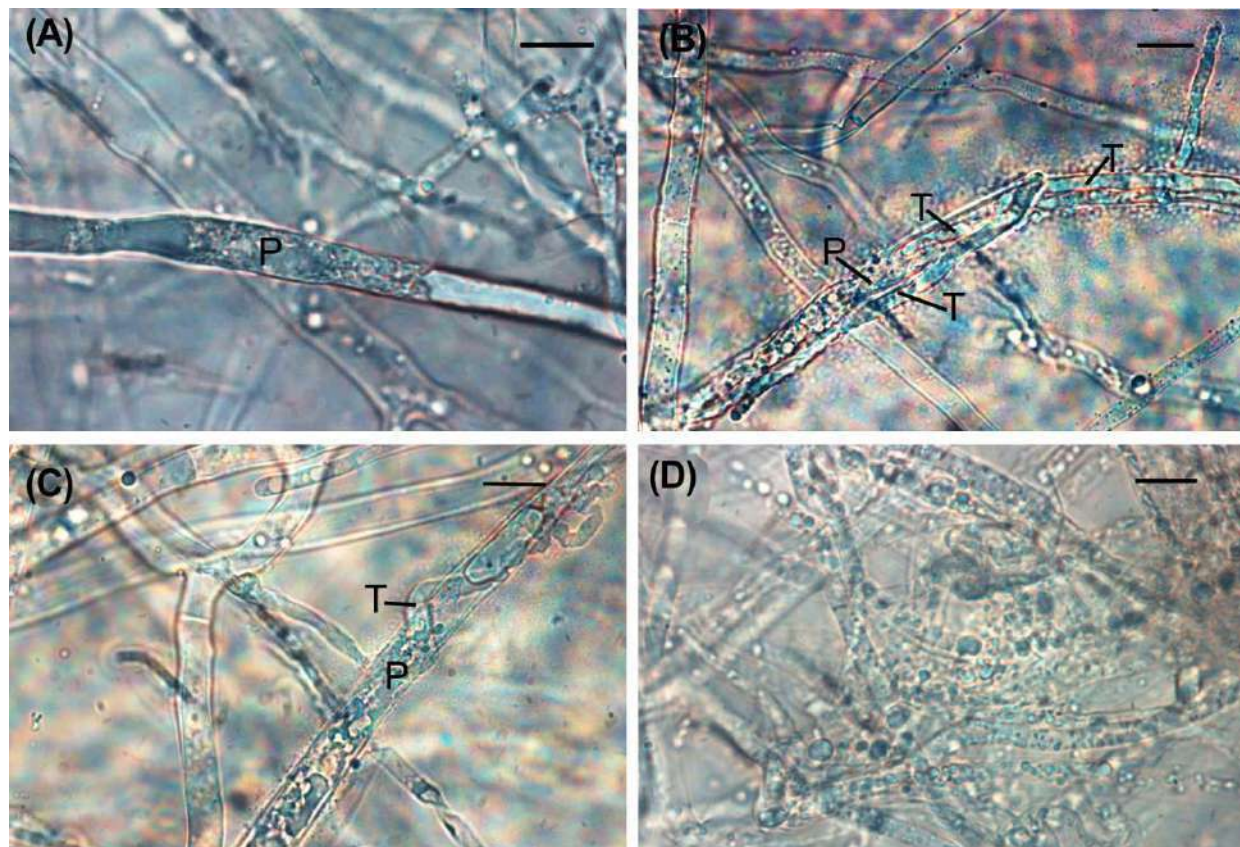
**Figure 3-7. Antagonism of *T. virens* HZA14 against *P. capsici* HZ07 in a collapsed interaction region after hyphae of *T. virens* overgrowing the colony of *P. capsici*.** A, A partially killed hypha of *P. capsici* (P). B, A hypha of *T. virens* (T) around disintegrated hypha of *P. capsici* (P). C, A hypha of *T. virens* (T) encircling a disintegrated hypha of *P. capsici*. D, Lots of disintegrated hypha of *P. capsici*. Scale bars = 10 μm.

### 3.3.2 Purification of active metabolites

Based on the results of inhibitory activity, potentially active compounds produced by *T. virens* HZA14 were extracted using ethyl acetate (Figure 3-8). The crude extract color of yellow and with weight 0.88 g had obtained. The TLC plates results exhibited that the crude extract contains separate to four fractions (A, B, C and D) (Figure 3-8A). Different amounts of factions, A, B, C and D were recovered. The activity tests using agar well diffusion method showed that among 4 fractions only fraction C dissolved in DMSO had the strong inhibitory activity against hyphal growth of *P. capsici* (Figure 3-8B). The fraction C was purified and collected with a RP-HPLC instrument (Figure 3-8C) for analyzed by the mass spectrometer.
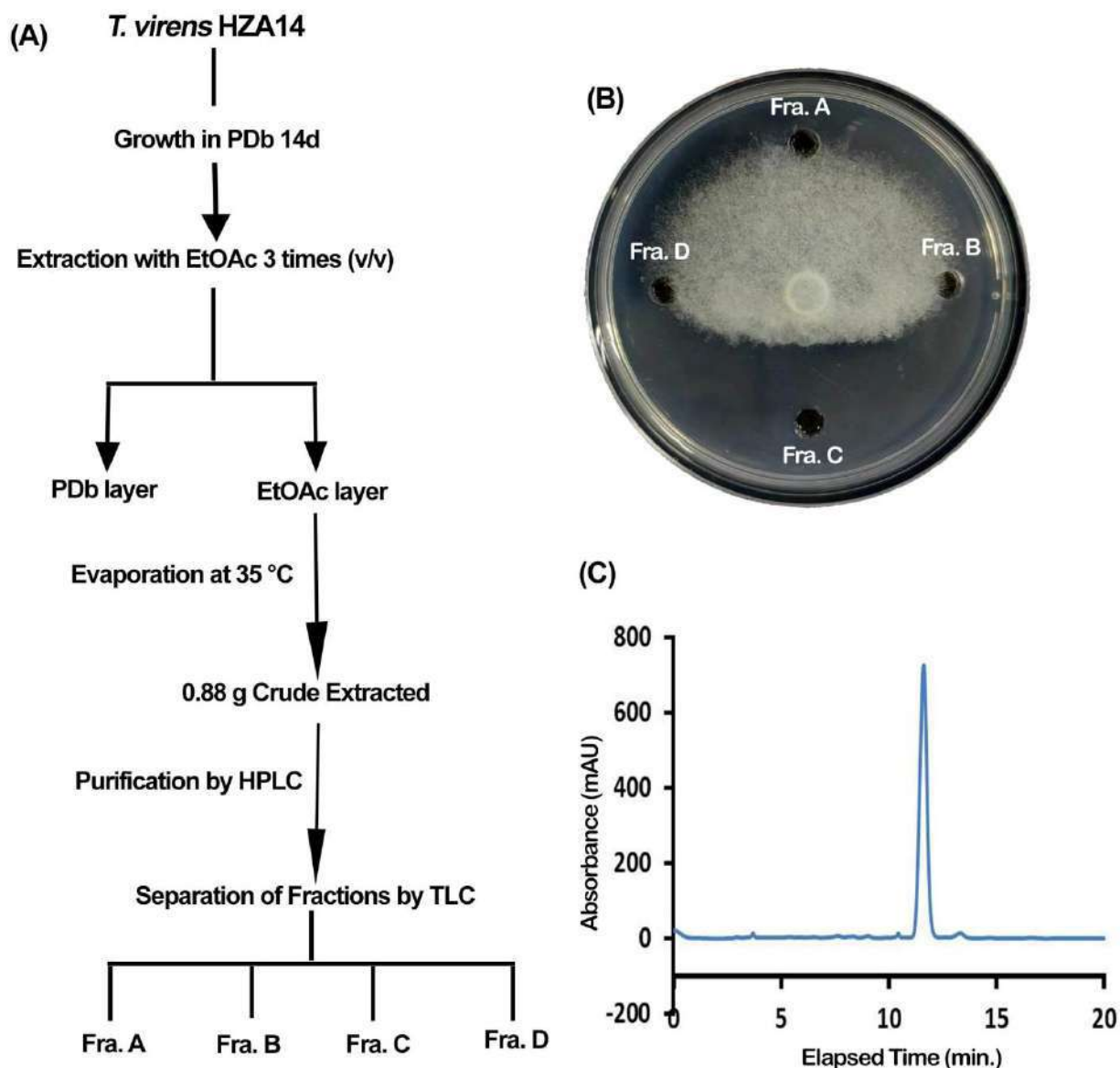
**Figure 3-8. Extraction, separation, bioactivity test, and purification of bioactive fraction of *T. virens* HZA14.**
A, Schematic diagram of extraction procedure for obtaining crude extracts and separate to four fractions (A, B, C and D) using TLC of *T. virens* HZA14. B, An anti-*Phytophthora* activity for the C fraction dissolved in DMSO against hypha growth of *P. capsici*. C, Great peak of fraction C purified using RP-HPLC.

### 3.3.3 Identification of C Fraction

Fullscan MS showed a ion at m/z 349 corresponding to the sodium adduct of gliotoxin [M + Na]$^+$ (Figure 3-9), which produced its single major daughter ion at m/z 263 corresponding to the dethiogliotoxin [M-2S]$^+$, as reported in previous MS studies of gliotoxin by electronic impact

mass spectrometry (Bose et al., 1968; Grovel et al., 2002). The isotopic distribution of this daughter ion confirmed a lack of two sulphur atoms in its composition (Bose et al., 1968).

The ions at m/z 245 correlated to [M−2S−H2O]$^+$ (Grovel et al., 2002), being attributable to a fragmentation of the daughter ions of the m/z 285 ion (Svahn et al., 2012). Subsequently, the activity test using purified gliotoxin was conducted on the plates containing V8 media (Figure 3-10). The activity tests showed that 0.5 μg/ml of gliotoxin inhibited in 40% mycelial growth after incubation for 4 days, 1.0 μg/ml in 66%, while 5.0 μg/ml and more completely inhibited the pathogen growth.
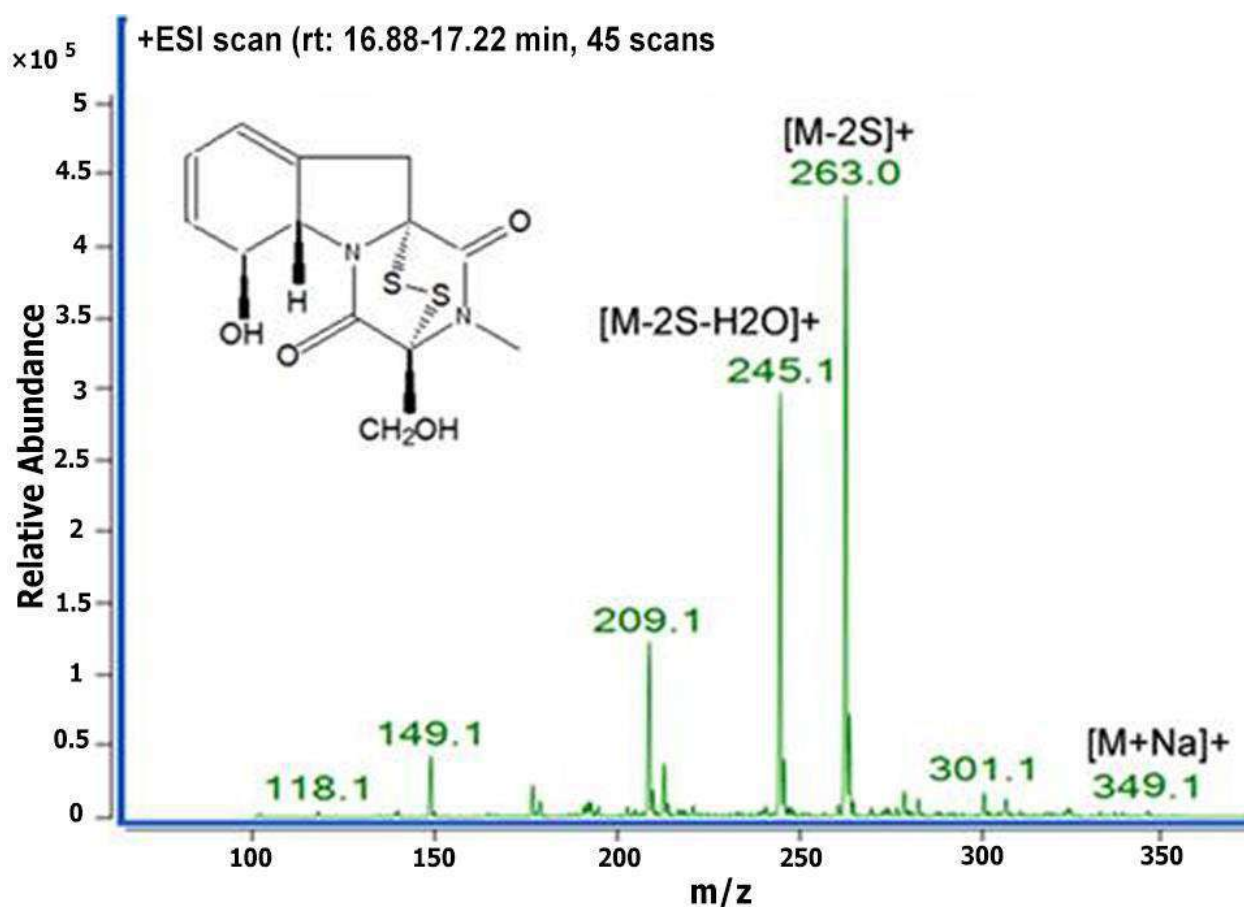


**Figure 3-9. Fullscan mass spectrum of fraction C. MS spectrum of fraction C showing loss of the two sulphur atoms leading to dethiogliotoxin at m/z 263.**
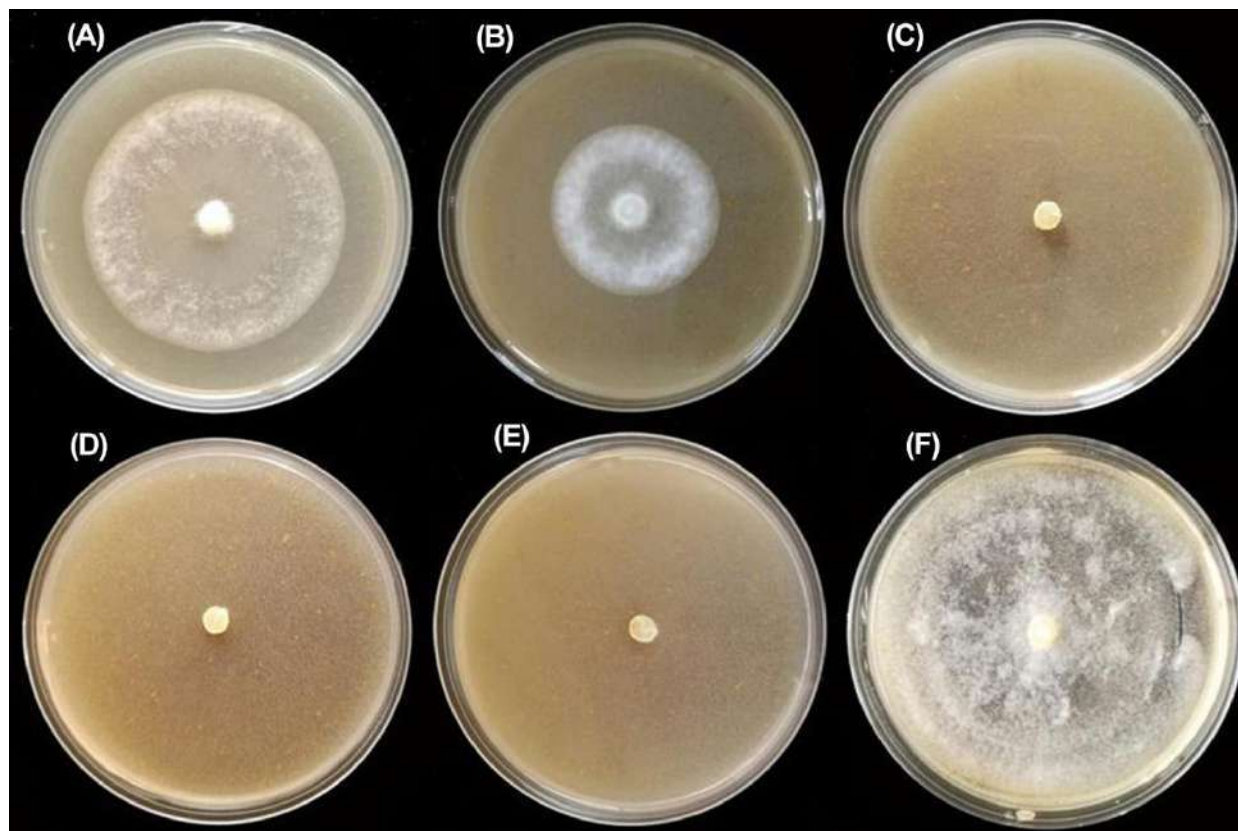
**Figure 3-10. The gliotoxin activity against hyphal growth of *P. capsici* on V8 medium plates with different concentrations of gliotoxin.** A, 0.5 µg/ml. B, 1.0 µg/ml. C, 5.0 µg/ml. D, 10.0 µg/ml. E, 15.0 µg/ml. F, Control.

### 3.3.4 Ultrastructure morphology changes in hyphal *P. capsici* caused by gliotoxin

In order to understand the effect of gliotoxin in suppression growth of *P. capsici* at low concentrations, mycelia of *P. capsici* were treated by gliotoxin at a concentration of 5.0 µg/ml for 6 and 12 h. A transmission electron microscopy analysis exhibited that the hyphae of *P. capsici* which exposed of gliotoxin had characterized by clearly structural changes depending to period of exposed (Figure 3-11). TEM analysis showed that the hyphae untreated with gliotoxin characterized by intact cellular structures, starting of the intact cell walls, membranes, nuclei, mitochondria, vacuoles (Figure 3-11A). That the exposure to 5.0 µg/ml of gliotoxin for 6 h caused marked alterations of the hyphal cells including to perforates on the cell wall which extending to the cell protoplast and disruption of parts of intracellular cytoplasm. Though lipid droplets and vacuoles were visible but, the nuclei and mitochondria had collapsed (Figure 3-11B). The 12 h of exposure by 5.0 µg/ml of gliotoxin had caused prominent changes including, perforates number had great increased to include most of cell wall, degrading of plasma lemma

and separated from the outer cell envelope, cytoplasmolysis by completely, led to collapsed each of nuclei, mitochondria, lipid droplets and vacuoles (Figure 3-11C). These results may indicate to mechanism of gliotoxin in its anti-*Phytophthora* activity.
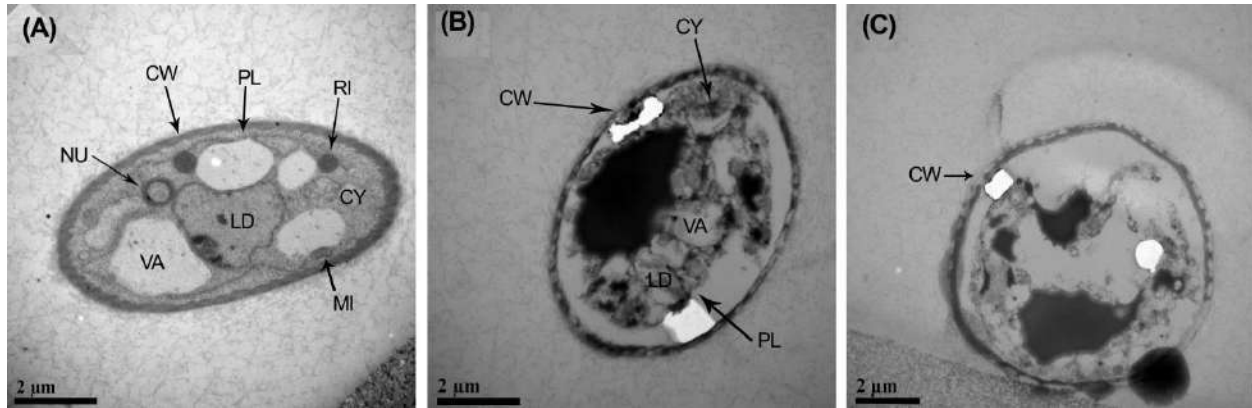


**Figure 3-11. Transmission electron microscopy analysis to hyphae cells of *P. capsici* exposed to gliotoxin.** A, Cross section of hyphae unexposed to gliotoxin. B, Cross section of hyphae treated to 5.0 μg/ml of gliotoxin for 6 h. C, Cross section of hyphae treated to 5.0 μg/ml of gliotoxin for 12 h. NU, nucleus; CW, cell wall; PL, plasma lemma; VA, vacuoles; LD, lipid droplets; RI, Ribosomes; CY, Cytoplasm MI, mitochondria. Bar = 2 μm.

### 3.3.5 Inhibitory efficacy against chili pepper blight

Inoculation tests showed that the *T. virens* HZA14 was able to delay disease occurrence and significantly reduced the disease incidence and severity. Five days after inoculation, dark brown lesions were observed on stem bases of few seedlings treated only with the zoospores suspension of *P. capsici* (control). Ten days after inoculation, symptoms of leaf wilting were observed in control plants but no symptom was found in plants coinoculated with the HZA14 isolate and zoospores suspension. However, typical symptoms appeared on stem bases of plants coinoculated with the HZA14 and zoospores suspension 12 days after inoculation. Fourteen days after inoculation, the lesion extension was obvious on stem bases of plants coinoculated with the HZA14 and zoospores suspension (Figure 3-12A).

During this period, wilt and damping-off occurred seriously on control plants (Figure 3-12B). Fifteen days after inoculation, the disease incidence and disease severity on plants coinoculated with *T. virens* HZA14 and zoospores suspension were 29.84±2.6% and 14.18±0.6%, respectively, compared with control with 92.48±2.1% DI and 88.38±2.9% DS, respectively (Figure 3-12C). The HZA14 significantly decreased the disease incidence (62.64%) and severity (64.2%), respectively.
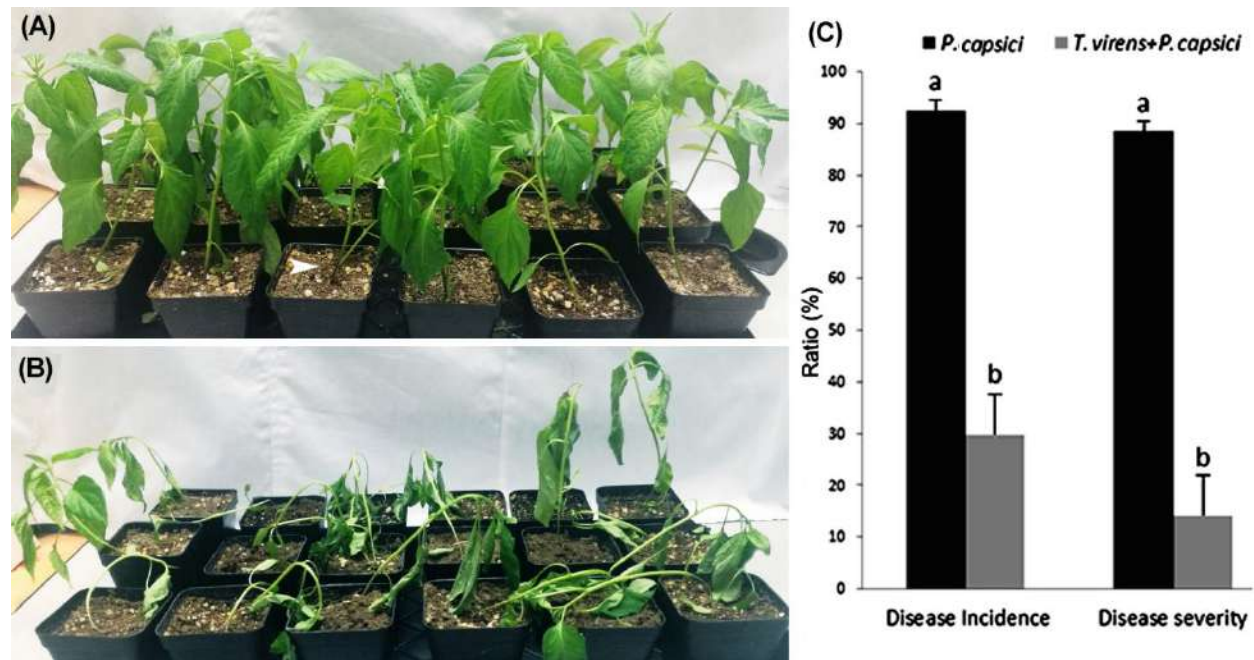
**Figure 3-12. Effect of inoculation with *T. virens* HZA14 on the disease incidence and severity of chili pepper blight 14 days after inoculation.** A–B. Disease symptoms 14 days after inoculation. A, Coinoculation with isolate HZA14 and zoospores suspension of *P. capsici*. The lesions spread upward (arrow). B, Inoculation with zoospores suspension (control). C, Disease incidence and severity 15 days after inoculation.

## 3.4 Discussion

Blight disease caused by the soil borne plant pathogen *P. capsici* is a destructive disease of pepper crop in China and worldwide. This disease is a major problem in pepper crop where, causing up to 100% yield loss in warm and humid environmental conditions (Foster and Hausbeck, 2010). Some of *Trichoderma* spp. is biocontrol agents efficient which often exhibit kinds of direct and indirect mechanisms of biocontrol against *P. capsici* (Bae et al., 2016; Segarra et al., 2013). Our results showed that *T. virens* HZA14 had high antagonistic activities against the mycelial growth of *P. capsici*, especially it caused a distinct interaction zone of hyphal disappearance of *P. capsici* HZ07 (Figure 3-6). This was considered to be related to its metabolites.

A few studies have showed that in interaction between mycoparasites and plant pathogens, interaction zone of hyphal disappearance are not observed (Cao et al., 2009). Although *T. virens* HZA14 possesses mycoparasitism, as showed in the Figure 3-7B and 3-7C, rapid colony disintegration is distinctly related to another mechanism. Microscopic observations demonstrated that a partially killed hypha of *P. capsici* could be related to antagonistic compounds produced

by *T. virens* in the interaction zone of *P. capsici* hyphal disappearance (Figure 3-7A). Chemical structure of an active fraction obtained from the culture liquid was identified as gliotoxin. Gliotoxin produced by *T. viride* has been known since it was discovered by Brian (1944).

Gliotoxin exhibits a wide variety of biological effects including anti-viral, anti-bacterial and immunosuppressive properties (Hebbar and Lumsden, 1999; Niide et al., 2006). Production of gliotoxin by *T. virens* has been proposed as an important component in antibiosis (Fravel, 1988). Gliotoxin has also been reported to act synergistically with chitinase in the antifungal activities of *T. virens* (Di Pietro et al., 1993). Similarly, the isolates producing gliotoxin were more effective in seed treatments for controlling diseases caused by *R. solani* (Howell et al., 1993). These studies showed that gliotoxin may play an important role in reducing pathogen development and disease occurrence, while this study charactered relationship of gliotoxin with formation of interaction zone of pathogen hyphal disappearance for first time and revealed its antioomycetes activity. Bioactivity of gliotoxin produced by the HZA14 against hyphal growth of *P. capsici* was very high in *in vitro* tests on PDA. Effects of gliotoxin in hyphal cells of *Sclerotia rolfsii* have been studied (Hua et al., 2021). However, the mechanism of impact gliotoxin in ultrastructure of *P. capsici* has not been detected in the previous studies. we detected the clear changes in the hyphal cells of *P. capsici* treated with gliotoxin including, perforating most of cell wall, cytoplasmolysis by completely, and collapse each of nuclei, mitochondria, lipid droplets and vacuoles. These details provided action mode of gliotoxin in killing the *P. capsici* hyphae. *In vivo* inoculation tests showed that the HZA14 isolate was able to delay disease occurrence and significantly reduce disease incidence and severity by 62.64% and 64.20%, respectively. Inhibitory role of the HZA14 against pathogen also involves in other mechanisms of action. A great number of studies showed that *Trichoderma* spp. can inhibit pathogens and reduce diseases possess by a wide range of mechanisms, including mycoparasitism, production of antagonistic compounds and extracellular enzymes such as amylase, cellulase, chitinase pectinase and protease as well as the  induced resistance (Atanasova et al., 2013; Cherkupally et al., 2017; Vargas et al., 2014).

As showed in Figure 3-6, the antagonistic *Trichoderma* spp. isolates colonized and degraded the colony growth of pathogen by means of penetration and encirclement (Figures 3-7C and 3-7D), obviously being associated with the mechanism of mycoparasitism involving in production of extracellularly lytic enzymes.

Thus the *T. virens* HZA14 possibly uses multiple mechanisms of action to synergistically inhibit pathogen, while gliotoxin produced by it could play an important role in inhibiting pathogen and controlling chili pepper blight. Our data indicate that the *T. virens* HZA14 and the gliotoxins that it produces have a great potential using as candidate biocontrol agent. However, its biocontrol efficacy needs to be confirmed under the field condition for generating useful products for management of pathogens in the agroecosystem. Further researches need focus on its control efficacy in the fields for development of biocontrol agent.

### 3.5 Conclusions

Here, identification of the best *Trichoderma* isolates as anti-*Phytophthora* has beed resulted. Where, *T. virens* HZA14 had been exhibited high active in inhibition *P. capsici in vitro* through detected of production of gliotoxin compound. We concluded that the *T. virens* HZA14 isolate belong to the Q strains of *T. virens*. We found that the gliotoxin produced from HZA14 isolate suppressed the *P. capsici* growth by low concentrations (5.0 μg/ml). Mechanism-gliotoxin in effecting to cells hyphal of *P. capsici* had by holeings of cell wall extending to inter the cell, degrading of membrane and separated from the outer cell envelope, collapsing and vanishing of cytoplasm, losing each of ribosome, nuclei, and lipid droplets. Intriguingly, cytotoxic influence of *Trichoderma*-gliotoxin on the clees and hyphal of *P. capsici* was reflected *in vivo* through protection chili pepper seedlings of infection by *P. capsici*. The obtained HZA14 isolate could be considered as successful alternative to chemical used in chili pepper blight disease control.

# Chapter 4

# Identification of *Trichoderma virens* genes responsible for microsclerotia degrading and control on *Verticillium* wilt disease in eggplant

## 4.1 Introduction

*Verticillium dahliae,* being a fungus belongs to the ascomycetes class, and a soil-borne pathogen that infects many vascular plants and causes the destructive diseases called the *Verticillium* wilt disease (Fradin and Thomma, 2006). *Verticillium* wilt disease of eggplant caused by *V. dahliae* leads to severe losses of eggplant in quantity and the quality in Zhejiang province. It is not easy to control because of the production of microsclerotia as the primary inoculum, which survive for more than 10 year in soil of the host plant absence (Wilhelm, 1955). Meanwhile, microsclerotia have thickened cell wall and melanin deposition that are resistant to some extreme environmental conditions such as UV irradiation, cold temperatures, enzymatic lysis as well as resistant to desiccation (Bell and Wheeler, 1986; Wheeler et al., 1978). Moreover, the completely resistant varieties are absent in production, crop rotation is limited due to limited cultivation and there is no registered fungicide available for this disease, leading to the disease occurrence annually.

To control this disease, most researches focus on biological control for *Verticillium* wilt of eggplant. This is due to environmentally friendly biocontrol agents having many advantages. *Trichoderma* species topped the list of biocontrol fungi that are used as biocontrol agents because the *Trichoderma* spp. possess many antagonistic mechanisms such as mycoparasitism and competition of spaces and nutrients (Harman et al., 2004). Apart from that, they also release active secondary metabolites against several plant pathogens as well as fungus cell wall-degrading enzymes (CWDEs) such as proteases, glucanases and chitinases (Chang and Stewart, 1998; Tronsmo, 1991). Specially, high levels of hydrolytic enzymes produced by *Trichoderma* spp. may cause microsclerotial degradation of *V. dahliae,* being involved in the expression of related genes. Recently, a lot of active genes have been identified from expressed-sequence-tag (EST) libraries of different *Trichoderma* strains attained under diverse stress conditions (Vizcaíno et al., 2007).

The use of EST analysis has been widespread in cDNA sequencing initiatives aimed at discovering new genes, studying gene expression patterns, and identifying genes that are differentially regulated, where the first EST libraries of *Trichoderma* were constructed from *T. reesei* QM6a to identify genes involved in biomass-degrading enzymes through cDNA clones (Diener et al., 2004). While the first EST study in a *T. harzianum* biocontrol species was carried out to investigate about the biocontrol process, its molecular mechanism and differentially expressed genes at mycelium stage (Liu and Yang, 2005). Transcriptome results showed when analyzing the gene expression changes during three stages of the *T. virens* mycoparasitic interaction with *R. solani*, the genes for biosynthesis of gliotoxin were involved (Atanasova et al., 2013). On the other hand, the result of this study demonstrated the involvement of the *Tvbgn3* gene (β-1, 6-glucanase-encoding) in mycoparasitism of *T. virens* against *P. ultimum* and its role in the biocontrol activity of *T. virens* (Djonovic et al., 2006). Furthermore, the co-overexpression of two b-glucanases (*Bgn2* and *Bgn3* genes) improved biocontrol effect of *T. virens* against *R. solani*, *P. ultimum*, and *Rhizopus oryzae* (Djonović et al., 2007). Besides, the active role of a laccase gene of *T. virens* during mycoparasitism on sclerotia of the plant pathogenic fungi *S. sclerotiorum* and *B. cinerea* was suggested (Catalano et al., 2011).

The aim of this study was to screen the *Trichoderma* isolates with high activity against hypha and microsclerotia of *V. dahliae* and reducing the *Verticillium* wilt disease of eggplant. Furthermore, the *Trichoderma* isolates with high activity were used for analysis of transcriptomes associated with hyperparasitism mechanism of hyphae of *Trichoderma* isolates interactions with microsclerotia of *V. dahliae*. The expression of enzyme-coding genes related to microsclerotial degradation was revealed by transcriptomics analysis and confirmed by the quantitative reverse transcription PCR (qRT-PCR).

**4.2 Materials and Methods**

**4.2.1 Fungal materials**

Fifteen *Trichoderma* isolates stored at -20°C in a 10% glycerol solution were used, including *T. atroviride* HZA1, *T. atroviride* HZA2 *T. afroharzianum* HZA3, *T. brevicompactum* HZA4, *T. dorothopsis* HZA5, *T. koningiopsis* HZA6, *T. brevicompactum* HZA7, *T. dorothopsis* HZA8, *T. citrinoviride* HZA9, *T. asperellum* HZA10, *T. harzianum* HZA11, *T. brevicompactum* HZA12, *T. atroviride* HZA13, *T. virens* HZA14, *T. dorothopsis* HZA15. The high aggressive phytopathogenic isolate H6 of *V. dahliae* was obtained from Plant Pathology Department, Agriculture and Biotechnology College, Zhejiang University, China (Sun et al., 2016). All the fungi isolates were cultured on the plates containing PDA at 25°C for five days for *Trichoderma* isolates and 14 days for *V. dahliae* isolate.

**4.2.2 Screening of *Trichoderma* isolates with antagonistic activity against *V. dahliae***

The potential *Trichoderma* isolates with high antagonistic activity were screened against *V. dahliae* in PDA medium. Fifteen *Trichoderma* isolates was screened by a dual culture method, as described by Morán-Diez et al. (2019) with slight modifications. In brief, mycelial discs (0.5-cm diameter) from *V. dahliae* isolate grown for 14 days on PDA at 20°C was transferred to one side of a plate containing PDA, and after the plate was incubated for three days, another mycelial discs (5-mm diameter) from *Trichoderma* isolate grown on PDA at 25°C for seven days was placed 1.5 cm apart on the same PDA plate. All plates were incubated at 23°C in darkness for 15 days and each treatment for each *Trichoderma* isolate was replicated three times. The growths of the pathogen *V. dahliae* and *Trichoderma* isolates were observed, and their antagonistic activities were evaluated according to the antagonism scale from class 1 to class 5 (Jiang et al., 2016a), Calss 1: *Trichoderma* grew on at the entire surface of the medium and covered the pathogen; Calss 2: *Trichoderma* grew on 2/3 of the medium and the pathogen grew on the last third; Calss 3: *Trichoderma* grew on 1/2 of the medium and the pathogen grew on the second half; Calss 4: pathogen grew on 2/3 of the medium and *Trichoderma* grew on at last-third; Calss 5: pathogen grew on the whole medium and covered the *Trichoderma*.

**4.2.3 Culture filtrate activity produced by *Trichoderma* isolates against *V. dahliae***

The six 0.5-cm-diameter discs for each *Trichoderma* isolate grown in PDA at 25°C for five days were placed into a 250-ml conical flask containing PD broth of 100 ml, and the flasks were incubated in a ZWY-211B rotary shaker at 150 rpm at 25°C for 14 days. After incubation, the partial liquid was filtered using cheesecloth, centrifuged at 6000 rpm for 5 min at 4°C, and the supernatant was filtered through Millipore filter paper of 0.22 μm diameter.

The bioactivity of culture filtrate against hyphal growth of the pathogen *V. dahliae* was evaluated using the poisoned food method. The 1.0 ml of culture filtrate with concentrations of 0, 25%, 50%, and 100% were mixed with 9 ml of PDA in a plate. After medium solidification, a 5-mm mycelial disc from a *V. dahliae* isolate grown for 14 days was placed onto the centre of a plate containing PDA and incubated at 23°C for 10 days. To determine the extent of inhibition of radial mycelial growth, a formula $[(V-T)/V] \times 100$ was employed, which involved calculating the percentage difference between the growth observed in the control (V) and the growth observed in the treatment (T) (Abuduaini et al., 2021). The well diffusion assay was performed for the evaluation of culture filtrate in the inhibition of the conidia germination of *V. dahliae*. 0.5 ml of fungal spore suspension ($10^6$ conidia/ml) was spread onto the surface of PDA in a plate after drying in a fume hood. Wells of 0.3 cm diameter were prepared in the centre of the plates using a sterilised stainless steel cork borer. The 30 μl of culture filtrates at 25%, 50%, and 100% were added to a well, respectively, and incubated at 23°C for three days. The diameters of inhibition zones around the wells were measured. Each treatment had three repeats, and no culture filtrate treatment was used as a control.

**4.2.4 Detection of siderophore and 3-indoleacetic acid (IAA) production**

A chrome azurol sulphonate (CAS) agar plate as described by Milagres et al. (1999) with slight modifications was used to evaluate ability of *Trichoderma* isolate to produce siderophore.

To prepare the CAS-blue agar medium, a series of steps were followed. Initially, 60.5 mg of CAS was dissolved in 50 ml of distilled, deionized water. Then, 10 ml of iron (III) solution (consisting of 1 mM $FeCl \cdot 6H_2O$ and 10 mM HCl) was added to the CAS solution. This mixture was slowly added to 72.9 mg of HDTMA, which was previously dissolved in 40 ml of water and stirred well. The resulting solution was dark blue in color and was autoclaved at 121°C for 25 min. In a separate container, another mixture was formed by combining 750 ml of water, 15 g of

agar, 30.24 g of pipes, and 12 g of a 50% (w/w) NaOH solution to adjust the pH to the pKa of pipes, which are 6.8. Finally, the dye solution was carefully poured along the glass wall of the container and agitated gently to avoid foaming (Schwyn and Neilands, 1987). Petri dishes plate of 10 cm divided into halves were prepared, the PDA poured in the first half and CAS-blue agar poured in the second half to be at the same level as the first half. A disc (0.5 cm diameter) from *Trichoderma* isolate grown for five days was inoculated onto the center of PDA side. The plates were incubated at 27°C. The color change was monitored in the second half after 14 days.

The potential of IAA production by *Trichoderma* isolate was analyzed using the Salkowski reagent described by (Glickmann and Dessaux, 1995). Five mycelial discs (5 mm) from 4-old days colony were put in a conical flask comprising of 100 ml PD broth added with 1.5 % of L-tryptophan, while treatments were used for PD broth as control and then incubated in a ZWY-211B rotary shaker at 150 rpm at 25°C in the darkness for 5, 10 and 15 days, respectively. The part liquid was filtered using cheesecloth, centrifuged at 6000 rpm for 5 min. at 4°C and then the supernatant was filtered through Millipore filter paper of 0.22 μm diameters. The supernatant was adjusted to pH 7 using 1 N NaOH. To determine IAA production, Salkowski reagent  was prepared (150 ml of $HClO_4$, 250 ml of $ddH_2O$, and 7.5 ml of 0.5 M $FeCl_3 \cdot 6H_2O$) and 2 ml from Salkowski reagent solution was mixed with 1 ml bacterial supernatant in a test tube (Gravel et al., 2007). The tubes were incubated in darkness at 25°C for 30 min and observed for the development of pink color compared with the control. The absorbance was measured at a wavelength of 530 nm using a UV–Vis spectrophotometer (Perkin Elmer Lambda 35, Waltham, MA, US). A standard curve was made from 1-100 μg/ml of commercial IAA (Sigma-Aldrich) solution in PD broth for a measure of the concentration of IAA in the *Trichoderma* isolate supernatant as μg/ml for both of period time incubation.

### 4.2.5 Preparation of fungal inoculations

The inoculum of *Trichoderma* isolate was prepared by culture in flasks containing boiled wheat grains autoclaved two times at 121°C for 2 h. The flasks were incubated at 25ºC with a 12/12 h photoperiod for 15 days. The conidia suspension was prepared by putting grains with conidia into sterile water, shaking well and filtrating by four layers of sterile cheesecloth (Zhang et al., 2013). The concentration of conidia suspension was adjusted using the hemacytometer. For preparing *V. dahliae* microsclerotia, the discs with pathogen hyphae were put onto a plate

containing a sterile, modified basal agar medium covered by a sterile cellophane membrane, a total of 20 plates were prepared and they were incubated at 20°C for 25 days in the darkness (Hu et al., 2013). The black microsclerotia were scraped using the sterile blade and were added to 200 ml water tap before mixed by blender. The resulting suspension was purified using a series of 125, 74, and 20 μm sieves (Atibalentja and Eastburn, 1997). The microsclerotia from the 20 μm sieve were washed two times in tap water and transferred to sterile water and centrifuged at 4000 rpm for 5 min. To kill mycelia and conidia, the tubes with microsclerotia were put in the water bath at 47°C for 5 min (Nelson and Wilhelm, 1958). Microsclerotia were suspended in sterile water and counted using Hemacytometer.

### 4.2.6 Greenhouse experiment

Effectiveness of the *Trichoderma* isolates in reducing the *Verticillium* wilt disease caused by a phytopathogenic *V. dahliae* was assessed on the eggplant seedlings. The field soil mixed with peat: vermiculite: sand (ratio of 3:1:1) was autoclaved, and conidia of *Trichoderma* isolates selected and microsclerotia of *V. dahliae* were prepared. The sterile soil was mixed with the microsclerotia and conidia 10, 20, and 30 days before sowing with final concentrations $1 \times 10^7$conidia g$^{-1}$ for *Trichoderma* isolates and 20 microsclerotia g$^{-1}$ for *V. dahliae* in soil, respectively (Angelopoulou et al., 2014; Mirmajlessi et al., 2016). No microsclerotial soil was used as control. The pots were filled with the soil and a susceptible variety of eggplant plants seeds from Hangzhou Academy of Agricultural Science (cv. Zheqie-3) were washed many times with sterile water after sterilizing with a 2% clorox solution for 2–3 min. The seeds were then planted into pots and subjected to four different time periods before being moved under controlled conditions of 75% humidity and temperatures ranging from 22-28°C. Experimental treatments were carried out in triplicate. Disease severity and control efficacy were assessed when the death of some plants appears in the control treatment (Lan et al., 2017). Assessment of disease severity was applied the following rating scale: 0 = no diseased leaf; 1 = <10%; 3 = 11–25%; 5 = 26–50%; 7 = >50%; 9; plant killed (Lan et al., 2017).

$$\textbf{Disease index} = \sum \frac{\text{(number of leaves with every scale} \times \text{disease severity score)}}{\text{(the total number of leaves examined} \times \text{the highest severity score)}} \times 100\%$$

$$\textbf{Control efficacy} = \frac{\text{(the mean disease index of control} - \text{the mean disease index of treatment)}}{\text{(the mean disease index of the control)}} \times 100\%$$

**4.2.7 Plant growth promotion (PGP) assay**

The potency of the *Trichoderma* isolate to improve plant growth was studied on eggplant seedlings. The seeds of cv. Zheqie-3 were sown into the pots filled with the mixed soil (as detailed in 4.2.6) with $1 \times 10^7$conidia g$^{-1}$ for *Trichoderma* isolate. No microsclerotial soil was utilized as a comparison treatment. Experimental treatments (twenty pots) had in triplicate. The pots were returned to the same controlled conditions as detailed in 4.2.6. The PGP potential of the isolate HZA14 was assessed by computing the seedlings heigh, the length of the taproots, and fresh and dry weights after 30 days from sowing. The dry weights were calculated after seedling organs were dried for 2 days at dry heat 65°C. The formula PGPE% = [(treatment – control)/control] × 100% was followed to calculate growth promotion efficacy.

**4.2.8 RNA extraction and purification**

The *Trichoderma* isolates with degradating microsclerotia of *V. dahliae* were selected and used for transcriptome analysis. A mycelial disc from *V. dahliae* isolate was transferred to one side of a plate containing PDA, and after the plate was incubated for three days, another mycelial disc from selected *Trichoderma* isolate grown on PDA at 25°C was placed 1.5 cm apart on the same PDA plate. All plates were incubated at 23°C in darkness, and then interaction zones between hyphae of *Trichoderma* isolate and microsclerotia of *V. dahliae* were cut 3, 6, 9, 12, and 15 day after incubation, respectively. Each treatment had three replicates during each period of time. The harvested interaction zones were frozen in liquid nitrogen immediately. The Trizol1 method was used to extract a total RNA, as described by the manufacturer. RNA purity was checked using the kaiaoK5500®Spectrophotometer (Kaiao, Beijing, China). The RNA was frozen in liquid nitrogen for 1 hour, stored at -80°C, and delivered to Zhejiang Annoroad Biotech Ltd for transcriptome sequencing.

**4.2.9 Library preparation for RNA sequencing**

To prepare the RNA sequencing libraries, 2 μg of RNA was used as input material for each sample. The NEBNext® Ultra™ RNA Library Prep Kit for Illumina® (#E7530L, NEB, USA) was used to generate sequencing libraries following the manufacturer's instructions, with index codes added to attribute sequences to each sample. The mRNA was isolated from total RNA using poly-T oligo-attached magnetic beads, and fragmentation was carried out using divalent cations under high temperature in NEBNext First Strand Synthesis Reaction Buffer (5X).

The first strand of double stranded cDNA was synthesized via RNase H and random hexamer primer. The second strand of the cDNA synthesized using dNTPs, RNase H, DNA polymerase I and buffer. The library fragments were purified using QiaQuick PCR kits and eluted with EB buffer. Terminal repair, A-tailing, and adapter addition were performed, and the aimed products were retrieved. PCR amplification was performed to complete the library. Qubit® RNA Assay Kit in Qubit® 3.0 was then used to determine RNA concentration of the library, after that, RNA was diluted to 1 ng/µl. Agilent Bioanalyzer 2100 system (Agilent Technologies, CA, USA) was used to measure the insert size and then StepOnePlus™ Real-Time PCR System (Library valid concentration＞10 nM) was used for precisely measuring the qualified insert size. Clustering of the index-coded samples was carried out on a cobalt cluster generation system using the HiSeq PE Cluster Kit v4-cBot-HS (Illumina) according to the manufacturer's instructions. After cluster generation, the libraries were sequenced on an Illumina platform with 150 bp paired-end reads.

## 4.2.10 Filter of original data

A Perl script was utilized to filter the raw data to ensure the accuracy and reliability of the data for analysis. The script removed adapter sequences, poly-N, and low-quality bases from the raw data to obtain clean reads. Quality control measures such as Q20, Q30, GC-content, and sequence duplication level were also calculated for the processed data. Reference genomes, annotation files and regulatory function were downloaded from the ensemble database (http://www.ensembl.org/index.html).

The genome index was built using Bowtie2 v2.2.3, and the clean data was aligned to the reference genome using HISAT2 v2.1.0. (Langmead et al., 2009). The mapping results were visualized using the Integrative Genomics Viewer (IGV) and displayed as a heatmap (Thorvaldsdóttir et al., 2013). HTSeq v0.6.0 was used to count the reads for each gene in each sample, and the correlation between samples was determined (Anders et al., 2015). The expression level of each gene in each sample was estimated using Fragments per Kilobase Million Mapped Reads (FPKM), which was calculated with Cufflinks v2.0.2. The formula used for calculating FPKM is FPKM = [106*F/(NL/103)], where F represents the number of fragments assigned to a certain gene, N represents the total number of mapped reads, and L represents the length of the gene (Trapnell et al., 2012).

**4.2.11 Analysis of differential gene expression**

DESeq2 is a statistical tool used for analyzing differential gene expression between two biological samples with replicates. It is based on the negative binomial distribution theory, which assumes that count values follow this distribution. DESeq2 estimates sample-specific and gene-specific depth parameters, and uses "linear regression" for dispersion to "shrink" the variance of gene expression, taking into account the similarity of gene expression levels. It then estimates the expression level of each gene in each sample using linear regression and calculates the p-value with the Wald test. Finally, the p-value is corrected by the BH method. Genes with q≤0.05 and |log2_ratio|≥1 are considered as differentially expressed genes (DEGs).

**4.2.12 Analysis of function enrichment of gene ontology**

Gene ontology (GO) enrichment analysis was performed using the hypergeometric test to identify the biological functions of differentially expressed genes (DEGs). The p-value was calculated and adjusted to q-value, with the data background being the genes in the whole genome. GO terms with q-value less than 0.05 were considered significantly enriched. This analysis helped to reveal the potential biological processes and molecular functions associated with the DEGs. Kyoto Encyclopedia of Genes and Genomes (KEGG) enrichment analysis was also performed to identify significantly enriched pathways related to the DEGs. The p-value was adjusted by multiple comparisons to obtain q-value. KEGG terms with q-value <0.05 were considered as significantly enriched. This analysis provided insight into the metabolic pathways and biological functions associated with the DEGs.

**4.2.13 Quantitative reverse transcription PCR (qRT-PCR)**

The cell walls in filamentous fungi are mainly composed of glucan, chitin and proteins that extensively cross-linked to form a complex network, which offer the structural basis of the cell wall. In light that, we took into account six of main enzyme-coding genes potentially involved in degradation of microsclerotia, including enzymes Endochitinase A1, Endochitinase 3, endo-1,3-beta-glucanase, Alpha-N-acetylglucosaminidase, Laccase-1 and Peroxidase. All positive matched hits with e-value≥1e−15 and coverage less than 0.5 were examined manually for each enzyme in genome based on the active domains in the enzyme database (Kloepper and Schroth, 1981).

To confirm the DEGs results obtained, RT-qPCR experiments were carried out (Livak and Schmittgen, 2001). The interaction zones between hyphae of *Trichoderma* isolate and microsclerotia of *V. dahliae* were cut 3, 6, 9, 12, and 15 day after incubation, respectively, as described above. Total RNAs from the five different time periods samples were extracted by using TRIZOL® reagent (TaKaRa RNAiso Reagent 9180). Reverse transcription of total RNA to cDNA was carried out by using protocol of the TAKARA fluorescence quantitation reagent (TB Green Premix Ex Taq™ RR420A) and TAKARA reverse transcription reagent (PrimeScript™RT reagent Kit with gDNA Eraser RR047A) (TaKaRa, Otsu, Japan).

(1) Reagents and usage amounts for reverse transcription of total RNA to cDNA and genomic DNA removal reactions were applied as follows:

$5 \times$ gDNA Eraser Buffer: 2.0 μl

gDNA Eraser: 1.0 μl

Total RNA 20 reaction system <1 μg

RNase Free $H_2O$: 10 μl

The reagent-added samples were reacted at 42°C for 2 min and stored at 4°C.

(2) Reagents and amounts for the reverse transcription reaction master mix were prepared according to the amount of reaction number +1 as follows:

$5 \times$ PrimerScript Buffer 2 (for Real Time): 4.0 μl

PrimerScript RT Enzyme Mix I: 1.0 μl

RT Primer Mix: 1.0 μl

Step (1) reaction solution: 10.0 μl

RNase Free $H_2O$: 2.0 μl

The reagent-added sample was reacted at 37°C for 15 min, then reacted at 85°C for 5 sec, and finally stored at -20°C.

The six of main genes potentially involved in degradation of microsclerotia were amplified by RT-qPCR using the primer pairs designed by the PerlPrimer v1.1.20 software, and the actin gene was used as an internal reference gene to normalize gene expression.

The 25 μl of reaction system was superimposed on TB Green Premix Ex Taq TM II (Tli RNaseH Plus), both forward and reverse primers, cDNA template, and nuclease-free water. The fluorescence quantification in reaction system was used with the Takara kit instrument Bio-Rad CFX96 as follows:

PCR F-Primer (10 μmol/l): 0.4 μl.

PCR R-Primer (10 μmol/l): 0.4 μl.

cDNA: 1.0 μl.

TB Green Premix Ex Taq II: 10.0 μl.

RNase Free $H_2O$: 8.2 μl.

Reaction program pre-denaturation were at 95°C for 30 sec; 95°C for 5 sec, 60°C for 30 sec, 45 cycles; 95°C for 15 sec, 60°C for 60 sec, 95°C for 15 sec. Fluorescence quantification was assessed using Takara kit and instrument Bio-Rad CFX96 Real-Time System (Bio-Rad, USA). The results of gene expression levels were calculated and statistically analyzed using the threshold cycle ($2^{-\Delta\Delta Ct}$) method, and the data were expressed as mean ± standard deviation.

## 4.3 Result

### 4.3.1 Dual culture assay

The antagonistic activities of the *Trichoderma* isolates toward *V. dahliae* were assessed in PDA. The 15 isolates of *Trichoderma* spp. were determined by the dual plate way on PDA media. All tested isolates exhibited different degree of antagonistic activity (Figure 4-13). Of the 15 isolates, isolate HZA14 showed the highest strong activity against *V. dahliae*, reaching to class I. Colonies of pathogen were completely covered by hyphae of isolate HZA14 on the PDA plate (Figure 4-13N), and its microsclerotia disappeared. By comparison, isolates of HZA1, HZA2, HZA10, HZA11, HZA12, and HZA13 showed higher antagonistic activity belonging to class II (Figure 4-13). The isolates of HZA3, HZA4, HZA5, HZA6, HZA7, HZA8, and HZA15 indicated slightly antagonistic activity, being divided into class III (Figure 4-13).
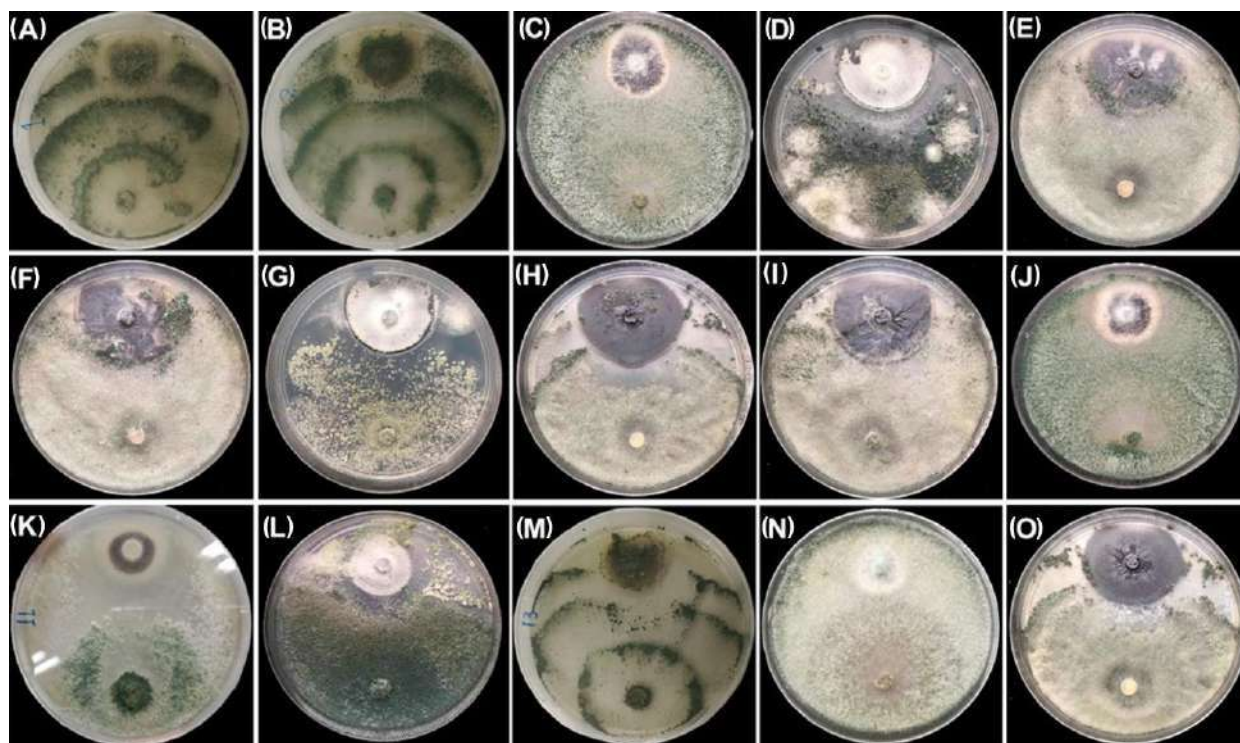


**Figure 4-13. Antagonistic activity of fifteen *Trichoderma* isolates against *V. dahliae* on PDA at 23°C for 15 days.** A, HZA1. B, HZA2. C, HZA3. D, HZA4. E, HZA5. F, HZA6. G, HZA7. H, HZA8. I, HZA9. J, HZA10. K, HZA11. L, HZA12. M, HZA13. N, HZA14. O, HZA15.

**4.3.2 Effect of culture filtrates of *Trichoderma* isolates on mycelial growth and conidial germination of *V. dahliae*.**

The activity of culture filtrates produced by *Trichoderma* isolates against the mycelial growth of *V. dahliae* was assessed. The plates containing culture filtrates of different concentrations were prepared. Among the 15 isolates, only isolate HZA14 showed significant inhibition of mycelial growth of *V. dahliae* in different dilutions (Figure 4-14A), and had complete growth inhibition at culture filtrate concentration of the 100%, following by 50% and 25%. To evaluate activity of culture filtrates against inhibition of conidia germination, wells diffusion assay was performed. Only inhibition zone with the culture filtrate produced by isolate HZA14 was the largest one at concentration of 100% (Figure 4-14B) and among inhibition zone diameters, there was significant difference ($p < 0.05$) (Table 4-3).
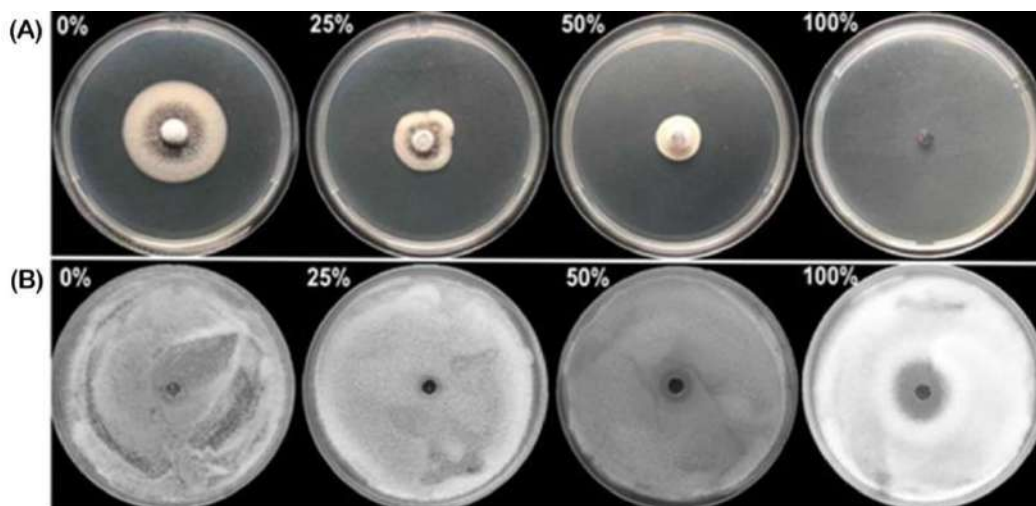


**Figure 4-14. The activities of culture filtrate produced by *T. virens* HZA14 against *V. dahliae*.** A, Percent inhibition of mycelial growth of the *V. dahliae* at the diluted concentration of 0, 25%, 50%, and 100%. B, Percent inhibition of conidia germination of *V. dahliae* at the diluted concentration of 0, 25%, 50%, and 100%.

**Table 4-3. Effect of culture filtrates produced by isolate HZA14 on mycelial growth and conidia germination of *V. dahliae*.**

| Concentration of CF | PIRMG (%) | IZD (mm) |
|---|---|---|
| 100% | 100.00±0.0 [a] | 10.13±0.3 [a] |
| 50% | 65.51±8.9 [b] | 3.49±0.1 [b] |
| 25% | 50.71±2.9 [c] | 1.48±0.1 [c] |
| 0 | ---------- | 0.00±0.0 [d] |

CF: culture filtrate; PIRMG: Percentage inhibition of radial mycelial growth; IZD: Inhibition zone diameters. Value are means ± standard deviations of three replicates, and the different lowercase letters in the same column are significantly different at p 0.05 according to LSD test.

### 4.3.3 Assessment of siderophore and IAA production

The CAS assay in solid medium, only tested *T. virens* HZA14 isolate showed a positive result with capability to produce siderophores. There was no color change before. The HZA14 isolate grow on the plate-half containing PDA for 3 days (Figure 4-15A), but visible orange halos on CAS media appeared when its hyphae grow on the surface of CAS media (Figure 4-15B), showing ability of the *T. virens* HZA14 to produce siderophores. For assessing ability to IAA, the *T. virens* HZA14 were cultured in PD broth with tryptophan. The pink color change was found from five days to 15 days after culture supernatants obtained from different culture times were mixed with the Salkowski's reagent, respectively, indicating that the *T. virens* HZA14 had ability to produce IAA color (Figure 4-15C). To quantify the IAA, IAA concentrations were determined. Maximum concentration was 218.61±1.96 μg/ml 15 day after incubation, following by 112.87±1.74 μg/ml for five days and 138.48±1.45 μg/ml for ten days, respectively (Figure 4-15D). This also showed that IAA content produced by the *T. virens* HZA14 was related to culture times.
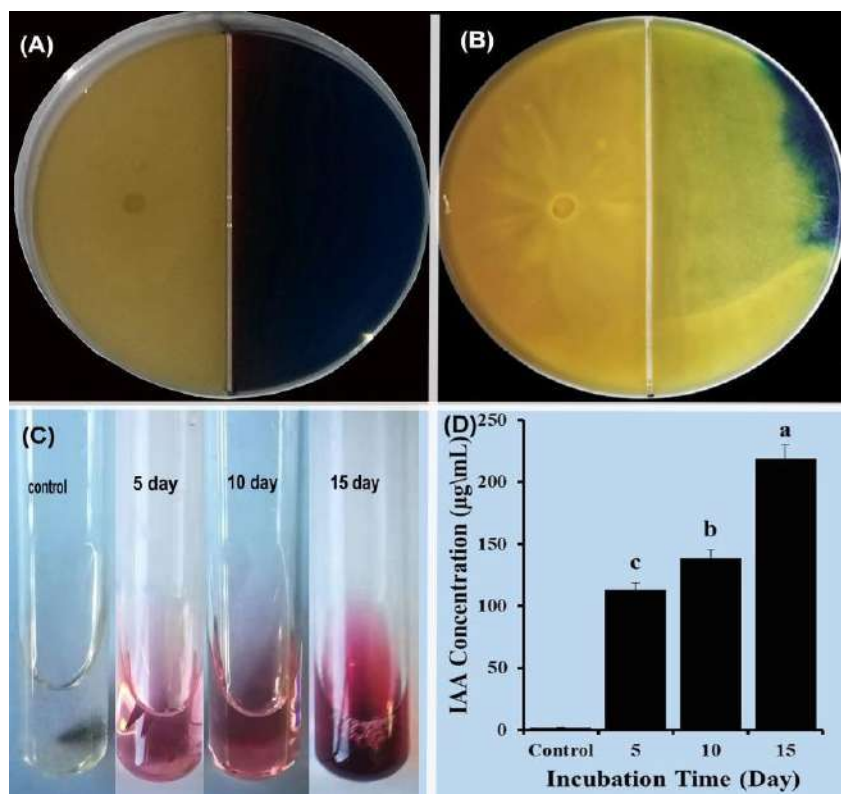


**Figure 4-15. Siderophore and IAA produced by isolate *T. virens* HZA14.** A, Growth of isolate HZA14 for three days. B, Hyphae of isolate HZA14 growing on CAS medium after 11 days. C, Color changes after culture supernatants mixed with Salkowski's reagent. D, Quantification of IAA.

## 4.3.4 Control efficiency of *T. virens* HZA14 against *Verticillium* wilt

The potential of *T. virens* HZA14 for controlling *Verticillium* wilt disease was determined in pots. The inoculation assays were carried out during different periods. The results of controlling assays showed that inoculation with *T. virens* HZA14 all could reduce incidence and disease severity of eggplant *Verticillium* wilt comparing to control (Figure 4-16). According to the results of statistical analysis, the effect of 30 days after inoculation with HZA14 was better than that of 10 and 20 days. The maximum reduction of disease severity (02.77±0.62) occurred at sowing 30 days after inoculation with *T. virens* HZA14, follwing by 23.88±0.62 at sowing for 20 days after inoculation and 44.43±0.95 at sowing for ten days after inoculation, while control efficacy in turn were 96.59±0.76, 67.99±0.83 and 39.10±1.30, respectively (Table 4-4).
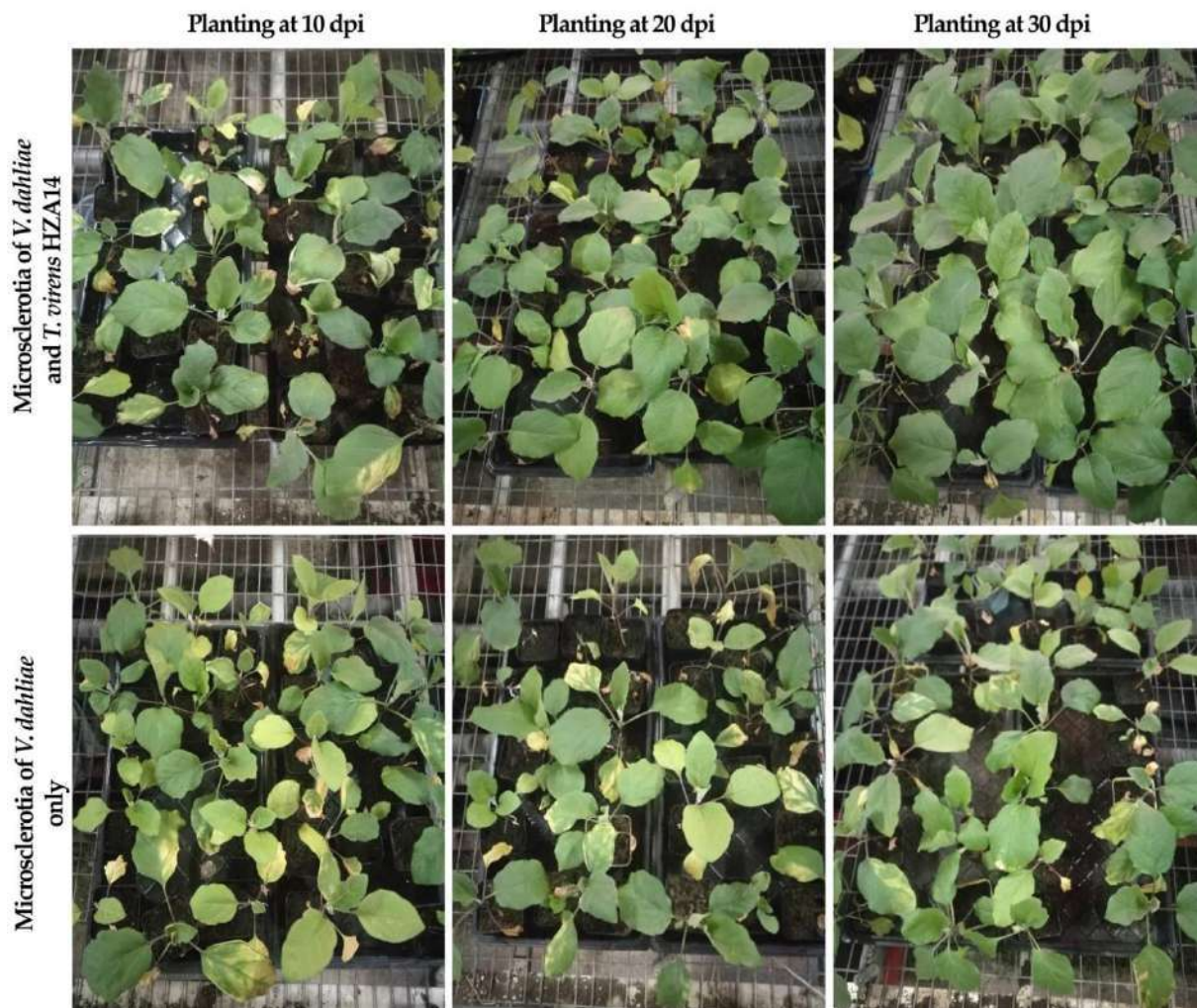


**Figure 4-16. The potential of HZA14 isolate in the reducing *Verticillium* wilt infestation on eggplant seedlings**

**Table 4-4. Control efficacy of HZA14 isolate against the *Verticillium* wilt of eggplant seedlings.**

| Periods/days | Disease severity (%) | | Control efficacy (%) |
| --- | --- | --- | --- |
| | *V. dahliae* alone | *T. virens*+*V. dahliae* | |
| 10 | 72.96±2.62 [a] | 44.43±0.95 [c] | 39.10±1.30 [c] |
| 20 | 74.63±0.96 [a] | 23.88±0.62 [b] | 67.99±0.83 [b] |
| 30 | 71.48±1.91 [a] | 2.77±0.62 [a] | 96.59±0.76 [a] |
| Average | 75.69 | 23.69 | 67.89 |

Value are means ± standard deviations of three replicates, and the different lowercase letters in the same column are significantly different at p 0.05 according to LSD test.

### 4.3.5 Plant growth promotion (PGP)

Based on the phenotypic observations noted in the pots experiment under the greenhouse, the eggplant seedlings treated with *T.virens* isolate HZA14 showed a significant increase in the plant height and length of each of the stems and roots in comparison to the untreated control plants 30 days after sowing (Figure 4-17A-D).
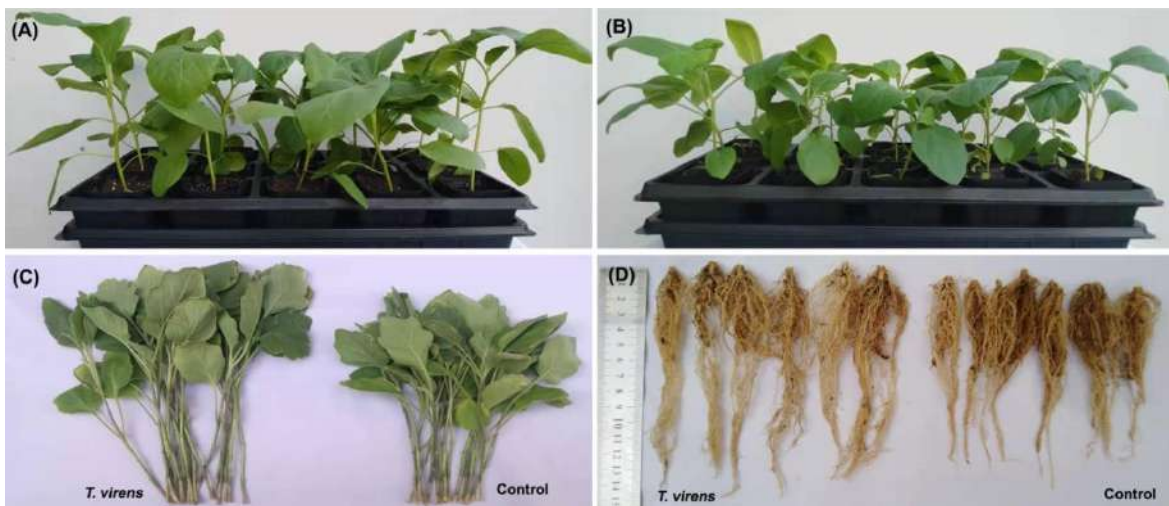


**Figure 4-17. Plant growth promotion ability of *T.virens* isolate HZA14 against eggplant seedlings 30 days after sowing.** A, Inoculation with HZA14 isolate. B, Control. C, Comparision of stem lengths between inoculation with HZA14 isolate and control. D, Comparision of root lengths.

In addition, the statistical analysis showed inoculation with isolate HZA14 increased growth promotion efficacy (GPE) of stem and root lengths by 16.54 and 13.50%, respectively (Table 4-5). Meantime, inoculation increased the GPE of stem and root fresh weigh (biomass) by 17.20% (or dry weight by 20.31%) and 28.00% (or dry weight by 54.55%), respectively (Table 4-5).

**Table 4-5. Percent differences of various growth parameters between treatment and control 30 days after inoculation with *T. virens* HZA14.**

| Treatments | Measured parameters | | | | | |
|---|---|---|---|---|---|---|
| | Stem length (cm) | Stem fresh weight (g) | Stem dry weight (g) | Root length (cm) | Root fresh weight (g) | Root dry weight (g) |
| **HZA14** | 15.58±0.47 [a] | 8.04±0.39 [a] | 0.77±0.01 [a] | 14.29±0.26 [a] | 0.64±0.029 [a] | 0.17±0.013 [a] |
| **Control** | 13.37±0.43 [b] | 6.86±0.38 [b] | 0.64±0.02 [b] | 12.59±0.21 [b] | 0.50±0.022 [b] | 0.11±0.011 [b] |
| **GPE (%)** | 16.54 | 17.20 | 20.31 | 13.50 | 28.00 | 54.55 |

Value are means ± standard deviations of three replicates, and the different lowercase letters in the same column are significantly different at p 0.05 according to LSD test.

### 4.3.6 Antagonism against *V. dahliae* and transcriptome sequencing

In order to determine further role of the isolate HZA14 against microsclerotial degradation of the *V. dahliae*, a dual culture method was used. Three days after incubation, hyphae of the isolate HZA14 covered entire surface of *V. dahliae* colony, but black microsclerotia forming a circle zone, produced by *V. dahliae*, were barely degraded (Figure 4-18A). Six days after incubation, microsclerotia began to be degraded. Subsequently, number of microsclerotia decreased significantly from 9 to 12 days. However, 15 days after incubation, microsclerotia hardly were observed, showing that *T.virens* isolate HZA14 had ability of great potential to degradate microsclerotia of *V. dahliae*. Similarly, process of microsclerotial degradation could be seen by the petri dish reverses (Figure 4-18B).



**Figure 4-18. Process of black microsclerotial degradation of *V. dahliae* on PDA medium.** A, The front of petri dishes. B, The reverse of petri dishes.

### 4.3.7 RNA sequencing

In the total of the five periods of time, the sequences for fifteen libraries were obtained. The high-quality clean reads were obtained by filtering low-quality reads, including the low-quality reads (1%), Ns reads (0%), and (2%) of adapter polluted reads (Table 4-6).

The analysis generated more than 695 million raw reads, with an average of 46.3 million reads in each sequencing library (Table 4-7). The total of the clean reads was 672.2 million, with an average of 44.8 and 97% of raw clean reads in each sample. The total of the mapped reads was more than 541 million, with an average of more than 36 million, and there were 79.91% clean mapped reads in each sample.

**Table 4-6. The summary of filtrating of data from 5 samples.**

| Sample | Low-quality Reads Number | Low-quality Reads (%) | Ns Reads Number | Ns Reads (%) | Adapter Polluted Reads Number | Adapter Polluted Reads (%) | Raw Q30 Bases (%) | Clean Q30 Bases (%) |
|---|---|---|---|---|---|---|---|---|
| 3 d1 | 247,666 | 0.51 | 80,350 | 0.17 | 1,422,250 | 2.92 | 94.28 | 94.53 |
| 3 d2 | 285,374 | 0.62 | 119,458 | 0.26 | 1,682,376 | 3.65 | 94.03 | 94.36 |
| 3 d3 | 258,734 | 0.56 | 104,576 | 0.23 | 1,955,898 | 4.21 | 94.7 | 95 |
| 6 d1 | 167,088 | 0.36 | 107,152 | 0.23 | 1,228,146 | 2.65 | 92.78 | 92.99 |
| 6 d2 | 168,518 | 0.35 | 99,602 | 0.21 | 1,378,994 | 2.86 | 92.36 | 92.55 |
| 6 d3 | 218,044 | 0.51 | 74,086 | 0.17 | 372,114 | 0.87 | 91.48 | 91.7 |
| 9 d1 | 272,842 | 0.59 | 113,518 | 0.24 | 774,844 | 1.68 | 92.17 | 92.46 |
| 9 d2 | 304,430 | 0.72 | 115,352 | 0.27 | 578,148 | 1.38 | 92.22 | 92.56 |
| 9 d3 | 373,630 | 0.86 | 72,444 | 0.17 | 1,463,248 | 3.39 | 91.34 | 91.8 |
| 12 d1 | 294,770 | 0.62 | 137,014 | 0.29 | 577,152 | 1.22 | 91.66 | 91.95 |
| 12 d2 | 231,074 | 0.51 | 117,782 | 0.26 | 617,152 | 1.37 | 92.32 | 92.58 |
| 12 d3 | 287,424 | 0.63 | 277,632 | 0.61 | 667,408 | 1.46 | 92.83 | 93.23 |
| 15 d1 | 223,532 | 0.47 | 41,360 | 0.09 | 1,052,474 | 2.23 | 94.46 | 94.67 |
| 15 d2 | 250,698 | 0.5 | 90,734 | 0.18 | 1,994,356 | 3.96 | 94.05 | 94.31 |
| 15 d3 | 217,032 | 0.44 | 38,672 | 0.08 | 1,686,662 | 3.43 | 94.47 | 94.67 |
| Total | 3,800,856 | 8 | 1,589,732 | 3 | 17,451,222 | 37 | 1,395 | 1,399 |
| Average | 253,390 | 1 | 105,982 | 0 | 1,163,415 | 2 | 93.01 | 93.29067 |

**Table 4-7. The summary of RNA-seq data from 5 samples**

| Sample | Raw Reads Number | Clean Reads | | Mapped reads | |
|---|---|---|---|---|---|
| | | Total | Raw reads | Total | Clean reads |
| **3 d1** | 48,694,098 | 46,943,832 | 96.41 | 45,610,346 | 97.16 |
| **3 d2** | 46,132,964 | 44,045,756 | 95.48 | 42,853,129 | 97.29 |
| **3 d3** | 46,500,864 | 44,181,656 | 95.01 | 43,061,345 | 97.46 |
| **6 d1** | 46,396,834 | 44,894,448 | 96.76 | 26,230,319 | 58.43 |
| **6 d2** | 48,263,138 | 46,616,024 | 96.59 | 38,260,921 | 82.08 |
| **6 d3** | 42,955,580 | 42,291,336 | 98.45 | 30,140,380 | 71.27 |
| **9 d1** | 46,271,222 | 45,110,018 | 97.49 | 25,308,591 | 56.10 |
| **9 d2** | 41,973,028 | 40,975,098 | 97.62 | 19,843,293 | 48.43 |
| **9 d3** | 43,182,142 | 41,272,820 | 95.58 | 17,491,240 | 42.38 |
| **12 d1** | 47,160,676 | 46,151,740 | 97.86 | 41,313,003 | 89.52 |
| **12 d2** | 45,191,892 | 44,225,884 | 97.86 | 33,912,174 | 76.68 |
| **12 d3** | 45,729,560 | 44,497,096 | 97.31 | 40,747,833 | 91.57 |
| **15 d1** | 47,125,420 | 45,808,054 | 97.20 | 44,612,998 | 97.39 |
| **15 d2** | 50,318,454 | 47,982,666 | 95.36 | 46,082,876 | 96.04 |
| **15 d3** | 49,164,158 | 47,221,792 | 96.05 | 45,765,333 | 96.92 |
| **Total** | 695,060,030 | 672,218,220 | 1,451 | 541,233,781 | 1198.72 |
| **Average** | 46,337,335 | 44,814,548 | 97 | 36,082,252 | 79.91466667 |

## 4.3.8 Correlation analysis of RNA-seq data among treated groups

The clean reads were spliced and aligned to the reference *Trichoderma virens* Gv29-8 genome retrieved from the *Trichoderma* genome website (https://www.ncbi.nlm.nih.gov /nuccore/ABDF02000077.1) using TopHat and assembled by Cufflinks software. The effects of sequencing depth and gene length on the mapped read counts were estimated by calculating the fragments per kilobase per transcript per million mapped reads (FPKM) values. To illustrate the gene expression profile among samples, genes expressed in 15 samples were analyzed by cluster analysis, and heatmap was drawn (Figure 4-19). The expression genes in the five different periods of time show large differences. It was also shows that the three replicates of each treatment were consistent within one group, which indicates that the dataset reproducibility was well done.
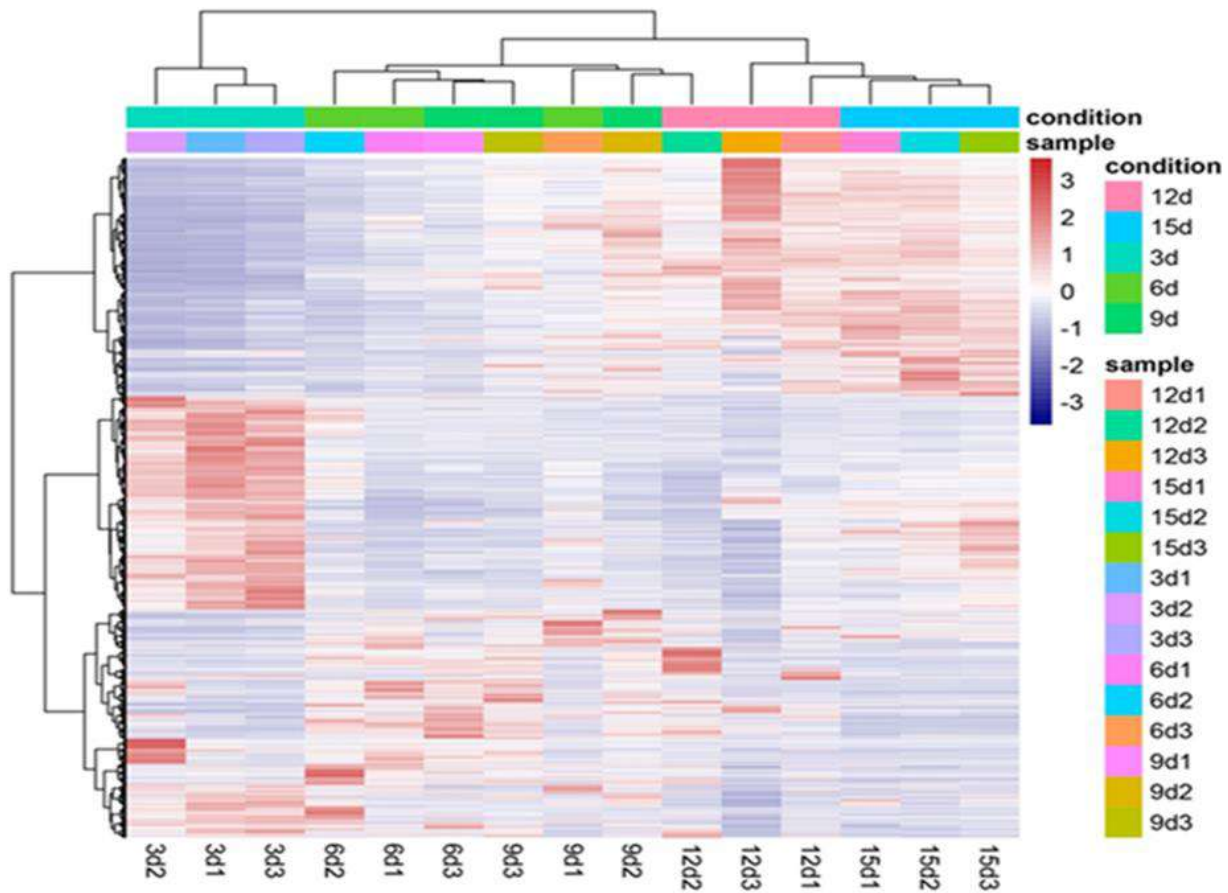
**Figure 4-19. Heatmap showing gene expression of *T. virens* in five different periods interaction between *T. virens* and *V. dahliae*.** The X-axis shows different time treatments and Y-axis shows expressed genes. Red indicates high expression levels and blue indicates low expression levels and. Data for gene expression level was normalized to Z-score.

### 4.3.9 DEGs analysis

Based on analysis of the differentially expressed genes (DEGs) (Figure 4-20), the biggest DEGs (up-regulation genes for 1914; down-regulated genes for 2114) was after 15 days (15 d vs 3 d), while the DEGs with minimal change (up-regulation genes for 1197; down-regulated genes for 1191) were after six days (6 d vs 3 d). After six days, the DEGs increased gradually from nine days (up-regulation genes for 1758; down-regulated genes for 1963) (9 d vs 3 d) to 12 days (up-regulation genes for 1936; down-regulated genes for 2050) (12 d vs 3 d), and more data visualized of the DEGs by volcano plot (Supplementary Figure 4-1).
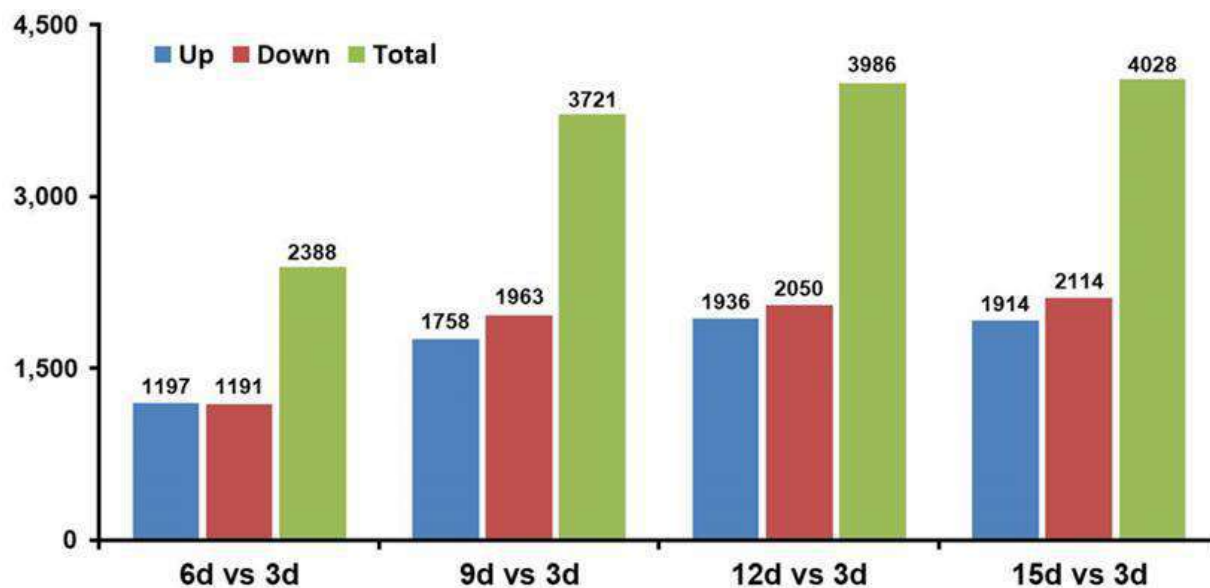
**Figure 4-20. Comparison of the identified differentially expressed genes (DEGs) of *T. virens* HZA14 during the mycoparasitic on the *V. dahliae* within different times periods.**

### 4.3.10 Gene ontology classification of differentially expressed genes (DEGs)

The main biological functions of differentially expressed genes (DEGs) and the pathways that they participate in were enriched by gene ontology (GO) functional significance enrichment analysis. The enrichment analysis for DEGs revealed that the down-regulated genes were more than the up-regulated genes in cellular components, biological-processes, and molecular-functions (Figure 4-21), showing that catabolic process was dominant. In cellular-components (Supplementary Table 4-1), mainly enriched terms (6 d vs 3 d) included membrane, organelle, organelle part, and cell part. In the (9 d vs 3 d) included protein-containing complex, organelle, organelle part, membrane part, and cell part. In the (12 d vs 3 d) were included membrane, protein-containing complex, organelle, organelle part, membrane part, cell part. In the (15 d vs 3 d) were included membrane, protein-containing complex, organelle, organelle part, membrane part, cell part.

In biological_process, mainly enriched terms (6 d vs 3 d) included biological regulation, cellular process, localization, metabolic process, and response to stimulus. In the (9 d vs 3 d) included biological regulation, cellular process, localization, metabolic process and response to stimulus. In the (12 d vs 3 d) included biogenesis, metabolic process, biological regulation, cellular component organization, cellular process, localization, and response to stimulus. In the (15 d vs 3 d) included biogenesis, biological regulation, cellular component organization cellular

process, localization, metabolic process, and response to stimulus. In molecular_function, mainly enriched terms (6 d vs 3 d) included catalytic activity, transporter activity, and binding. In the (9 d vs 3 d) included catalytic activity, binding, and transporter activity. In the (12 d vs 3 d) included binding, catalytic activity, molecular function regulator, transporter activity, and transcription regulator activity. In the (15 d vs 3 d) included binding, catalytic activity, molecular function regulator, transporter activity, and transcription regulator activity.
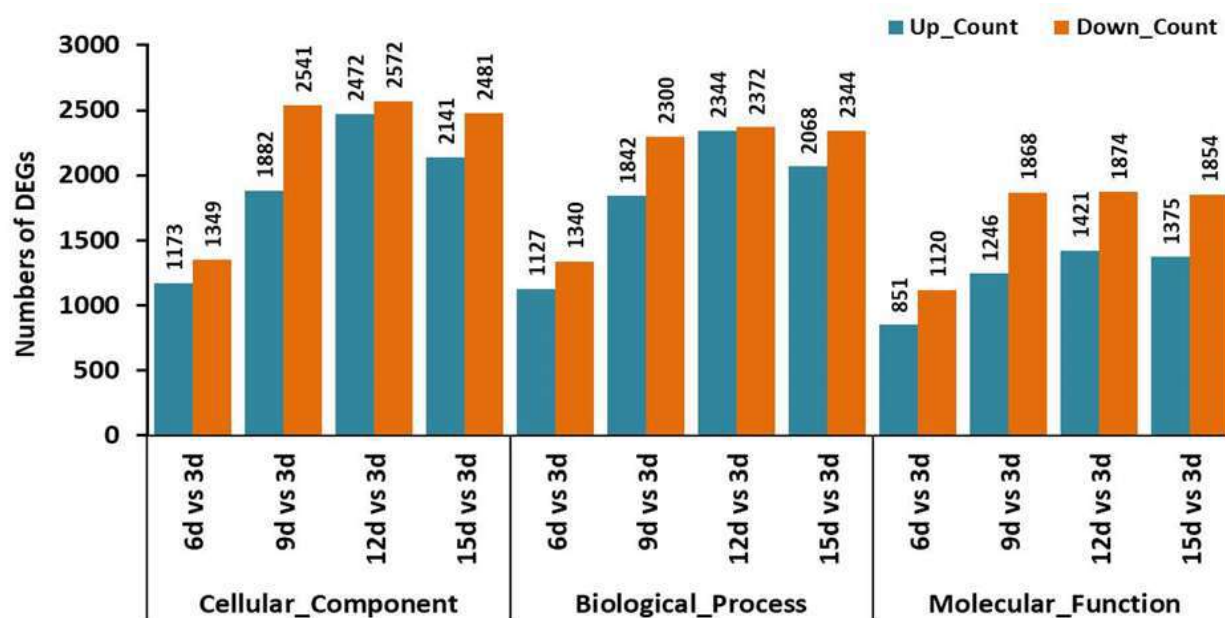


**Figure 4-21. Gene ontology classification of differentially expressed genes (DEGs) 15 samples.**

## 4.3.11 KEGG enrichment analysis of DEGs

Kyoto Encyclopedia of Genes and Genomes (KEGG) pathway annotation and enrichment analysis were used to evaluate significantly enriched DEGs using FDR ≤0.05. During interaction between *T. virens* and *V. dahliae*, the KEGG pathway analysis revealed that the DEGs were distributed in different metabolic pathways (Figure 4-22). In four interaction stages, metabolic pathway of ribosome all contained the highest DEGs, carbon metabolite pathway also all had relative high DEGs and the other pathways appear in different stages. In 6 d vs 3 d, metabolite pathways still were associated with the glyoxylate and dicarboxylate metabolism and indole alkaloid biosynthesis. In the 9 d vs 3 d, more metabolite pathways were involved, including glyoxylate and dicarboxylate metabolism, fructose and mannose metabolism, indole alkaloid biosynthesis, pyruvate metabolism and glutathione metabolism.

In the 12 d vs 3 d, just glyoxylate and dicarboxylate metabolism pathways were found. However, in the 15 d vs 3 d, metabolism pathways only had glyoxylate and dicarboxylate metabolism, fructose and mannose metabolism and glutathione metabolism (Figure 4-22). This indicates that the microsclerotia degradation of *V. dahliae* might involve in the enzymes of different pathways.
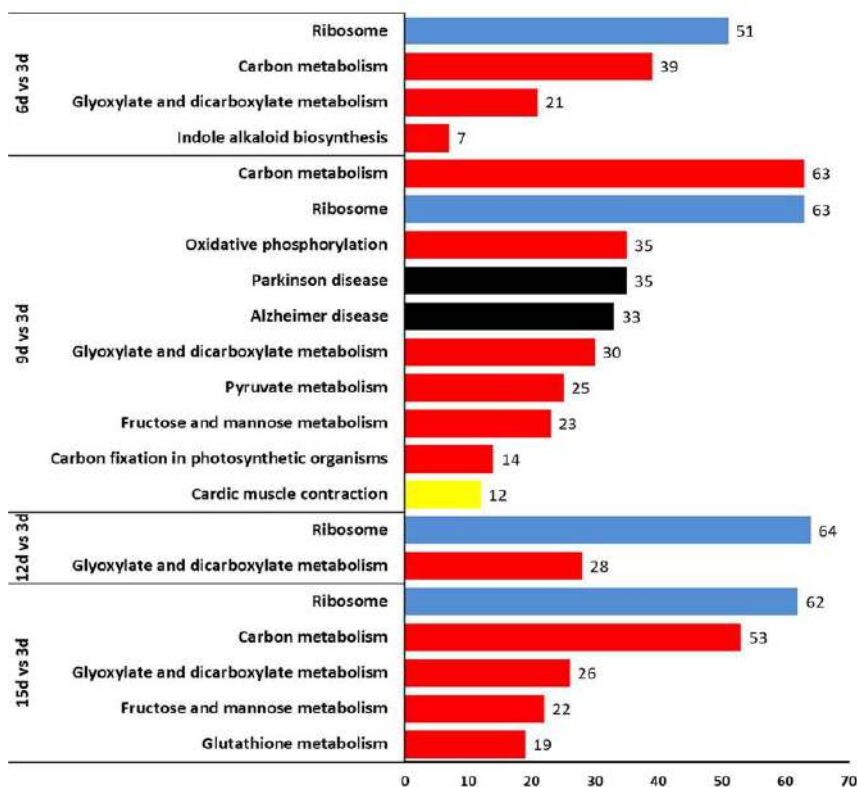


**Figure 4-22. KEGG pathway enrichment analysis, the significant pathways for differentially expressed genes on periods time 6 d vs 3 d, 9 d vs 3 d, 12 d vs 3 d, and 15 d vs 3 d.** Genes were divided into four categories according to the involvement of KEGG pathway. Blue, Environmental information processing; Red, Metabolism; Black, Human diseases; Yellow; Organismal system.

## 4.3.12 Analysis of DEGs related to enzymes of microsclerotial degradation

The cell wall is a characteristic structure of fungi and is composed mainly of glucans, chitins and glycoproteins, while microsclerotia is composed of dense mycelia. So the cell wall degrading enzymes (CWDEs) genes is related to enzymes of microsclerotial degradation. In addition, alpha-N-acetylglucosaminidase, laccase-1, peroxidase also is involved in microsclerotial degradation. Therefore, the DEGs being related to microsclerotial degradation were selected, including Endochitinase A1, Endochitinase 3, Endo-1,3-beta-glucanas, Alpha-N-acetylglucosaminidase, Laccase-1 and peroxidase.

The statistical analysis indicated that six enzyme-coding genes all were up-regulation, but the Log2FC values of enzyme-coding DEGs variated with time change in process of interaction between hyphae of *T. virens* HZA14 and microsclerotia of *V. dahliae* (Figure 4-23). For examples, Log2FC values of Endochitinase A1-coding DEG after 3, 6, 9, 12 and15 day were 3.39, 7.42, 11.81, 18.27, and 3.51, respectively, Endochitinase 3 for 2.54, 2.51, 14.82, 7.87, and 8.37, Endo-1,3-beta-glucanase for 15.11, 21.42, 42.02, 12.42, and 12.40, Alpha-N-acetylglucosaminidase for 4.83, 12.52, 11.64, 11.56, and 4.04, Laccase-1 for 34.87, 33.19, 64.58, 65.09, and 22.98 and peroxidase for 56.37, 53.32, 67.94, 85.51, and 55.59, respectively.
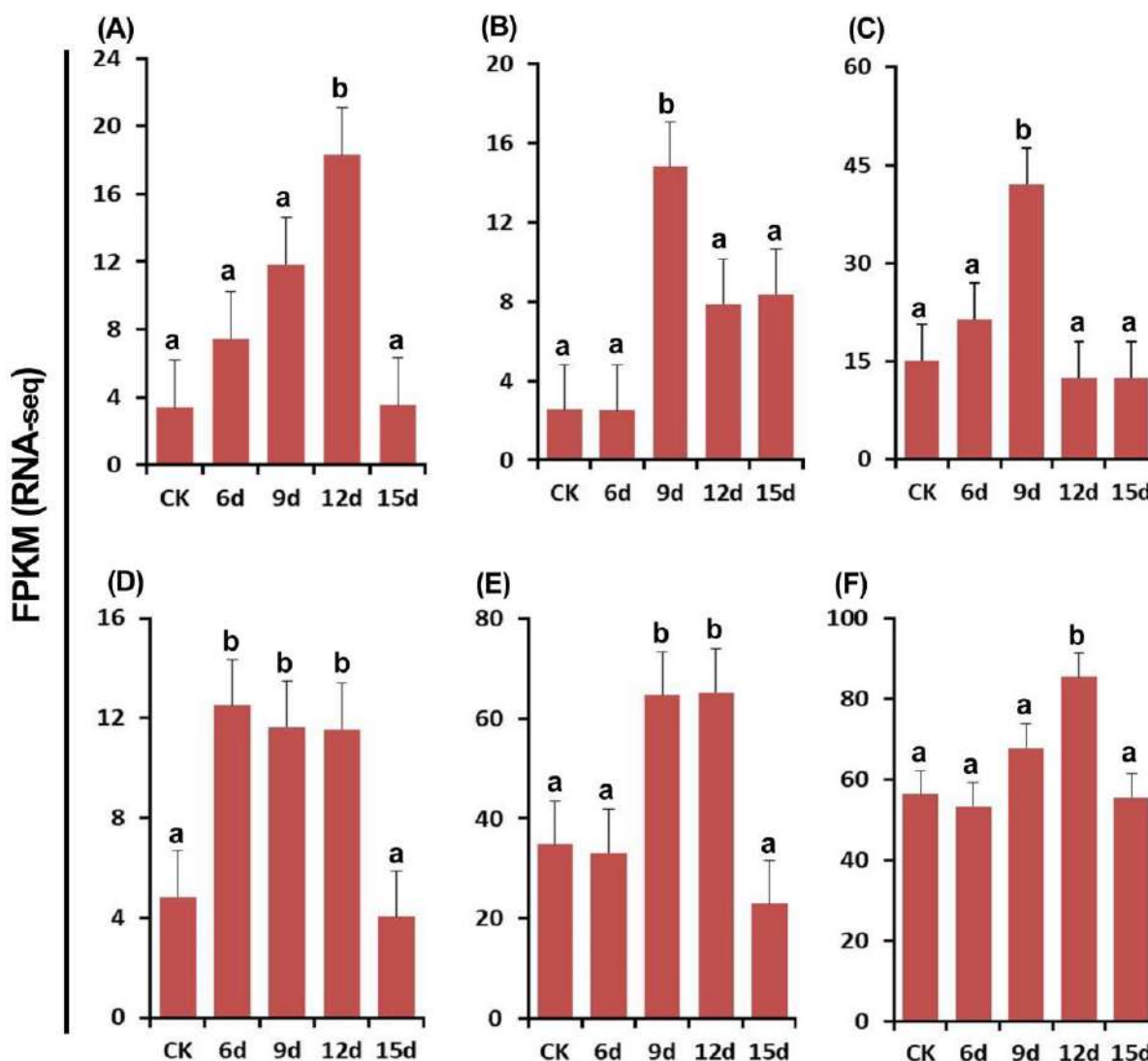


**Figure 4-23. Analysis of enzyme-coding DEGs related to enzymes of microsclerotial degradation of *V. dahliae* after 3, 6, 9, 12 and 15 days.** A, Endochitinase A1. B, Endochitinase 3. C, Endo-1,3-beta-glucanase. D, Alpha-N-acetylglucosaminidase. E,  Laccase-1. F, Peroxidase. The columns represent the mean FPKM for three replicates.

### 4.3.13 Detection of RT-qPCR

RT-qPCR analysis was used to validate the DEGs in the mycoparasitic process between *T. virens* HZA14 and the microsclerotia of *V. dahliae* for different interaction stages in PDA medium. The six enzyme-coding genes, including Endochitinase A1 (XM_014096114.1), Endochitinase 3 (XM_014099969.1), Endo-1,3-beta-glucanase (XM_014101914.1), Alpha-N-acetylglucosaminidase (XM_014095377.1), Laccase-1 (XM_014095593.1), and Peroxidase (XM_014105606.1), possibly involving in microsclerotial degradation was confirmed by RT-qPCR analysis using the primer pairs designed by the PerlPrimer v1.1.20 software (Table 4-8), and the actin gene was used as an internal reference gene to normalize gene expression. (Figure 4-24). The results showed that these gene expressions profiles were similar to that of the DEGs in transcriptome analysis (Figure 4-23), confirming the reliability of transcriptome data.

**Table 4-8. Primers utilized in qPCR experiments.**

| Gene Name | Forward and Reverse of Primers (5' to 3') |
|---|---|
| Endochitinase A1 | F: ACCCCGTAACTGGCTTGCCCACACA |
| | R:TGGAAGGGAAGAGAGTAGAGTTGCT |
| Endochitinase 3 | F: CTACCCTCCGTCCCTTTGGCACTGT |
| | R: GGCGTCGGGAAAGGGGCACTGGGGA |
| Endo-1,3-beta-glucanase | F: CACACCACCGTCCTCAAGGGCTCCG |
| | R: GTGGGTGAATCGGGCGACAATGAGA |
| Alpha-N-acetylglucosaminidase | F: ATTCGTCCCCCGCAACATCTCTCGC |
| | R: CCACTGAGGAGCGGATTCGGCAAAC |
| Laccase-1 | F: TGAGGGGCACGAGGACGATGATGAG |
| | R: GCGTTAGGATAAAATAGCAGAGGGT |
| Peroxidase | F: TCCGACGCCTGGGACGCCCTCACTG |
| | R: CGAAGTAGCGGAAGCCCTGGGTGTC |
| Actin | F: GGTCAGGTCATCACCATCGGCAACG |
| | R: GCTGCTGTGTGAATGGATGGGAAAA |
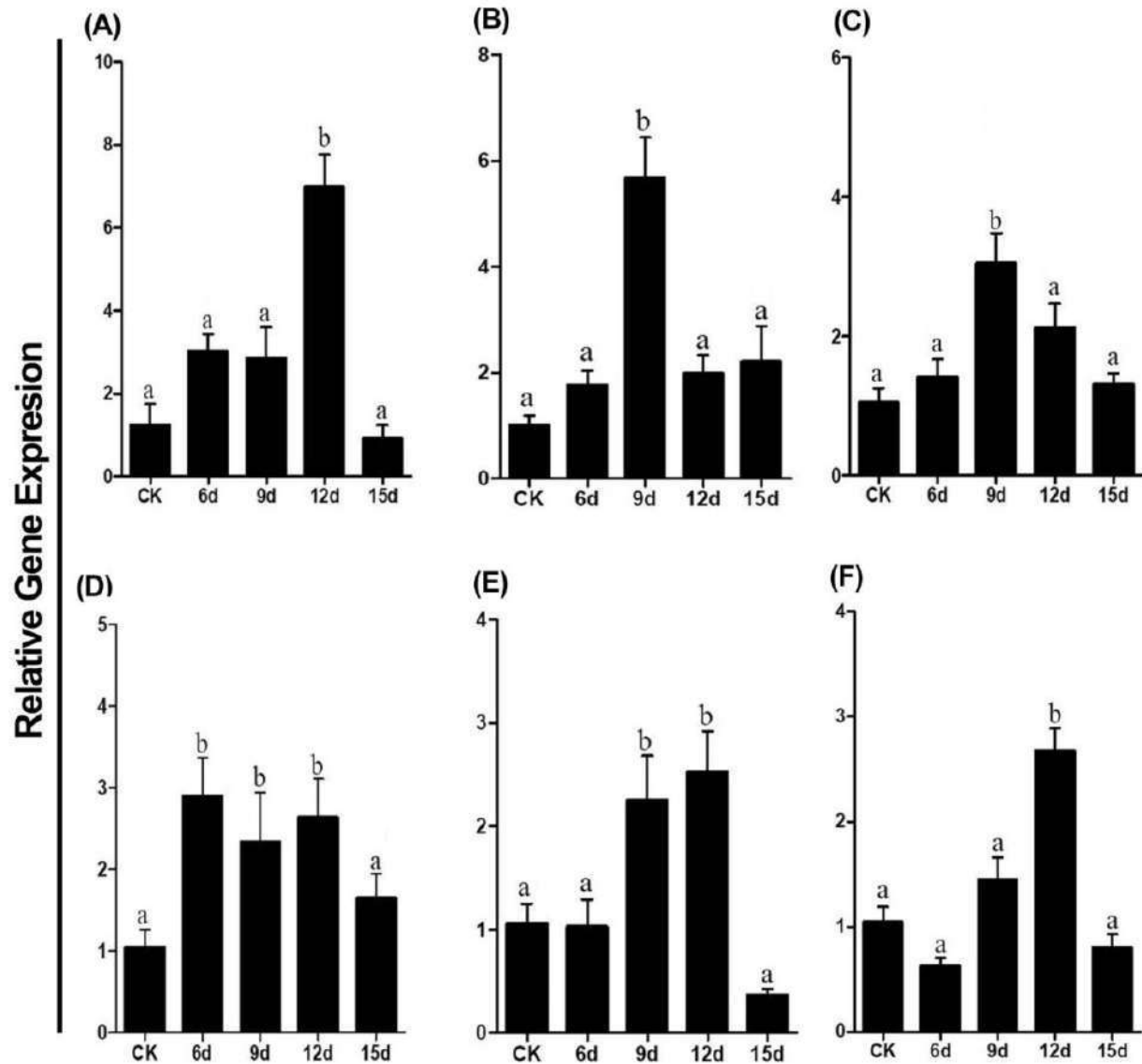
**Figure 4-24. Expression level of six genes in RT-qPCR detection after 3, 6, 9, 12 and 15 days.** A, Endochitinase A1. B, Endochitinase 3. C, Endo-1,3-beta-glucanase. D, Alpha-N-acetylglucosaminidase. E, Laccase-1. F, Peroxidase. The columns represent the mean relative gene expression for three replicates.

## 4.4 Discussion

*Verticillium* wilt disease caused by the *V. dahliae* is a major disease that severely affects eggplant production in China (Zhu et al., 2021). The *Trichoderma* species have been used commercially wide applied as a biological control agent against many important plant fungal pathogens (Mukherjee et al., 2012a). The successful application of these species in suppressing plant pathogens is depending on many mechanisms that work directly or indirectly (Lorito et al., 1996).

In the current study, from a total of 15 *Trichoderma* isolates tested, *T. virens* HZA14 exhibited an antagonism to the colony of *V. dahliae* in the class I, being consistent with the results reported by D'ercole et al. (2000), El-Rafai et al. (2003) and Reghmit et al. (2021). The mycoparasitism leading to a change in the color of the colony from black to light-brown, the stereomicroscope showed that the microsclerotia of *V. dahliae* were degraded during their interaction, being consistent with the results studied by Jabnoun-Khiareddine et al. (2009). Moreover, the results for culture filtrate of *T. virens* HZA14 inhibiting mycelial growth and conidia germination indicated that antibiosis was also involved in the biocontrol activity against *V. dahliae* (Anita et al., 2012; Fotoohiyan et al., 2017; Marques et al., 2018). Here, both mycoparasitism and antibiosis are important modes of action of *Trichoderma* spp. against microsclerotial degradation, mycelial growth, and conidia germination of *V. dahliae* (Xiaojun et al., 2014). *Trichoderma* species have been shown to be effective in controlling soil-borne diseases in many studies due to their having mechanisms such as mycoparasites, antagonists, and competition that can be exploited as biological fungicides to fight against pathogenic fungi (Vinale et al., 2009). In the present study, *Verticillium* disease severity was reduced in eggplant seedlings when the pot's soil was inoculated with *T. virens* conidia suspensions at different periods of times compared to the soil in the untreated pot. Similarly, the use of the different *Trichoderma* species all showed antagonistic activities against *V. dahliae* in different plants such as *T. harzianum*, *T. viride* and *T. virens* against the Tomato plants (Jabnoun-Khiareddine et al., 2009), *T. asperellum* against the olive Plants (Carrero-Carrón et al., 2016), *T. harzianum* against the pistachio plants (Fotoohiyan et al., 2017). Many of *Trichoderma* strains evaluated have showed the ability to produce siderophores on a CAS agar medium and indole-3-acetic acid on PD broth supplemented with tryptophan (Bogumił et al., 2013). In this study, the results of tests revealed the ability of *T. virens* HZA14 to produce siderophores and 3-indoleacetic acid (Figures 4-15A and C).

A Fe-chelating complex, known as siderophore, is secreted by some of *Trichoderma* strains limiting the growth of plant pathogens by reducing the efficiency of iron uptake (Srivastava et al., 2018). The siderophores reduce $Fe_3^+$ ions to $Fe_2^+$ ions, which can be utilized by plants and then efficiently transported from the roots to the shoots. While the Indole-3-acetic acid as an auxin stimulates plant growth and development (Sood et al., 2020). The production of plant growth hormones 3-indoleacetic acid (IAA) and its role in enhancing plant growth are

importantly specified mechanisms in many *Trichoderma* strains (Nieto-Jacobo et al., 2017). Also, *T. asperellum* Q1 was found to be able to promote the growth of *Arabidopsis thaliana* in an iron-deficient or insoluble iron-containing ($Fe_2O_3$) medium (Zhao et al., 2020). *Trichoderma* isolates that produced siderophores and IAA showed the ability to promote plant growth in beans (Hoyos-Carvajal et al., 2009). These reports are in agreement with our study results. The *T. virens* HZA14 increased the seedling height, taproot length, and dry or fresh weights of eggplant seedlings in pot experiments. These results all confirmed the role of siderophore and IAA for promoting eggplant seedling growth.

The microsclerotia of *V. dahliae* are arise by budding from septate, swollen hyphae composed of compact, thick-walled, melanized cells and it capable survive e in a dormant stat from 10 to up 30 years in agricultural soils (Duressa et al., 2013; Griffiths, 1970; Tjamos and Fravel, 1995). Consequently, the degradating process of microsclerotia is critically important way in the breaking disease cycle. Mycoparasitic role of *Trichoderma* species are considered most important direct mechanism being able to reducing inocula of pathogens (Gruber and Zeilinger, 2014; Mukherjee et al., 2022). Mycoparasitism is an ancestral trait in *Trichoderma* strain which involves chemotrophic growth, recognition and coiling, as well as the interaction of hyphae with secretion of specific lytic enzymes (Mukherjee et al., 2022).

The chitin and glucan are the major constituents of cell walls in many fungal pathogens (Lam and Gaffney, 1993). Correspondingly, *Trichoderma* strains are typically characterized by their ability to secrete lytic enzymes such as chitinases, glucanases, and proteases that can hydrolyze the cell walls of pathogenic fungi during the mycoparasitic process (Halifu et al., 2020). Studies of genome-wide expression for many *Trichoderma* species toward plant-fungal pathogenic were demonstrated (Atanasova et al., 2013; Ji et al., 2019; Steindorff et al., 2014). In addition, there is one study of microarray approach concerning in mycoparasitic mechanism to *T. atroviride* against *Verticillium* hyphae, but without targeting the microsclerotia (Morán-Diez et al., 2019). However, the mechanism of biocontrol related to *T. virens* during mycoparasitic action on microsclerotia of *V. dahliae* have not been yet addressed at the genetic level. Based on the differentially expressed genes (DEGs) using the Illumina sequencing, gene expression profiling involved in biosynthesis may be revealed (Shentu et al., 2014a). Our study provides transcriptome information about gene expression of *T. virens* HZA14 during mycoparasitism of *T. virens* against microsclerotia in different periods.

Based on the transcriptome analysis, 12037 differentially expressed genes (DEGs) were revealed during *T. virens* mycoparasitism from five different periods. The number of the DEGs very close to that of annotated genes (12,428) in whole genome of *T.virens* Gv29-8 (Kubicek et al., 2011). The GO analysis enriched 53 terms, which were divided into three classes (including cellular components, biological processes, and molecular function categories). Among them, the protein-containing complex, metabolic process, and catalytic activity showed the largest number of GO terms in different periods (9 d vs 3 d and 12 d vs 3 d, respectively) (Supplementary Table 4-1). This fact is consistent with the extensive metabolic activity expected for *Trichoderma* during mycoparasitism mechanism (Vieira et al., 2013). A total of nine pathways were also categorized with different expression levels by KEGG analysis under four categories: metabolism, environmental information processing, the cellular system, and human diseases. The diagrams in 4–22 showed the largest number of KEGG pathways in different periods (9 d vs 3 d and 12 d vs 3 d, respectively). The important pathway was the glyoxylate and dicarboxylate metabolisms, which have demonstrated a clear relationship with the metabolism functions required during the mechanism of biocontrol (Vieira et al., 2013).

In analysis of the differentially expressed genes being related to microsclerotia degrading enzymes, six genes of *T. virens* HZA14 were selected. These enzymes divided to three classes, including Endochitinase A1, Endochitinase 3 and Alpha-N-acetylglucosaminidase, Glucanases endo-1,3-beta-glucanase, Laccase-1 and Peroxidase. These enzymes had released mainly by Trichoderma species during mycoparasitism process in order to penetrate fungal cell wall (Steyaert et al., 2003). The endochitinase and endo-1,3-beta-glucanase enzymes acted on cell-wall degradation through cleaving ß-linkages internally in both ß-glucan and chitin and their oligomers at random along the polysaccharide chain (Caseiro et al., 2022; Marco and Felix, 2007). While, protease enzymes attack specific amino acid residues within the polypeptide chain (Steyaert et al., 2003).

Melanin in the microsclerotia are composed of oxidative polymerization of various phenolic compounds which degraded by phenol-oxidases, such as laccase. The few studies indicate that the laccase gene Lcc1 is specifically highly expressed in *T. virens* during mycoparasitic process against sclerotia of *B. cinerea* (Catalano et al., 2011; Giardina et al., 2010). These enzymes act synergistically in a mycoparasitic process, resulting in weakening and

hydrolysis of cell walls of fungal hosts and allowing for easier access of *Trichoderma* to nutrients (Morán-Diez et al., 2019).

In this study, the enzyme-coding genes being related to microsclerotial degradation were analyzed by transcriptome data and confirmed by RT-qPCR (Figure 4-23). The results showed that DEGs profiles of six of enzyme-coding genes in transcriptome analysis all were up-regulated after 3, 6, 9,12 and 15 days, but their Log2FC values had similar patterns from low to high and change among different enzyme-coding genes in stage of different interaction between hyphae of *T. virens* HZA14 and microsclerotia of *V. dahliae* (Figure 4-23). Similarly, expression patterns of six of enzyme-coding genes in the same transcriptome samples were confirmed by RT-qPCR (Figure 4-24), showing reliability of transcriptome data. In process of microsclerotial degradation, fungal hyphae begin to contact; secrete different enzymes to help infected hyphae invade microsclerotia (Atanasova et al., 2013; Seidl et al., 2009), causing solid microsclerotia to disintegrate finally. Obviously, the cell wall degrading enzymes play a key role. However, order in which these enzymes appear is not entirely clear based only on transcriptome data.

## 4.5 Conclusion

Microsclerotia that serve as the primary inoculum on many hosts are the main survival and dormancy structures of this fungal pathogen *V. dahliae*. While, microsclerotial degradation by *T. virens* HZA14 selected in this study had providing an important means to control *Verticillium* wilt. Meantimes, this study showed that *T. virens* HZA14 had plant promoting growth ability due to siderophore and IAA production, and high control efficiency against *Verticillium* wilt disease of eggplant. In process of microsclerotial degradation, the gene expression profiles were revealed by transcriptome analysis, and the DEGs being related to microsclerotial degradation were analyzed by transcriptome data and confirmed by RT-qPCR. These results provide important information for understanding molecular mechanisms of microsclerotial degradation and integrated management of *Verticillium* wilt in eggplant and other crops.

# Chapter 5

## Antifungal activity of silver nanoparticles by mycosynthesis using screened isolates of *Trichoderma* and its antifungal mechanism toward *Sclerotinia sclerotiorum*

### 5.1 Introduction

*S. sclerotiorum* (Lib.) de Bary is a significant plant pathogenic fungus that leads to sclerotium disease on many crops and causes economical substantial losses in throughout the world (Purdy, 1979). *S. sclerotiorum* has a wide host range, which include at least 408 described plant species (Boland and Hall, 1994).

The pathogen infects the host plants to cause the diseases including cottony roton stems, watery soft roton leaves, crown rot, blossom blight, and perhaps most common, *Sclerotinia* stem rot (SSR) or white mold and so on (Purdy, 1979). This pathogen produces the melanized multicellular structure, known as sclerotia that can survive for years in the soil (Coley-Smith and Cooke, 1971). The infection of host plants occurs from ascospores that originate from the germination of sclerotia in soil (Purdy, 1979). Plant diseases caused by *S. sclerotiorum* were difficult to control using traditional methods because of lacking resistance of high level in some major crops, which makes it difficult to improve the resistance to this disease using classical plant breeding techniques (Bolton et al., 2006). The management of this disease mainly depends on the widespread application of various fungicides, but this often cause severe environmental problems (Wang et al., 2019). In addition, the emergence of *S. sclerotiorum* strains resistant to fungicides, such as carbendazim and benzimidazole in china, has been found (Xilin et al., 2003).

Due to lack of more efficient disease control methods, this has stimulated researchers to developed new biotechnology. The nanoparticles (NPs) been highly noticed because of the high bioactivity and a wide antimicrobial spectrum with low doses (Rai et al., 2009). While biogenic synthesis of NPs is considered to be an effective alternate for its non-toxic and green procedures (Rudakiya and Pawar, 2017). Biosynthesis of NPs using organisms such as microorganism and plants, or their metabolisms has been explored and among them, silver nanoparticles (AgNPs)

can be highlighted for their broad-spectrum antimicrobial potential (Gupta et al., 2017; Loo et al., 2018; Prabhu and Poulose, 2012; Rai et al., 2014).

Especially, use of fungi in biosynthesis of AgNPs is attractive due to the production of diversity proteins (Guilger-Casagrande and Lima, 2019). Among different fungi genera, biosynthesis of AgNPs using *Trichoderma* spp. is more convincing and safer for environment in comparison with synthesis by other pathogenic fungi (Elamawi et al., 2018; Mukherjee et al., 2008; Othman et al., 2017; Sundaravadivelan and Padmanabhan, 2014; Tripathi et al., 2013; Vahabi and Dorcheh, 2014; Vahabi et al., 2011). Meanwhile, *Trichoderma* spp. produces the rich metabolites with different metabolic compounds, which depend on species or isolates, but less information was achieved regarding the biosynthesized AgNPs and its interactions with proteins and metabolic compounds produced by *Trichoderma*.

In addition, physiochemical properties of synthesized AgNPs differ in terms of their size, surface charge and shape, depending on different metabolites produced of different fungal species (Guilger-Casagrande and Lima, 2019). Although synthesis mechanisms have not yet been fully elucidated, interaction of AgNPs with fungal biomolecules is considered to be mainly responsible for the process of synthesis (Guilger-Casagrande and Lima, 2019). In this process, the toxic $Ag^+$ ions are reduced to the non-toxic metallic AgNPs (Vahabi et al., 2011). AgNPs synthesized by fungi have several effects on plant pathogens, including accumulation of $Ag^0$ in transport systems, disturbance in the flow of ions and interruption of cellular processes (such as respiration and metabolism pathway) (Lamsal et al., 2011). However, the AgNPs synthesized by *T. harzianum* against inhibition of mycelial growth and myceliogenic germination of sclerotia in *S. sclerotiorum* has been revealed but mechanism of AgNPs action on fungal hyphae were not analyzed (Guilger et al., 2017).

Thus, the main purpose of this research was to screen *Trichoderma* isolates for efficient synthesis of AgNPs, to characterize AgNPs using scanning electron microscope (SEM), energy dispersive spectroscopy (EDS), X-ray diffraction (XRD), transmission electron microscope (TEM) and fourier transform infrared spectroscopy (FTIR), to evaluate the antifungal activity of biosynthesized AgNPs against plant pathogenic *S. sclerotiorum* and to reveal its mode of action.

## 5.2 Materials and methods

### 5.2.1 Fungal isolates and mycelial growth

Fifteen *Trichoderma* isolates, including the *T. atroviride* HZA1, *T. atroviride* HZA2, *T. afroharzianum* HZA3, *T. brevicompactum* HZA4, *T. dorothopsis* HZA5, *T. koningiopsis* HZA6, *T. brevicompactum* HZA7, *T. dorothopsis* HZA8, *T. citrinoviride* HZA9, *T. asperellum* HZA10, *T. harzianum* HZA11, *T. brevicompactum* HZA12, *T. atroviride* HZA13, *T. virens* HZA14, and *T. dorothopsis* HZA15, were utilized in this study. They were acquired from our first study in this lab. Plant pathogenic fungus *S. sclerotiorum* YY01 was a highly aggressive isolate and it was previously isolated from the diseased tuber mustard (*Brassica juncea* var. *tumida*), identified and deposited in the Culture Collection of the Institute of Biotechnology, Zhejiang University, Hangzhou, Zhejiang Province, China. Fifteen *Trichoderma* isolates were grown in 250 ml Erlenmeyer flasks comprising 100 ml liquid broth consisting of (g/l) $KH_2PO_4$, 7; $K_2HPO_4$, 2; $MgSO_4 \times 7H_2O$, 0.1; $(NH_2)SO_4$, 1; yeast extract, 0.6; glucose, 10  (Bhainsa and D'souza, 2006), which were incubated in a ZWY-211B rotating shaker at 25°C and 150 rpm for 72 h. Subsequently, the mycelia were collected after filtrating them with the clean cloth–cheese, and washed using sterile double-distilled water ($ddH_2O$), before they were used for the synthesis of silver nanoparticles (AgNPs).

### 5.2.2 Synthesis of silver nanoparticles using *Trichoderma* isolates

For the biosynthesis of AgNPs, 10 g of mycelia (fresh weight) for each of the *Trichoderma* isolates were put into a 250 ml flask comprising 100 ml of sterile $ddH_2O$ and put in a rotating shaker at 25°C and 150 rpm for 96 h (Fayaz et al., 2010). The cell-free filtrate was obtained for each isolate after moving mycelia with Whatman filter paper No.1 and adjusting the pH to 7.0. The filtrate for each isolate was mixed with 1mM of $AgNO_3$ solution, which was prepared by Silver nitrate ($AgNO_3$) from Sinopharm Chemical Reagent Co., Ltd. (Shanghai, China), and dissolved in distilled water as a silver source for AgNPs biosynthesis (Othman et al., 2017). Reaction mixtures were incubated in a rotating shaker at 25°C and 150 rpm in dark conditions for 1 h (Mukherjee et al., 2008). All experiments were done in triplicate. The color change of each reaction liquid was observed, and the isolates were selected based on the reaction liquid with a strong color change for re-synthesizing the AgNPs.

The synthesis procedure and conditions were the same as described above but the time of synthesis was kept for 24, 48, 72, 96 and 120 h, respectively. The experimental flasks without the silver ion but with mycelia were used for control and the experiments were done in triplicate. To ensure the formation of AgNPs, the absorbance spectra (UV–Visible) of colloidal suspension were measured as a wavelength function using a UV2550 UV-Vis spectrophotometer (Shimadzu, Kyoto, Japan) at 1.0 nm of data intervals. The obtained colloidal suspension of AgNPs was retrieval by speed centrifuge (20,000 rpm) it for 10 min and washing with $ddH_2O$ to remove the silver ion residue. These precipitates were freeze-dried by Alpha 1-2 LDplus dryer (Osterode, Germany) into AgNPs powder for characterization study.

### 5.2.3 Characterization of AgNPs

The morphology and size of the produced AgNPs were monitored utilizing a Su8010 scanning electron microscope (SEM) (HITACHI, Japan). The energy dispersive spectroscopy (EDS) of Nano-silver elements density was confirmed using an Oxford instruments EDS (X-MaxN 80, Oxford, UK) at 20 keV in conjunction with scanning electron microscopy (SEM). The shape and size features of AgNPs were detected by using a JEM-1010 transmission electron microscope (TEM) (JEOL USA Inc., Peabody, MA, USA). To provide the AgNPs sample for TEM, copper grid was dipped in AgNPs solution and dried under vacuum. The crystalline nature of AgNPs powder was detected by X-ray Diffraction (XRD) analysis using a Siemens D5000 diffract meter (Munich, Germany) with an operating voltage of 45 kV and a current of 0.8 mA. The FT-IR spectra were recorded to determination the biomolecules accosite in the reduction of the $Ag^+$ ions and capping of the bioreduced AgNPs synthesized by the *T. virens* extract. The correlation between functional groups of supernatant extract with AgNPs was analyzed using a Fourier transform infrared (FTIR) spectrometer (Bruker Vector 22, Ettlingen, Germany), where dried powder of fungal extract and AgNPs were mixed with KBr crystals, respectively, and compressed to form pieces for analysis in the mid-infrared light region of 490–4000 cm$^{-1}$ with a resolution of 4 cm$^{-1}$. In addition, purified gliotoxin powder, obtained from *T. virens* HZA14 (Tomah et al., 2020), was also analyzed by FTIR spectra as control.

**5.2.4 Inhibitory activity of synthetic AgNPs against mycelial growth**

The effect of AgNPs synthesized by *T. virens* HZA14 against mycelial growth of *S. sclerotiorum* was investigated in vitro using PDA medium. The AgNPs mother solution (1000 µg/ml) was prepared after being dissolved in sterile ddH$_2$O by using ultrasonic waves (Bahrami-Teimoori et al., 2017). The series solution of AgNPs solutions were mixed with the melted PDA after the mother solution was diluted, and the plates containing the AgNPs of different concentrations (50, 100, 150, and 200 µg/ml) were obtained. A disc (5 mm) containing hyphae of *S. sclerotiorum* from 5-day-old colonies was put into the center of a plate, which was incubated at 23°C for 10 days. The 1.0 ml fungal cell-free culture liquid (CFCL) diluted by twice as much, or sterile, ddH$_2$O was mixed with the melted PDA, as with the controls. All experiments were done in triplicate. Diameters of colonies were measured and the formula PI (%) = [(C-N)/C)] ×100 was used to compute the inhibition percentage, where I was the percentage inhibition of the radial growth of *S. sclerotiorum* hyphae, C was the colony diameter in the plate with sterile ddH$_2$O and N was the colony diameter in the plate with AgNPs or 50% CFCL.

**5.2.5 Effect of AgNPs on sclerotial production**

The effect of biosynthetic AgNPs on the sclerotial production of *S. sclerotiorum* was tested using cellophane membrane. Plates containing PDA were covered with the sterile cellophane membrane. A disc (3 mm) containing the 5-day-old hyphae of *S. sclerotiorum* was put into the center of a plate and incubated at 23°C for 4 days and the cellophane membranes with colonies were transferred into the plates containing PDA with AgNPs of different concentrations (50, 100, 150, and 200 µg/ml), 50% CFCL and sterile ddH$_2$O, as described above. The petri dishes were kept at 23°C for 15 days. The number of sclerotia was counted on each plate and the percentage inhibition of produce using the same formula that was described in (5.2.4).

**5.2.6 Effect of AgNPs on myceliogenic germination of sclerotia**

Antifungal effects of the synthetic AgNPs on sclerotial viability were also tested *in vitro* using the sterile soil (Soylu et al., 2007). The 20 g of sterilized farmyard soil mixed with peat in a 1:2 ratio was put in sterile glass plates (9 cm in diameter). Sterilized sclerotia were moved randomly into the soil surface, and then the plates were sprayed using 20 ml AgNPs solutions of different concentrations (50, 100, 150, and 200 µg/ml) or 50% CFCL or sterile ddH$_2$O.

Plates were sealed by parafilm strips and incubated at 23°C in dark conditions for five days. Sclerotia were surface-sterilized in 50% ethanol for two minutes, and dried on sterile filter paper under a laminar flow hood after rinsing with sterile water. Partial sclerotia were placed into the PDA plates and kept at 23°C for three days. Sclerotia producing hyphae were counted and the percentage of germination inhibition was evaluated using the formula as described in (5.2.4).

### 5.2.7 Effect of AgNPs on sclerotia morphology

The interaction of AgNPs with fungal hyphae cells was observed by the TEM tool. sclerotia incubated for five and seven days as experiment described in (5.2.6) were fixed in glutaraldehyde solution of 2.5% overnight for SEM observation, as described by (Li et al., 2017). Briefly, The 1% (w/v) of osmium tetroxide solution was utiluzed to fixation of samples and then dehydrated in a series graded containing of 50%, 70%, 80%, 90%, 95%, and 100% of ethanol. Before the critical-point drying, the samples were mounted onto an aluminum stub, screened and photographed in a SEM after covered with gold. The Nano-silver elements' density was confirmed using the Oxford Instruments energy dispersive spectroscope (EDS) (X-MaxN 80, Oxford, UK) at 20 keV, as described in (5.2.3).

### 5.2.8 Statistical Analysis

The analysis was carried out on the data of the inhibition experiment depending on the analysis of variance (ANOVA) using the SAS software version 9.1.3. To compare the means, the LSD test level of significance of 0.05 was used. The experiment had been analyzed using three replicates.

## 5.3 Results

### 5.3.1 Synthesis of nanoparticles

The realization of AgNPs fabrication was confirmed using visual color change and UV-visible spectroscopy. The experiment results showed that the color change markedly occurred from yellowish colour to reddish color only in the reaction mixture produced by *T. virens* HZA14 among 15 isolates (Figure 5-25 A and B), indicating the formation of maximum AgNPs after 120 h of incubation. Subsequently, the screened isolate HZA14 was used for the synthesis of AgNPs after different incubation times (24, 48, 72, 96 and 120 h).

Analysis of the UV-Visible spectra revealed that the sharp surface plasma resonance peaks were all observed at 419 nm after different incubation times (Figure 5-25C). Obviously, peaks were the representative characteristic of AgNPs formation. Meanwhile, with time extension of incubation, enhancement of absorption increased and the maximum absorbance peak was observed after 120 h (Figure 5-25C). On the other hand, any color alteration was not observed in the control solution with cell-free filtrate without $AgNO_3$, and the peak absorbance was not observed at 419 nm after 120 h of incubation.
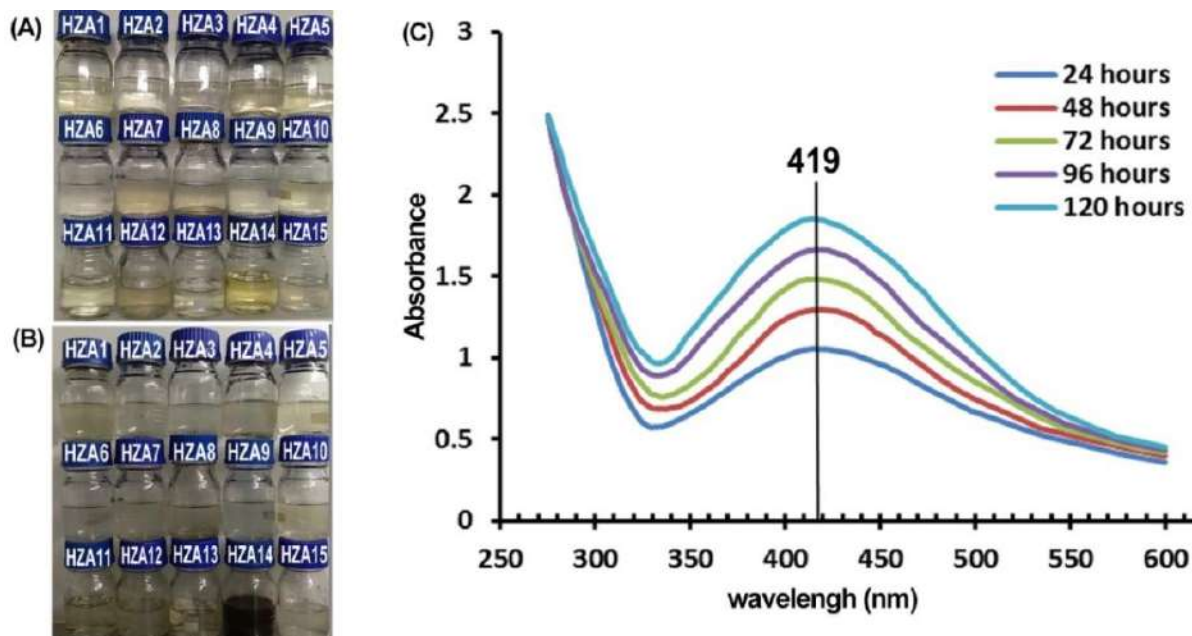


**Figure 5-25. Biosynthesis of AgNPs using 15 *Trichoderma* spp. isolates and UV-Visible spectra of synthetic AgNPs using cell-free filtrate of *T. virens* HZA14**. A, Cell-free filtrate produced by *Trichoderma* spp. isolates in different bottles. B, Synthetic AgNPs suspensions in different bottles after 120 h of incubation. The dark brown suspension in a bottle shows the formation of AgNPs. C, UV-Visible spectra of synthetic AgNPs after different time.

### 5.3.2 Characterization of AgNPs

The prepared AgNPs were characterized by scanning electron microscopy (SEM), energy dispersive spectroscopy EDS, TEM, XRD and FT-IR spectroscopy analysis. The SEM micrographs showed that the external surfaces of spherical AgNPs synthesized by cell-free filtrate of *T. virens* HZA14 were smooth (Figure 5-26A). The EDS analysis of AgNPs revealed the pure silver (28.85%) at 3 KeV was the second major constituent element compared to oxygen, nitrogen, carbon, and sulphur elements (Figure 5-26B), confirming the existence of the silver element in the synthesized AgNPs.

In addition, the EDS data also indicated that the relative proportion (1.24%) of the sulphur element was higher than that (1.04%) of the nitrogen element, which was an unusual finding.

The TEM micrographs showed that the different size and shape of AgNPs ranged from 5 to 50 nm (Figure 5-26C). The AgNPs exhibited a difference in their size but the majority of nanoparticles were spherical, while others were oval-shaped, irregular and larger sized nanoparticles are also visualized in Figure 5-26C. Furthermore, XRD analysis demonstrated that the emission peaks at 2values of 38.2, 44.2, 64.6, 77.5 and 81.5 corresponded to the silver crystal planes (111), (200), (220), (311) and (222), respectively (Figure 5-26D), confirming the crystalline nature of AgNPs. The XRD pattern thus clearly illustrates that the synthesized AgNPs were crystalline in nature as well as monodispersed in colloidal form. The line broadening of peaks was related to the presence of small particles in the medium. A few unassigned peaks were also observed in the vicinity of the characteristic peaks (Figure 5-26D). The unassigned peaks were recorded in the XRD pattern and they could be due to the crystallization of the bioorganic phase that occurs on the surface of the nanoparticles (Amargeetha and Velavan, 2018).
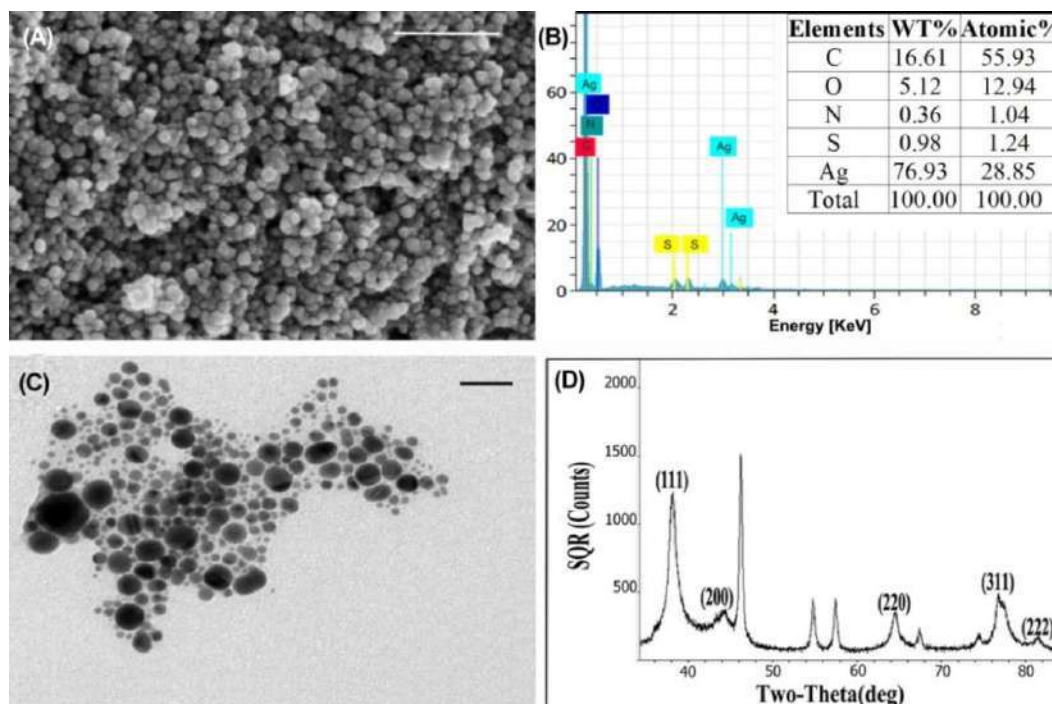
**Figure 5-26. Characterization of the synthesized AgNPs after 120 h of incubation.** A, Scanning electron microscopy. Scale bar = 250 nm. B, Energy dispersive spectroscopy. C, Transmission electron microscopy. Scale bar = 50 nm. D, X-ray diffractogram pattern.

FT-IR assessments were performed to identify the functional groups associated with the AgNPs' creation (Figure 5-27). The broad and strong bands at 3421 $cm^{-1}$ and 3292 $cm^{-1}$ were due to the bonded amine groups (–NH) or hydroxyl (–OH) in the interaction of fungal extract with AgNPs powder, respectively (Kumar and Mamidyala, 2011).

The peaks that appeared at 2959, 2923 and 2851 $cm^{-1}$ were attributed to asymmetric $CH_3$, and symmetric and asymmetric $CH_2$, stretching modes of carbohydrates and fatty acids. The peaks at 2360 and 2340 $cm^{-1}$ were due to O=C=O stretching vibrations ($CO_2$). The peaks at 1653, 1540 and 1077 $cm^{-1}$ were attributed to the C=O (carboxylic group), C=C-C (aromatic ring or amide II group) and C–O or C–O–C stretching vibrations, respectively (Shameli et al., 2012). A stronger absorption peak at 832 $cm^{-1}$ was assigned to the C-H bending vibration that was adjacent to the substituent group, indicative of heterocyclic compounds secreted by *T. virens*, which acted as the capping agent (Jain et al., 2011). The peaks for the binding of the C–S–H groups were assigned at 668 $cm^{-1}$. The peaks for the [O–C and P–O–C] groups in phosphatides, aromatics, amino acids (rocking vibrations) and ketones could be assigned near 568 $cm^{-1}$ (Rudakiya and Pawar, 2017). Similarly, the absorption band at near 472 $cm^{-1}$ was attributed to the AgNPs binding with oxygen (Gupta et al., 2010; Shameli et al., 2012).
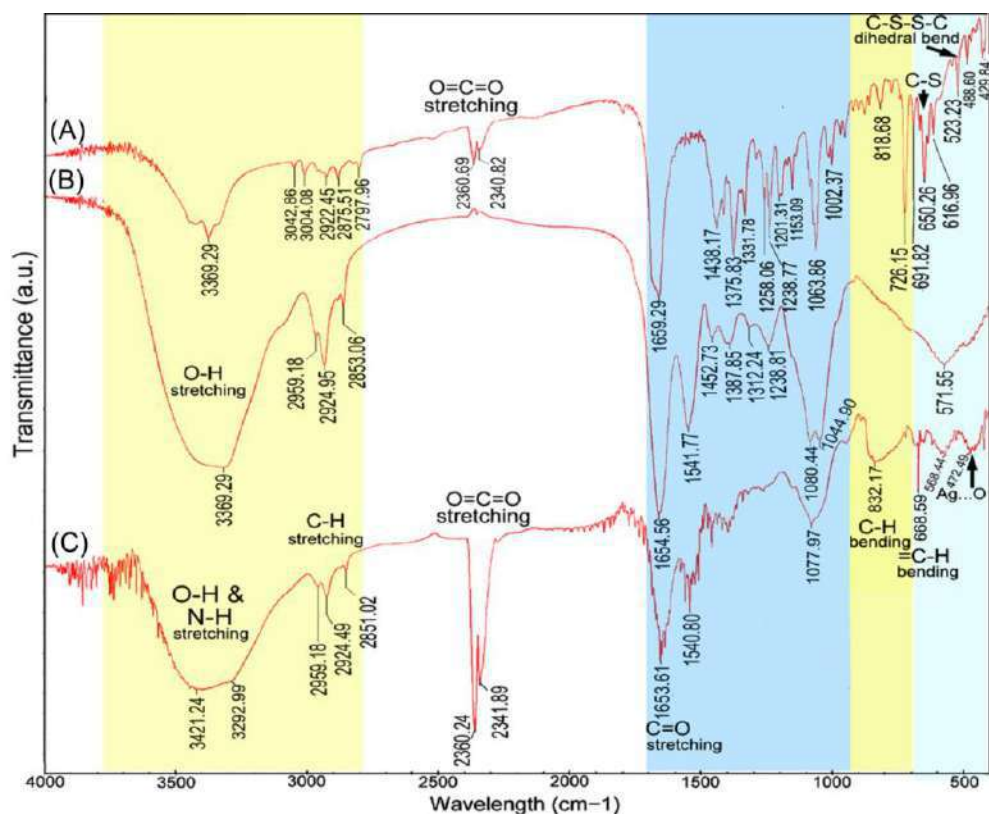
**Figure 5-27. FT-IR spectra of three samples: A, Gliotoxin. B, *T. virens* extract. C, AgNPs.**

Properties of FT-IR spectra and explain of produced shift changes in the new AgNPs product are exhibited in Table 5-9. The peak at 3292 cm$^{-1}$ with a large shift change (-76.20 cm$^{-1}$, compared to fungal extract) revealed the AgNPs binding strongly with oxygen from the oxidized form of gliotoxin or negatively charged carboxyl groups in proteins. Secondly, the peak of the C–S–H group stretching vibrations, with remarkable shift change (+18.33 cm$^{-1}$, compared to the FT-IR spectrum of gliotoxin), was assigned at 668 cm$^{-1}$ and suggested that the AgNPs were binding with sulphur from the reduced forms of gliotoxin (Abreu et al., 2017).

This could be confirmed by obvious shift change (+13.49 cm$^{-1}$) of the peak at 832 cm$^{-1}$ for the C–H bending vibration being adjacent to the substituent group. In addition, the peak of the R–CO–NH$_2$ stretching vibrations near 1077 cm$^{-1}$ also revealed the presence of proteins in synthetic AgNPs (Jain et al., 2011). These informations evidently revealed the role that biological components played in the fabrication of nano-silver and their stabilization (Rudakiya and Pawar, 2017).

**Table 5-9. Fourier-transform infrared spectral characteristics of fungal extract and AgNPs powder.**

| No. | Description | Wavenumber ($cm^{-1}$) | | Differences | Possible reason for the shift alteration |
| --- | --- | --- | --- | --- | --- |
| | | Fungal extract | AgNPs powder | | |
| 1 | N–H stretching vibrations | – | 3421.24 | – | Interaction with proteins |
| 2 | O–H stretching vibrations | 3369 | 3292.99 | -76.20 | Interaction with proteins or negatively charged carboxyl groups in gliotoxin |
| 3 | C–H stretching vibration (alkanes) | 2853.06 | 2851.02 | -2.04 | Interaction with fatty acids and carbohydrates |
| 4 | $CO_2$ stretching vibrations | – | 2360.24 and 2341.89 | – | an increase of carbon dioxide in the extract or poor purge stability of the instrument |
| 5 | Carbonyl group (C=O), amide I group stretching vibrations | 1654.56 | 1653.61 | -0.95 | Binding with proteins |
| 6 | Amide II group stretching vibrations | 1541.77 | 1540.80 | -0.97 | Interaction with proteins |
| 7 | P=O stretching in phosphatides and C=O group in polysaccharides | 1080.44 | 1077.96 | -2.48 | Interactions with lipids and carbohydrates |
| 8 | C-H bending vibration that was adjacent to the substituent group | – | 832.17 | + 13.49 [*] | Interactions with heterocyclic compounds |
| 9 | C–S–H group stretching vibrations | – | 668.59 | + 18.33 [*] | Ag binding with sulfur from the reduced forms of gliotoxin |
| 10 | C–O–C and P–O–C on phosphatides aromatics, amino acids and ketones stretching vibrations | 571.55 | 568.44 | -3.11 | Interactions with phospholipids, aromatics, amino acids and ketones. |
| 11 | O-Ag stretching vibrations | – | 472.49 | – | Ag binding with oxygen from hydroxyl groups of gliotoxin |

[*] comparing with gliotoxin.

### 5.3.3 Inhibitory activity against hyphal growth

The inhibitory activity of AgNPs synthesized by the cell-free filtrate produced by *T. virens* HZA14 against hyphal growth of *S. sclerotiorum* was assessed. The experiment results exhibited

that the AgNPs significantly inhibited the development of fungal hyphae (Figure 5-28). The highest percentage inhibition (PI%) of colony diameters was 100% at a concentration of 200 µg/ml, followed by 82.75, 72.03 and 66.70% at the concentrations of 150, 100, and 50 µg/ml ($p < 0.05$), respectively (Table 5-10). In addition, 50% cell-free culture liquid (CFCL) of *T. virens* HZA14 also had markedly antifungal activity compared with control (ddH$_2$O).
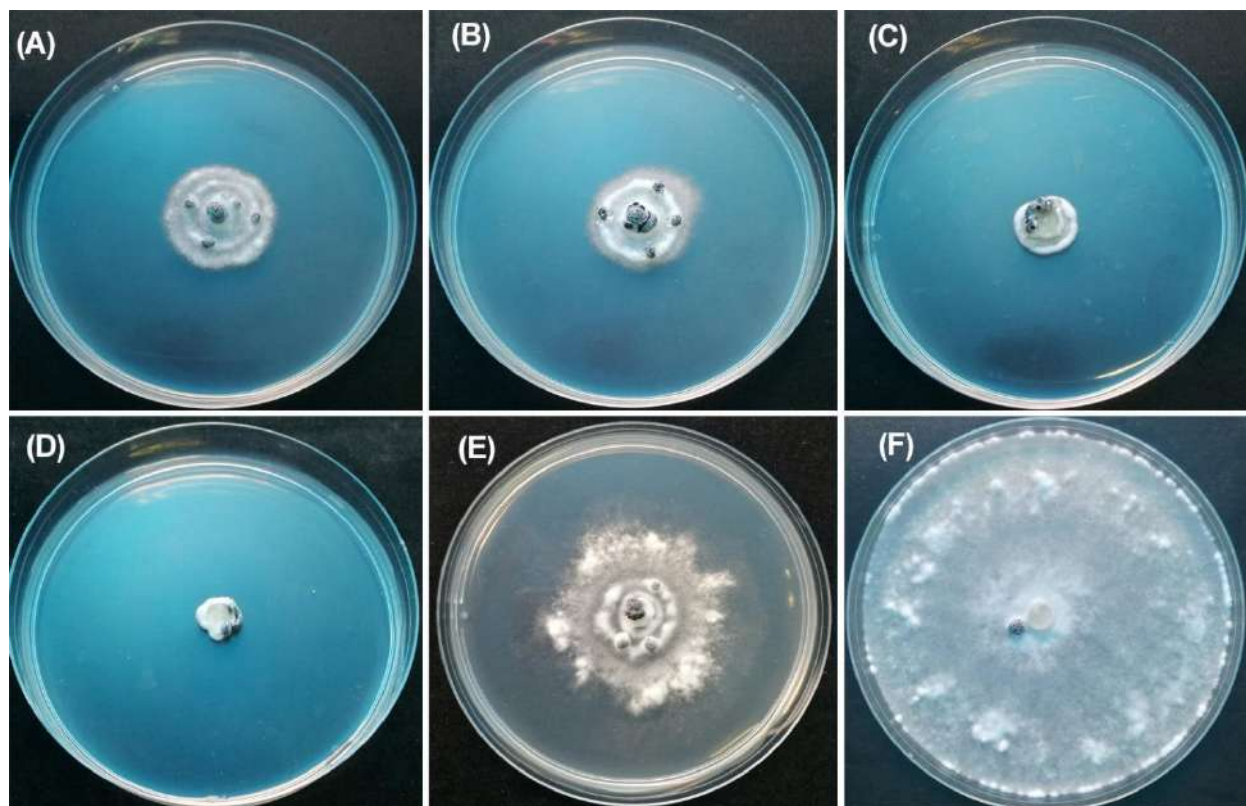


**Figure 5-28. Effect of AgNPs on hyphal growth of *S. sclerotium* on PDA 10 days after inoculation.** A, 50 µg/ml. B, 100 µg/ml. C, 150 µg/ml. D, 200 µg/ml. E, 50% cell-free culture liquid (CFCL) of *T. virens* HZA14. F, ddH$_2$O.

### 5.3.4 Inhibitory activity against sclerotial production

In experiment of determine the inhibitory activity of AgNPs against sclerotial production, cellophane membranes of 9-diameter with colony of *S. sclerotiorum* were covered onto the plates containing PDA with the AgNPs of different concentrations (50, 100, 150, and 200 µg/ml) for 15 days. The results showed that the synthesized AgNPs significantly reduced the number of sclerotia produced (Figure 5-29). The percentage inhibition (PI) of sclerotia production was 93.81%, 76.33%, 54.63% and 23.7% at concentrations of 200, 150, 100 and 50 µg/ml, respectively (Table 5-10). By comparison, the PI of 50% cell-free culture liquid (CFCL) was 18.55% comparing with control (ddH$_2$O).
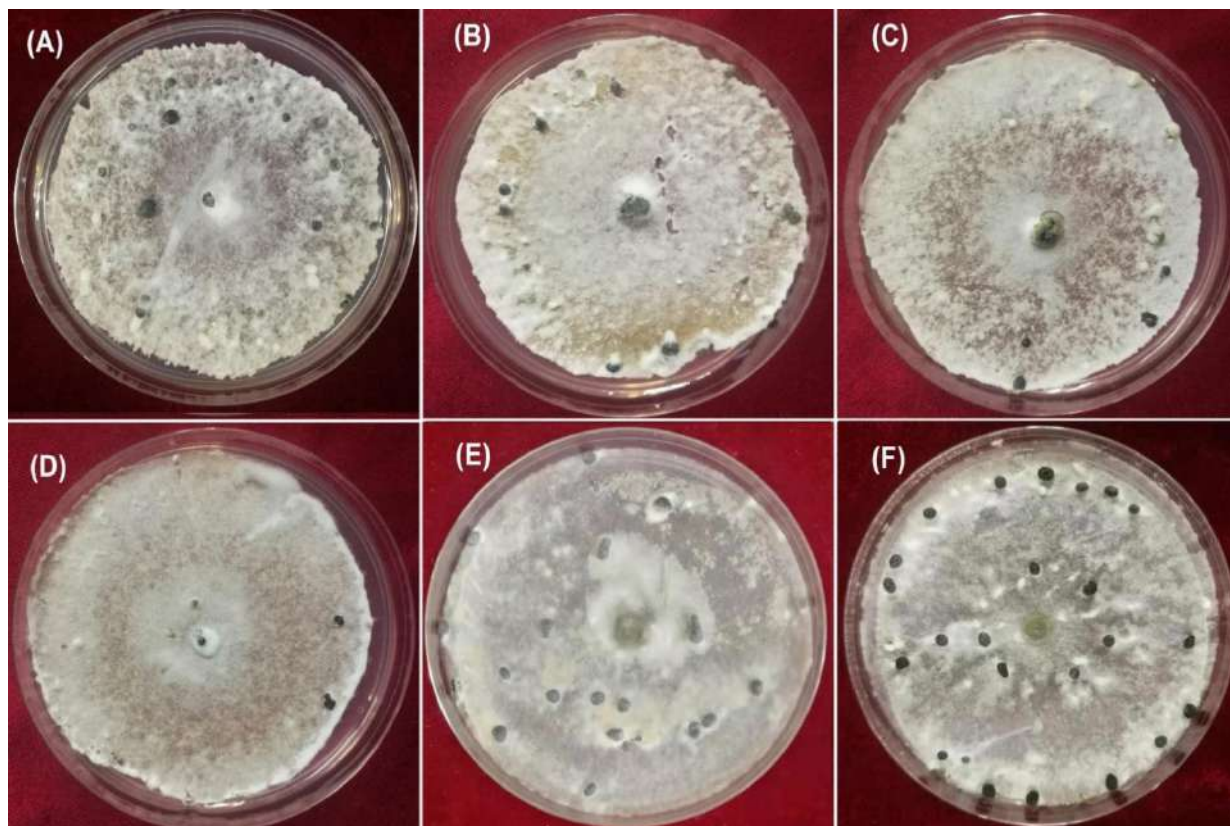
**Figure 5-29. Effect of AgNPs on the sclerotia production of *S. sclerotium* 15 days after inoculation.** A, 50 µg/ml. B, 100 µg/ml. C, 150 µg/ml. D, 200 µg/ml. E, 50% cell-free culture liquid (CFCL). F, ddH$_2$O.

### 5.3.5 Inhibitory activity against myceliogenic germination of sclerotia

The inhibitory activity of AgNPs against myceliogenic germination of sclerotia (MGS) was determined using field soil. The 20 ml AgNPs suspension with diverse levels of concentrations (50, 100, 150, and 200 µg/ml) were sprayed on sclerotia on the surface of the soil and treated at 23°C for five days. The results of myceliogenic germination of sclerotia on PDA indicated that the MGS was completely inhibited after treatment with three different concentrations of AgNPs (100, 150 and 200 µg/ml AgNPs) (Figure 5-30). The 80% PI of the MGS was observed at a concentration of 50 µg/ml AgNPs ($p < 0.05$) (Table 5-10). Comparatively, 50% CFCL also showed the higher inhibitory activity against the MGS (PI of 45%).
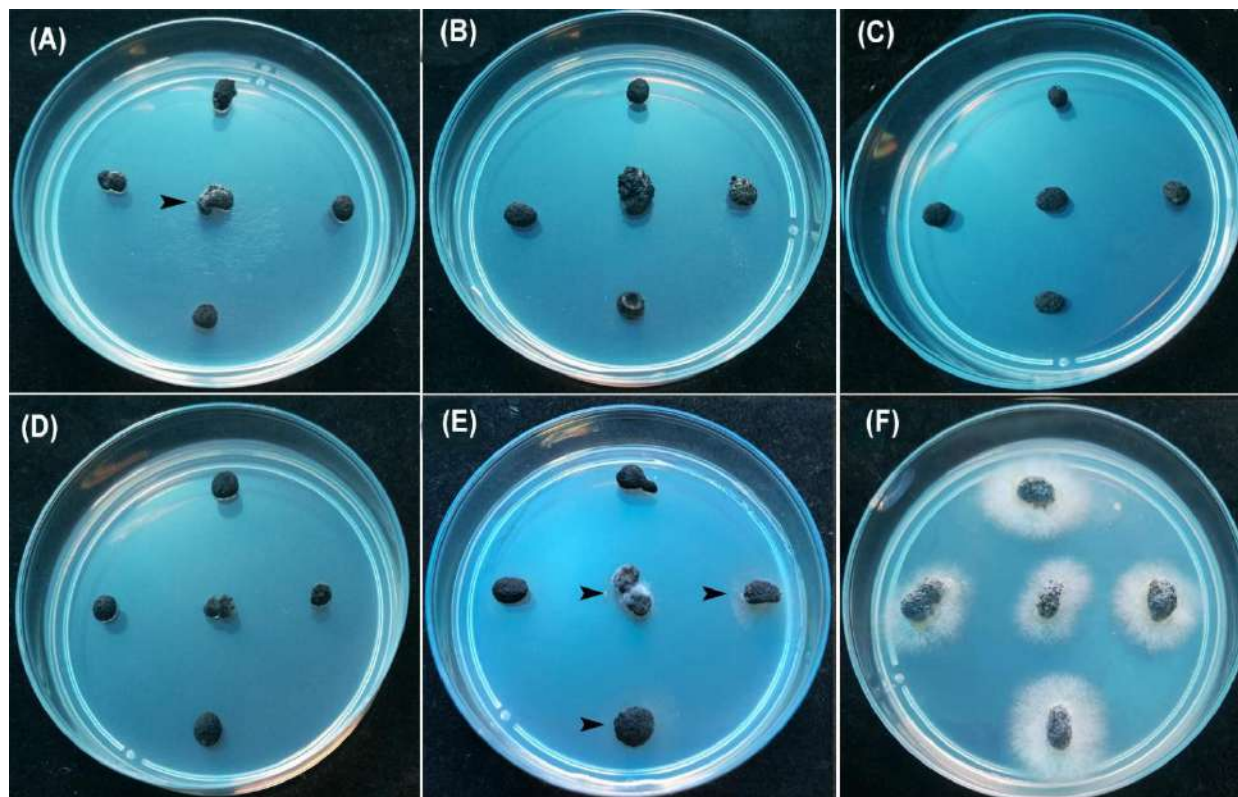
**Figure 5-30. Effect of different concentrations of AgNPs on myceliogenic germination of sclerotia on PDA for 3 days.** A, 50 µg/ml. B, 100 µg/ml. C, 150 µg/ml. D, 200 µg/ml. E, 50% cell-free culture liquid (CFCL). F, ddH$_2$O.

**Table 5-10. Effect of AgNPs of different concentrations against the hyphal growth, sclerotia production, and myceliogenic germination of sclerotia of *S. sclerotiorum*.**

| Treatments | HG (mm) | PICD (%) | SP (no.) | PISP (%) | MSG (no.) | PISG (%) |
|---|---|---|---|---|---|---|
| **AgNPs (50 µg/ml)** | 28.31±0.8 [c] | 66.70±0.9 [d] | 18.50±0.5 [c] | 23.70±2.3 [d] | 1.00±0.8 [c] | 80±16.0 [b] |
| **AgNPs (100 µg/ml)** | 23.78±1.1 [d] | 72.03±1.3 [c] | 11.00±0.8 [d] | 54.63±3.3 [c] | 0.00±0.0 [d] | 100±0.0 [a] |
| **AgNPs (150 µg/ml)** | 14.66±0.1 [e] | 82.75±0.1 [b] | 5.75±0.9 [e] | 76.33±3.4 [b] | 0.00±0.0 [d] | 100±0.0 [a] |
| **AgNPs (200 µg/ml)** | 0.0±0.0 [f] | 100 ±0.0 [a] | 1.50±0.5 [f] | 93.81±2.0 [a] | 0.00±0.0 [d] | 100±0.0 [a] |
| **Tv-CFA (50%)** | 64.75±0.4 [b] | 23.82±0.4 [e] | 19.75±0.9 [b] | 18.55±3.8 [e] | 2.75±0.5 [b] | 45±9.7 [c] |
| **ddH$_2$O** | 85.00±0.0 [a] | ------------ | 24.25±0.9 [a] | ------------- | 5.00±0.0 [a] | ----------- |

HG: hyphal growth; PICD: percentage inhibition of colony diameter; SP: sclerotia production; PISP: percentage inhibition of sclerotia production; MSG: myceliogenic germination of sclerotia; PISG: percentage inhibition of sclerotia germination. Value are means ± standard deviations of three replicates, and the different lowercase letters in the same column are significantly different at p 0.05 according to LSD test.

### 5.3.6 Morphological changes on the surface of sclerotia

SEM photographs were used to observe the interaction of AgNPs with hyphae cells. The morphological changes on the surfaces of sclerotia were seen by SEM after sclerotia were treated at a concentration of 200 μg/ml AgNPs for five or seven days. The micrographs of SEM showed that the small lamellar fragments (Figure 5-31A) or micropores or fissures (Figure 5-31B) appeared on the surfaces of hyphae cells on samples treated for five days, revealed damage of hyphae cells integrity. After seven days, complete collapse of hyphae cells occurred on the surface of a sclerotium (Figure 5-31C). By comparison, regular hyphae cell structure was observed on control samples (Figure 5-31D). The energy dispersive spectroscopy (EDS) analysis indicated the presence and accumulation of Ag as well as O, N, C, and S elements on hyphae cell surfaces of the sclerotia on samples treated for five days (Figure 5-31E).
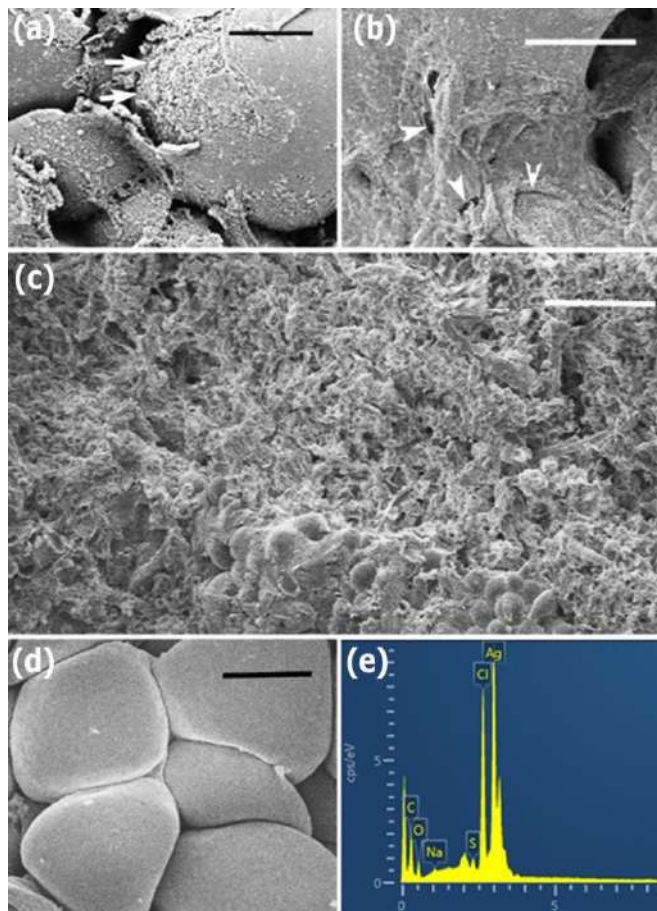


**Figure 5-31. The micrographs of scanning electron microscopy and energy dispersive spectroscopy, after sclerotia were treated by 200 μg/ml AgNPs: (A-B) Five days.** A, Lamellar fragments (arrows) on surfaces hyphae cells. Scale bar = 4 μm. B, Micropores or fissures (arrowheads) on surfaces of hyphae cells. Scale bar = 4 μm. C, Seven days. Mycelia die on the surfaces of a sclerotium. Scale bar = 50 μm. D, Control. Hyphae cells indicate regular shapes on the surfaces of a sclerotium. Scale bar = 5 μm. E, Energy dispersive spectroscopy.

**5.4 Discussion**

AgNPs have unique optical, electrical, and thermal properties, which constitute the basis of novel applications in Industrial, Pharmaceutical, and Agricultural activities (Firdhouse and Lalitha, 2015). They are able to adhere to the surface of fungi cell walls or bacteria membranes and then may gain access to the cells internal components, leading to cellular structural damage and interruption of the signaling pathway (Dakal et al., 2016; Kim et al., 2011). These properties enable AgNPs to become promising application prospects in the management of human and plant pathogenic microorganisms (Saklani et al., 2012). With research and development in the synthesis of nanoparticles, these activities have attracted increasing interest in biogenic synthesis methods using a variety of productions of organisms due to their stability rate is higher, lower level toxicity, and its properties of physicochemical are high quality (Iravani et al., 2014). However, although various organisms have potential for use in biogenic synthesis, the synthetic yield has a considerable difference, depending on the species or strain of the organism (Saklani et al., 2012).

In this study, the highest AgNPs formation occurred in the synthesis of AgNPs using the *T. virens* HZA14, showing great difference among isolates of different species (Figure 5-25). The synthetic yield was involved in components of secondary metabolites secreted by *Trichoderma* spp. and synthesis mechanisms of AgNPs. The isolate HZA14 produces gliotoxin, which has been identified previously (Tomah et al., 2020). Characterizations of AgNPs synthesized using the *T. virens* HZA14 revealed that the gliotoxin took part in the synthesis of AgNPs. The EDS data also indicated that the relative proportion (1.24%) of the sulphur element was higher than that (1.04%) of the nitrogen element. The result of FTIR exhibited the existence and binding of protein, carbohydrates and heterocyclic compounds and fatty acids with AgNPs. Furthermore, It has been well known that the proteins normaly bind with nanoparticles by cysteine residues or free amino groups (Jeevan et al., 2012), while the negatively charged carboxyl groups in proteins or in heterocyclic compounds also bind with nanoparticles (Rudakiya and Pawar, 2017). However, the peak with a larger shift change revealed the AgNPs binding strongly with oxygen from oxidized or reduced forms of gliotoxin (Table 5-9). Therefore, interaction patterns for the AgNPs binding negatively charged carboxyl groups or dithiol groups in gliotoxin are proposed and the schematic illustration of the synthesis of AgNPs capped with gliotoxin is depicted in Figure 5-32.

Although a previous study also found that the largest amount of AgNPs could be biosynthesized by *T. virens* (Devi et al., 2013), the interaction of AgNPs with fungal metabolites was not characterized. In the biosynthesis of AgNPs using *T. longibrachiatum* (Elamawi et al., 2018), synthesized AgNPs interacted only with proteins by carbonyl groups of amino acid residues and peptides, while, in this study, interaction patterns of AgNPs with metabolites, especially with gliotoxin, provide new insight for understanding the synthesized mechanisms of AgNPs.
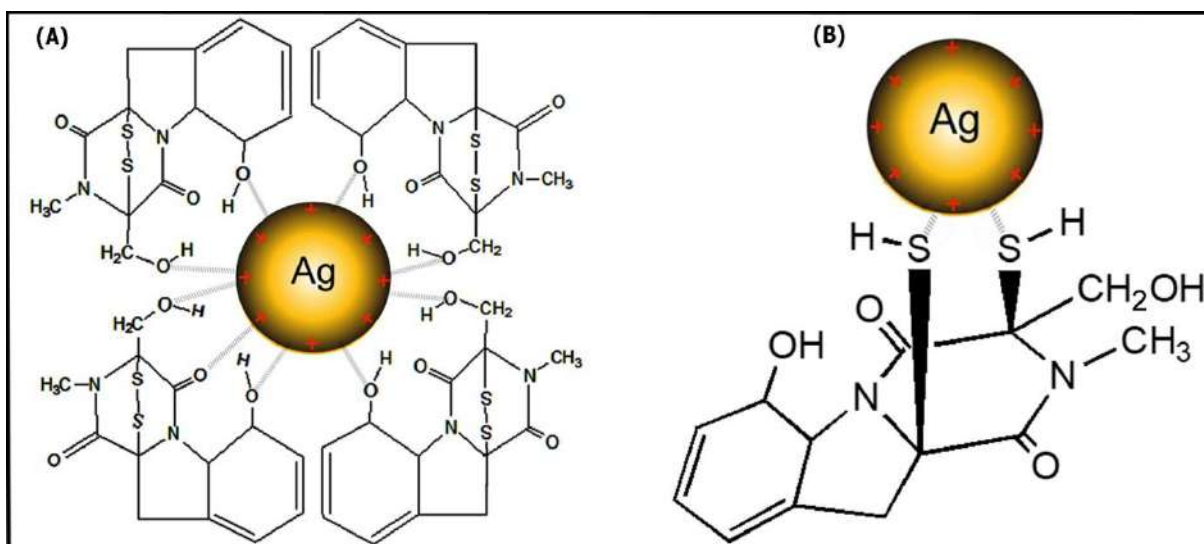


**Figure 5-32. Schematic illustration showing the interactions between the oxidized A or reduced B form of gliotoxin with the surface of positive charge of silver nanoparticles (AgNPs).**

The AgNPs exhibit their antimicrobial potential through multifaceted mechanisms (Dakal et al., 2016). It is interesting that AgNPs are preponderantly used for diseases management due to their antimicrobial activity against a diverse and broad range of plant pathogens (Mishra and Singh, 2015). In this study, synthesized AgNPs exhibited high inhibitory activity against mycelial growth, sclerotial fashioning, and myceliogenic emergence of sclerotia of *S. sclerotium*, showing their potential applications against white mold, which is partially similar to a previous report (Guilger et al., 2017). However, in this study, the mode of AgNPs on fungal hyphae was characterized by SEM based on the morphological changes of fungal hyphae on the sclerotia and the presence of nanoparticles was confirmed by EDS, providing evidence of direct physical interaction between nanoparticles and fungal cells.

These findings revealed that direct physical interaction of AgNPs with fungal hyphal cells causes an alteration in the fungal cell wall structure; consist of AgNPs touch, acumulation,

laminar fragment, and establishment of fissures or micropores, possibly allowing AgNPs into the cell interior. Similar works also found that the antifungal role of nanoparticles arose from an initial direct contact with fungal cell walls, inducing ROS production, destroying membrane integrity, and altering morphological characteristics (Chen et al., 2020; Dakal et al., 2016).

However, the gliotoxin is an epipolythiodioxopiperazine class toxin, containing a disulfide bridge, with high agonistic activity against plant pathogens (Tomah et al., 2020). Whether or not the prepared AgNPs with gliotoxin possess higher inhibitory activity than those without gliotoxin needs to be confirmed further. This study will extend our understanding of nanoparticles that could potentially be adopted as an effective strategy for preventing diversified fungal disease. The use of AgNPs in the form of nanopesticides in agroecosystems is not fully explored, and further research should focus on its risk assessment, such as using the statutory scopes depended in European (Villaverde et al., 2018), for achieving safer and more efficient agricultural practices.

### 5.5 Conclusions

In conclusion, this project expounded for the first time the prominent antifungal activity of AgNPs synthesized using a derived aqueous filtrate of *T. virens* HZA14 that produces gliotoxin against the soilborne pathogen *S. sclerotiorum in vitro*. Characterization of AgNPs revealed that the highest yield was related to gliotoxin produced by *T. virens* HZA14, and meanwhile, interaction patterns of AgNPs with gliotoxin molecules were proposed. The biosynthesized AgNPs exhibited a high percentage inhibition against the mycelial growth, sclerotial fashioning, and myceliogenic emergence of sclerotia. All the inhibitory behaviors observed using SEM/EDS technologies may be mostly attributed to nanoparticle–cell direct touch, acumulation, laminar fragment, and establishment of fissures or micropores on fungal cell walls and may be related to the alteration of fungal cell walls, while these changes provide the channels for the AgNPs to enter the cells. The final cell death may be associated with cell membrane damage, oxidative stress, and altered transport activity and signal transduction pathways.

# Chapter 6

## Research Conclusion and Prospects

**Conclusion**

For controlling horticultural crop diseases causing by soil-borne pathogens, *Trichoderma* isolates were screened and identified, mechanisms of their interaction with pathogens were analyzed, silver nanoparticles were synthesized, and some of important results were achieved as following:

1. An isolate of *Trichoderma* with highest antagonistic activity were screened from 77 isolates and it was identified as *T. virens* HZA14. It was able to cause colony collapse and degradation of *P. capsici* and produce a main secondary metabolite gliotoxin with antimicrobial activity. The biocontrol tests demonstrated that the HZA14 delayed the occurrence of chili pepper blight and significantly reduced the disease incidence and severity. This provides a potential biocontrol agent for developing biocontrol product for management of *P. capsici* in pepper.

2. A new species was found, and it was described as *T. dorothopsis* based on morphological characteristics and phylogenetic analysis. This will provide a good example for excavating natural resources.

3. The *T. virens* HZA14 had ability to produce the siderophore and IAA (3-indol acetic acid), and significantly promoted increase of eggplant biomass in the plant stem height and root length. This also shows that the HZA14 has great potential for developing plant promoting growth agent.

4. Antagonism tests showed that *T. virens* HZA14 had possessed ability to degradate microsclerotia of *V. dahliae* to disintegrate. Transcriptome analysis and RT-qPCR verification revealed that six differentially expressed genes (DEGs) possibly being related to cell wall degrading enzymes (CWDEs, EndochitinaseA1, Endochitinase3, Endo-1,3-beta-glucanase, Alpha-N-acetylglucosaminidase, Laccase-1 and Peroxidase) were high up-regulated in interaction of hyphae *T. virens* HZA14 with microsclerotia of *V. dahliae* during 3, 6, 9, 12 and 15 days periods. These provide a new approach to insights for

understanding mycoparasitic process of *T. virens* against microsclerotia of *V. dahliae* in different interaction stages.

5. Silver nanoparticles (AgNPs) was synthesized by using fermentation broth produced by *T. virens* HZA14. The synthetic AgNPs were charactered by SEM, EDS, TEM, XRD, and FTIR. Electron microscopic observations revealed that the AgNPs with size ranging from 5–50 nm had spherical and oval shapes with smooth surfaces. This provides an excellent method for green synthesized silver nanoparticles preparation using as a fungicide.

6. The antifungal activity of the synthetic AgNPs demonstrated that percentage inhibition of the obtained AgNPs was 100%, 93.8% and 100%, respectively, against the mycelial growth, sclerotial fashioning, and myceliogenic emergence of *S. sclerotiorum* sclerotia at a concentration of 200 µg/ml. The direct interaction between nanoparticles and fungal cells revealed by SEM and EDS consist of AgNPs touch, acumulation, laminar fragment, and establishment of fissures or micropores on fungal cell walls. These findings will deep enlarge our understanding of the action mechanisms of AgNPs for controling diversified fungal disease.

**Prospects**

In this study, we investigated the significance of *Trichoderma* species in biological control against the soil-borne plant disease *Phytophthora capsici* and identified the *Trichoderma virens* HZA14 as antagonism fungus, and production of bioactive compound (Gliotoxin) is the mechanism followed by the antagonist to inhibiting the plant pathogen. This mechanism will help in the development of plant-pathogen control strategies. However, still, there are more strains of *Trichoderma* non-discovered yet that may provide other bioactive compounds. Thus, more soil samples from different cropped areas need to be collected, isolate the *Trichoderma* spp. from it and tested for their bio-control potential against the major soil-borne diseases and also, need to execute more number and diverse range of field experiments for evaluation of real effectiveness of selected strains of *Trichoderma*.

In this subject, *T. virens* HZA14 had showed the characteristics that are desirable as a biocontrol agent against *Verticillium* wilt disease on eggplant, and the *T. virens* HZA14 had resulted in the degradation of microsclerotia of *V. dahliae* in vitro. We found the *Trichoderma* direct antagonism is mycoparasitism and the associated production of extracellular lytic enzymes. By transcriptome data and the RT-qPCR analysis we found the enzymes involved in microsclerotial degradation included endochitinase A1, endochitinase 3, alpha-N-acetylglucosaminidase, endo-1,3-beta-glucanase, laccase-1 , and  peroxidase. Furthermore, potential Trichoderma should be screened in conditions that resemble the field situation to increase the chance of successful use in practice; large scale production, preservation conditions, and application methods should be considered in the process of selecting *Trichoderma* against *Verticillium*.

In the modern pattern, the biosynthesis of AgNPs by metabolites, especially with the binding negatively charged carboxyl groups or dithiol groups in gliotoxin of *T. virens* HZA14 had obtained. The capping of the AgNPs with gliotoxin led to good control against a phytopathogenic *Sclerotinia sclerotiorum*. But, the more intensive study is needed when considering AgNPs to control plant diseases as they clearly have negative impacts on fungal soil communities. At the same time these also the disadvantages of AgNPs as they affect non-target microorganisms. Future work should consider the effects of AgNPs on soil functional capability in long-term experiments.

# References

Abdenaceur, R., Farida, B., Mourad, D., Rima, H., Zahia, O. and Fatma, S. 2022. Effective biofertilizer *Trichoderma* spp. isolates with enzymatic activity and metabolites enhancing plant growth. International Microbiology, 25: 817-829.

Abreu, D. S., Sousa, T. P., Castro, C. B., Sousa, M. N. V., Silva, T. T., Almeida-Neto, F. W. Q., Queiros, M. V. A., Rodrigues, B. S. F., Oliveira, M. C. F. and Paulo, T. F. 2017. SAM of gliotoxin on gold: A natural product platform for sugar recognition based on the immobilization of *Canavalia brasiliensis* lectin (ConBr). Electrochimica Acta, 241: 116-123.

Abuduaini, X., Aili, A., Lin, R., Song, G., Huang, Y., Chen, Z., Zhao, H., Luo, Q. and Zhao, H. 2021. The lethal effect of *Bacillus subtilis* z15 secondary metabolites on *Verticillium dahliae*. Natural Product Communications, 16: 1-11.

Acciarri, N., Restaino, F., Vitelli, G., Perrone, D., Zottini, M., Pandolfini, T., Spena, A. and Rotino, G. L. 2002. Genetically modified parthenocarpic Eggplants: improved fruit productivity under both greenhouse and open field cultivation. BMC Biotechnology, 2: 1-7.

Ahluwalia, V., Kumar, J., Rana, V. S., Sati, O. P. and Walia, S. 2015. Comparative evaluation of two *Trichoderma harzianum* strains for major secondary metabolite production and antifungal activity. Natural Product Research, 29: 914-920.

Ai, P., Jin, K., Alengebawy, A., Elsayed, M., Meng, L., Chen, M. and Ran, Y. 2020. Effect of application of different biogas fertilizer on eggplant production: Analysis of fertilizer value and risk assessment. Environmental Technology and Innovation, 19: 101019.

Al-Abboud, M. A. 2018. Fungal biosynthesis of silver nanoparticles and their role in control of *Fusarium* wilt of sweet pepper and soil-borne fungi *in vitro*. International Journal of Pharmacology, 14: 773-780.

Alabouvette, C., Olivain, C. and Steinberg, C. 2006. Biological control of plant diseases: the European situation. European Journal of Plant Pathology, 114: 329-341.

Alam, I. and Salimullah, M. d. 2021. Genetic engineering of Eggplant (*Solanum melongena* L.): Progress, controversy and potential. Horticulturae, 7: 78.

Alghuthaymi, M. A., Almoammar, H., Rai, M., Said-Galiev, E. and Abd-Elsalam, K. A. 2015. Myconanoparticles: synthesis and their role in phytopathogens management. Biotechnology and Biotechnological Equipment, 29: 221-236.

Ali, M., Ahmad, H., Amin, B., Atif, M. J. and Cheng, Z. 2022. Induce defense response of DADS in Eggplants during the biotrophic phase of *Verticillium dahliae*. BMC Plant Biology, 22: 1-15.

Amargeetha, A. and Velavan, S. 2018. X-ray diffraction (XRD) and energy dispersive spectroscopy (EDS) analysis of silver nanoparticles synthesized from *Erythrina indica* flowers. Nanoscience and Technology, 5: 1-5.

Amira, M. B., Lopez, D., Mohamed, A. T., Khouaja, A., Chaar, H., Fumanal, B., Gousset-Dupont, A., Bonhomme, L., Label, P. and Goupil, P. 2017. Beneficial effect of *Trichoderma harzianum* strain Ths97 in biocontrolling *Fusarium solani* causal agent of root rot disease in olive trees. Biological Control, 110: 70-78.

Anders, S., Pyl, P. T. and Huber, W. 2015. HTSeq—a Python framework to work with high-throughput sequencing data. Bioinformatics, 31: 166-169.

Angelopoulou, D. J., Naska, E. J., Paplomatas, E. J. and Tjamos, S. E. 2014. Biological control agents (BCAs) of *Verticillium* wilt: influence of application rates and delivery method on plant protection, triggering of host defence mechanisms and rhizosphere populations of BCAs. Plant Pathology, 63: 1062-1069.

Anita, S., Ponmurugan, P. and Babu, R. G. 2012. Significance of secondary metabolites and enzymes secreted by *Trichoderma atroviride* isolates for the biological control of *Phomopsis* canker disease. African Journal of Biotechnology, 11: 10350-10357.

Anitha, R. and Murugesan, K. 2005. Production of gliotoxin on natural substrates by *Trichoderma virens*. Journal of Basic Microbiology, 45: 12-19.

Arya, S., Sonawane, H., Math, S., Tambade, P., Chaskar, M. and Shinde, D. 2020. Biogenic titanium nanoparticles (TiO 2 NPs) from *Tricoderma citrinoviride* extract: synthesis, characterization and antibacterial activity against extremely drug-resistant *Pseudomonas aeruginosa*. International Nano Letters, 13: 1-8.

Atanasova, L., Crom, S. L., Gruber, S., Coulpier, F., Seidl-Seiboth, V., Kubicek, C. P. and Druzhinina, I. S. 2013. Comparative transcriptomics reveals different strategies of *Trichoderma* mycoparasitism. BMC Genomics, 14: 1-15.

Atibalentja, N. and Eastburn, D. M. 1997. Evaluation of inoculation methods for screening horseradish cultivars for resistance to *Verticillium dahliae*. Plant Disease, 81: 356-362.

Bae, S., Mohanta, T. K., Chung, J. Y., Ryu, M., Park, G., Shim, S., Hong, S., Seo, H., Bae, D. and Bae, I. 2016. *Trichoderma* metabolites as biological control agents against Phytophthora pathogens. Biological Control, 92: 128-138.

Baek, J., Howell, C. R. and Kenerley, C. M. 1999. The role of an extracellular chitinase from *Trichoderma virens* Gv29-8 in the biocontrol of *Rhizoctonia solani*. Current Genetics, 35: 41-50.

Bahrami-Teimoori, B., Nikparast, Y., Hojatianfar, M., Akhlaghi, M., Ghorbani, R. and Pourianfar, H. R. 2017. Characterisation and antifungal activity of silver nanoparticles biologically synthesised by *Amaranthus retroflexus* leaf extract. Journal of Experimental Nanoscience, 12: 129-139.

Banerjee, K. and Rai, V. R. 2018. A review on mycosynthesis, mechanism, and characterization of silver and gold nanoparticles. BioNanoScience, 8: 17-31.

Barchenger, D. W., Lamour, K. H. and Bosland, P. W. 2018. Challenges and strategies for breeding resistance in *Capsicum annuum* to the multifarious pathogen, *Phytophthora capsici*. Frontiers in Plant Science, 9: 628.

Bardin, M., Ajouz, S., Comby, M., Lopez-Ferber, M., Graillot, B., Siegwart, M. and Nicot, P. C. 2015. Is the efficacy of biological control against plant diseases likely to be more durable than that of chemical pesticides. Frontiers in Plant Science, 6: 566.

Bell, A. A. and Wheeler, M. H. 1986. Biosynthesis and functions of fungal melanins. Annual Review of Phytopathology, 24: 411-451.

Benítez, T., Rincón, A. M., Limón, M. C. and Codon, A. C. 2004. Biocontrol mechanisms of *Trichoderma* strains. International Microbiology, 7: 249-260.

Berdy, J. 2005. Bioactive microbial metabolites. The Journal of Antibiotics, 58: 1-26.

Bhainsa, K. C. and D'souza, S. F. 2006. Extracellular biosynthesis of silver nanoparticles using the fungus *Aspergillus fumigatus*. Colloids and Surfaces B: Biointerfaces, 47: 160-164.

Bilesky-Jose, N., Maruyama, C., Germano-Costa, T., Campos, E., Carvalho, L., Grillo, R., Fraceto, L. F. and De Lima, R. 2021. Biogenic α-Fe2O3 nanoparticles enhance the biological activity of *Trichoderma* against the plant pathogen *Sclerotinia sclerotiorum*. ACS Sustainable Chemistry and Engineering, 9: 1669-1683.

Bissett, J. 1984. A revision of the genus *Trichoderma*. I. Section *Longibrachiatum* sect. nov. Canadian Journal of Botany, 62: 924-931.

Bissett, J. 1991. A revision of the genus *Trichoderma*. II. Infrageneric classification. Canadian Journal of Botany, 69: 2357-2372.

Bissett, J., Gams, W., Jaklitsch, W. and Samuels, G. J. 2015. Accepted *Trichoderma* names in the year 2015. IMA Fungus, 6: 263-295.

Bissett, J., Szakacs, G., Nolan, C. A., Druzhinina, I., Gradinger, C. and Kubicek, C. P. 2003. New species of *Trichoderma* from Asia. Canadian Journal of Botany, 81: 570-586.

Bogumił, A., Paszt, L. S., Lisek, A., Trzciński, P. and Harbuzov, A. 2013. Identification of new *Trichoderma* strains with antagonistic activity against *Botrytis cinerea*. Folia Horticulturae, 25: 123-132.

Boland, G. J. and Hall, R. 1994. Index of plant hosts of *Sclerotinia sclerotiorum*. Canadian Journal of Plant Pathology, 16: 93-108.

Bolton, M. D., Thomma, B. P. H. J. and Nelson, B. D. 2006. *Sclerotinia sclerotiorum* (Lib.) de Bary: biology and molecular traits of a cosmopolitan pathogen. Molecular Plant Pathology, 7: 1-16.

Bose, A. K., Das, K. G., Funke, P. T., Kugajevsky, I., Shukla, O., Khanchandani, K. S. and Suhadolnik, R. J. 1968. Biosynthetic studies on gliotoxin using stable isotopes and mass spectral methods. Journal of the American Chemical Society, 90: 1038-1041.

Bosland, P. and Lindsey, D. 1991. A seedling screen for *Phytophthora* root rot of pepper, *Capsicum annuum*. Plant Disease, 75: 1048-1050.

Bosland, P. W. 2008. Think global, breed local: specificity and complexity of *Phytophthora capsici*. In Think global, breed local: specificity and complexity of *Phytophthora capsici*, 19th International Pepper Conference. Atlantic City, NJ.

Brian, P. W. 1944. Production of gliotoxin by *Trichoderma viride*. Nature, 154: 667-668.

Brian, P. W. and Hemming, H. G. 1945. Gliotoxin, a fungistatic metabolic product of *Trichoderma viride*. Annals of Applied Biology, 32: 214-220.

Cai, F. and Druzhinina, I. S. 2021. In honor of John Bissett: authoritative guidelines on molecular identification of Trichoderma. Fungal Diversity, 107: 1-69.

Callaghan, S. E., Williams, A. P., Burgess, T., White, D., Keovorlajak, T., Phitsanoukane, P., Phantavong, S., Vilavong, S., Ireland, K. B. and Duckitt, G. S. 2016. First report of *Phytophthora capsici* in the Lao PDR. Australasian Plant Disease Notes, 11: 1-4.

Cao, R., Liu, X., Gao, K., Mendgen, K., Kang, Z., Gao, J., Dai, Y. and Wang, X. 2009. Mycoparasitism of endophytic fungi isolated from reed on soilborne phytopathogenic fungi and production of cell wall-degrading enzymes in vitro. Current Microbiology, 59: 584-592.

Carbone, I. and Kohn, L. M. 1999. A method for designing primer sets for speciation studies in filamentous ascomycetes. Mycologia, 91: 553-556.

Carrero-Carrón, I., Trapero-Casas, J. L., Olivares-García, C., Monte, E., Hermosa, R. and Jiménez-Díaz, R. M. 2016. *Trichoderma asperellum* is effective for biocontrol of *Verticillium* wilt in olive caused by the defoliating pathotype of *Verticillium dahliae*. Crop Protection, 88: 45-52.

Caseiro, C., Dias, J. N., de Andrade Fontes, C. M. and Bule, P. 2022. From cancer therapy to winemaking: The molecular structure and applications of β-glucans and β-1, 3-glucanases. International Journal of Molecular Sciences, 23: 3156.

Castro-Longoria, E., Vilchis-Nestor, A. R. and Avalos-Borja, M. 2011. Biosynthesis of silver, gold and bimetallic nanoparticles using the filamentous fungus *Neurospora crassa*. Colloids and Surfaces B: Biointerfaces, 83: 42-48.

Catalano, V., Vergara, M., Hauzenberger, J. R., Seiboth, B., Sarrocco, S., Vannacci, G., Kubicek, C. P. and Seidl-Seiboth, V. 2011. Use of a non-homologous end-joining-deficient strain (delta-ku70) of the biocontrol fungus *Trichoderma virens* to investigate the function of the laccase gene lcc1 in sclerotia degradation. Current Genetics, 57: 13-23.

Chang, C. and Stewart, R. C. 1998. The two-component system: regulation of diverse signaling pathways in prokaryotes and eukaryotes. Plant Physiology, 117: 723-731.

Chaverri, P., Branco-Rocha, F., Jaklitsch, W., Gazis, R., Degenkolb, T. and Samuels, G. J. 2015. Systematics of the *Trichoderma harzianum* species complex and the re-identification of commercial biocontrol strains. Mycologia, 107: 558-590.

Chaverri, P., Gazis, R. O. and Samuels, G. J. 2011. *Trichoderma amazonicum*, a new endophytic species on *Hevea brasiliensis* and *H. guianensis* from the Amazon basin. Mycologia, 103: 139-151.

Chaverri, P. and Samuels, G. J. 2003. *Hypocrea/Trichoderma* (ascomycota, hypocreales, hypocreaceae): species with green ascospores. Studies in Mycology, 48: 1-116.

Chen, D., Hou, Q., Jia, L. and Sun, K. 2021. Combined use of two *Trichoderma* strains to promote growth of pakchoi (*Brassica chinensis* L.). Agronomy, 11: 726.

Chen, J., Wu, L., Lu, M., Lu, S., Li, Z. and Ding, W. 2020. Comparative study on the fungicidal activity of metallic MgO nanoparticles and macroscale MgO against soilborne fungal phytopathogens. Frontiers in Microbiology, 11: 365.

Chen, K., Li, J.-S., Zhang, G.-Z. and Zho, X.-Y. 2016. The Identification and Functional Assessmentof *Trichoderma gamsii* Strain TW20050. Science Technology and Engineering, 16: 156-160.

Chen, K. and Zhuang, W.-Y. 2017. Discovery from a large-scaled survey of *Trichoderma* in soil of China. Scientific Reports, 7: 9090.

Chen, M., Liu, Q., Gao, S., Young, A. E., Jacobsen, S. E. and Tang, Y. 2019. Genome mining and biosynthesis of a polyketide from a biofertilizer fungus that can facilitate reductive iron assimilation in plant. Proceedings of the National Academy of Sciences, 116: 5499-5504.

Cherkupally, R., Amballa, H. and Reddy, B. N. 2017. In vitro screening for enzymatic activity of *Trichoderma* species for biocontrol potential. Annals Plant Sciences, 6: 1784-1789.

Chet, I. and Inbar, J. 1994. Biological control of fungal pathogens. Applied Biochemistry and Biotechnology, 48: 37-43.

Coley-Smith, J. R. and Cooke, R. C. 1971. Survival and germination of fungal sclerotia. Annual Review of Phytopathology, 9: 65-92.

Consolo, V. F., Torres-Nicolini, A. and Alvarez, V. A. 2020. Mycosinthetized Ag, CuO and ZnO nanoparticles from a promising *Trichoderma harzianum* strain and their antifungal potential against important phytopathogens. Scientific Reports, 10: 1-9.

Contreras-Cornejo, H. A., Macías-Rodríguez, L., Cortés-Penagos, C. and López-Bucio, J. 2009. *Trichoderma virens*, a plant beneficial fungus, enhances biomass production and promotes lateral root growth through an auxin-dependent mechanism in *Arabidopsis*. Plant Physiology, 149: 1579-1592.

D'ercole, N., Nipoti, P., Di Pillo, L. and Gavina, F. 2000. In vitro and in vivo tests of *Trichoderma* spp. as a biocontrol agent of *Verticillium dahliae* Kleb. in eggplants. In

Advances in *Verticillium*: Research and Disease Management, , ed. Rowe R. C. Tjamos E. C., Heale J. B., Fravel D. R., 260-263. St. Paul, MN,USA: APS Press, .

Daintith, J. and Martin, E. 2005. A Dictionary of Science (Oxford Paperback Reference Series).

Dakal, T. C., Kumar, A., Majumdar, R. S. and Yadav, V. 2016. Mechanistic basis of antimicrobial actions of silver nanoparticles. Frontiers in Microbiology, 7: 1831.

Darriba, D., Taboada, G. L., Doallo, R. and Posada, D. 2012. jModelTest 2: more models, new heuristics and parallel computing. Nature Methods, 9: 772-772.

Degenkolb, T., Dieckmann, R., Nielsen, K. F., Gräfenhan, T., Theis, C., Zafari, D., Chaverri, P., Ismaiel, A., Brückner, H. and Von Döhren, H. 2008. The *Trichoderma brevicompactum* clade: a separate lineage with new species, new peptaibiotics, and mycotoxins. Mycological Progress, 7: 177-219.

Dennis, C. and Webster, J. 1971. Antagonistic properties of species-groups of *Trichoderma*: I. Production of non-volatile antibiotics. Transactions of the British Mycological Society, 57: 25-IN23.

Devi, T. P., Kulanthaivel, S., Kamil, D., Borah, J. L., Prabhakaran, N. and Srinivasa, N. 2013. Biosynthesis of silver nanoparticles from *Trichoderma* species. Indian Journal of Experimental Biology, 51: 543-547.

Devi, T. P., Prabhakaran, N. and Deeba, K. 2017. Development of species specific markers for the identification of *Trichoderma asperellum* and *Trichoderma harzianum*. Vegetos, 30: 94-100.

Di Pietro, A., Lorito, M., Hayes, C. K., Broadway, R. M. and Harman, G. E. 1993. Endochitinase from *Gliocladium virens:* isolation, characterization, and synergistic antifungal activity in combination with gliotoxin. Phytopathology, 83: 308-318.

Diener, S. E., Chellappan, M. K., Mitchell, T. K., Dunn-Coleman, N., Ward, M. and Dean, R. A. 2004. Insight into *Trichoderma reesei* genome content, organization and evolution revealed through BAC library characterization. Fungal Genetics and Biology, 41: 1077-1087.

Djonovic, S., Pozo, M. J. and Kenerley, C. M. 2006. Tvbgn3, a β-1, 6-glucanase from the biocontrol fungus *Trichoderma virens*, is involved in mycoparasitism and control of *Pythium ultimum*. Applied and Environmental Microbiology, 72: 7661-7670.

Djonović, S., Vittone, G., Mendoza-Herrera, A. and Kenerley, C. M. 2007. Enhanced biocontrol activity of *Trichoderma virens* transformants constitutively coexpressing β-1, 3-and β-1, 6-glucanase genes. Molecular Plant Pathology, 8: 469-480.

Dodd, S. L., Lieckfeldt, E. and Samuels, G. J. 2003. *Hypocrea atroviridis* sp. nov., the teleomorph of *Trichoderma atroviride*. Mycologia, 95: 27-40.

Druzhinina, I. and Kopchinski, A. 2006. TrichOKEY v. 2-a DNA oligonucliotide BarCode program for the identification of multiple seqences of *Hypocrea* and *Trichoderma*. In TrichOKEY v. 2-a DNA oligonucliotide BarCode program for the identification of multiple seqences of *Hypocrea* and *Trichoderma*, IMC8 2006 Cairns, 53-59. Cairns, Australia. Medimond S.r.l, Bologna, Italy.: Medimond-Monduzzi Editore International.

Druzhinina, I. and Kubicek, C. P. 2005. Species concepts and biodiversity in *Trichoderma* and *Hypocrea*: from aggregate species to species clusters? Journal of Zhejiang University Science B, 6: 100.

Druzhinina, I. S., Kopchinskiy, A. G., Komoń, M., Bissett, J., Szakacs, G. and Kubicek, C. P. 2005. An oligonucleotide barcode for species identification in *Trichoderma* and *Hypocrea*. Fungal Genetics and Biology, 42: 813-828.

Druzhinina, I. S., Seidl-Seiboth, V., Herrera-Estrella, A., Horwitz, B. A., Kenerley, C. M., Monte, E., Mukherjee, P. K., Zeilinger, S., Grigoriev, I. V. and Kubicek, C. P. 2011. *Trichoderma*: the genomics of opportunistic success. Nature Reviews Microbiology, 9: 749-759.

du Plessis, I. L., Druzhinina, I. S., Atanasova, L., Yarden, O. and Jacobs, K. 2018. The diversity of *Trichoderma* species from soil in South Africa, with five new additions. Mycologia, 110: 559-583.

Dunn, A. R. and Smart, C. D. 2015. Interactions of *Phytophthora capsici* with resistant and susceptible pepper roots and stems. Phytopathology, 105: 1355-1361.

Duressa, D., Anchieta, A., Chen, D., Klimes, A., Garcia-Pedrajas, M. D., Dobinson, K. F. and Klosterman, S. J. 2013. RNA-seq analyses of gene expression in the microsclerotia of *Verticillium dahliae*. BMC Genomics, 14: 1-18.

El-Hasan, A., Walker, F., Schöne, J. and Buchenauer, H. 2009. Detection of viridiofungin A and other antifungal metabolites excreted by *Trichoderma harzianum* active against different plant pathogens. European Journal of Plant Pathology, 124: 457-470.

El-Moslamy, S. H., Elkady, M. F., Rezk, A. H. and Abdel-Fattah, Y. R. 2017. Applying Taguchi design and large-scale strategy for mycosynthesis of nano-silver from endophytic *Trichoderma harzianum* SYA. F4 and its application against phytopathogens. Scientific Reports, 7: 1-22.

El-Rafai, I. M., Asswah, S. M. and Awdalla, O. A. 2003. Biocontrol of some tomato disease using some antagonistic microorganisms. Pakistan Journal of Biological Sciences (Pakistan), 6: 399-406.

Elad, Y., Chet, I. and Henis, Y. 1981. A selective medium for improving quantitative isolation of *Trichoderma* spp. from soil. Phytoparasitica, 9: 59-67.

Elamawi, R. M., Al-Harbi, R. E. and Hendi, A. A. 2018. Biosynthesis and characterization of silver nanoparticles using *Trichoderma longibrachiatum* and their effect on phytopathogenic fungi. Egyptian Journal of Biological Pest Control, 28: 1-11.

Ezziyyani, M., Requena, M., Egea-Gilabert, C. and Candela, M. 2007. Biological control of Phytophthora root rot of pepper using *Trichoderma harzianum* and *Streptomyces rochei* in combination. Journal of Phytopathology, 155: 342-349.

Faostat. 2011. Food and Agriculture Organization of the United Nations. FAO, 2011, 11: 1817-7077.

Farhat, M., Haggag, W., Thabet, M. and Mosa, A. 2018. Efficacy of silicon and titanium nanoparticles biosynthesis by some antagonistic fungi and bacteria for controlling powdery mildew disease of wheat plants. Technology, 14: 661-674.

Fayaz, A. M., Balaji, K., Girilal, M., Yadav, R., Kalaichelvan, P. T. and Venketesan, R. 2010. Biogenic synthesis of silver nanoparticles and their synergistic effect with antibiotics: a study against gram-positive and gram-negative bacteria. Nanomedicine: Nanotechnology, Biology and Medicine, 6: 103-109.

Ferguson, B. J. and Beveridge, C. A. 2009. Roles for auxin, cytokinin, and strigolactone in regulating shoot branching. Plant Physiology, 149: 1929-1944.

Ferreira, F. V. and Musumeci, M. A. 2021. *Trichoderma* as biological control agent: Scope and prospects to improve efficacy. World Journal of Microbiology and Biotechnology 37: 1-17.

Firdhouse, M. J. and Lalitha, P. 2015. Biosynthesis of silver nanoparticles and its applications. Journal of Nanotechnology, 28: 1-15.

Flores, A., Chet, I. and Herrera-Estrella, A. 1997. Improved biocontrol activity of *Trichoderma harzianum* by over-expression of the proteinase-encoding gene prb1. Current Genetics, 31: 30-37.

Foster, J. M. and Hausbeck, M. K. 2010. Resistance of pepper to Phytophthora crown, root, and fruit rot is affected by isolate virulence. Plant Disease, 94: 24-30.

Fotoohiyan, Z., Rezaee, S., Bonjar, G. H., Mohammadi, A. H. and Moradi, M. 2017. Biocontrol potential of *Trichoderma harzianum* in controlling wilt disease of pistachio caused by *Verticillium dahliae*. Journal of Plant Protection Research, 57: 185-193.

Fradin, E. F. and Thomma, B. 2006. Physiology and molecular aspects of *Verticillium* wilt diseases caused by *Verticillium dahliae* and *Verticillium albo-atrum*. Molecular Plant Pathology, 7: 71-86.

Fravel, D. R. 1988. Role of antibiosis in the biocontrol of plant diseases. Annual Review of Phytopathology, 26: 75-91.

Gams, W. and Bissett, J. 2002. Morphology and identification of *Trichoderma* and *Glioclodium*. In Basic biology, taxonomy and genetics, ed. Harman GE (Eds) In: Kubicek CP, 3-31. Lindon: Taylor and Francis Ltd.

Gams, W., Bissett, J., Kubicek, C. and Harman, G. 1998. *Trichoderma* and *Gliocladium*. Vol. 1. Basic biology, taxonomy and genetics. Taylor & Francis, London.

Gardiner, D. M., Waring, P. and Howlett, B. J. 2005. The epipolythiodioxopiperazine (ETP) class of fungal toxins: distribution, mode of action, functions and biosynthesis. Microbiology, 151: 1021-1032.

Gemishev, O. T., Panayotova, M. I., Mintcheva, N. N., Djerahov, L. P., Tyuliev, G. T. and Gicheva, G. D. 2019. A green approach for silver nanoparticles preparation by cell-free extract from *Trichoderma reesei* fungi and their characterization. Materials Research Express, 6: 095040.

Gerbore, J., Benhamou, N., Vallance, J., Le Floch, G., Grizard, D., Regnault-Roger, C. and Rey, P. 2014. Biological control of plant pathogens: advantages and limitations seen through the case study of *Pythium oligandrum*. Environmental Science and Pollution Research, 21: 4847-4860.

Ghisalberti, E. L. and Sivasithamparam, K. 1991. Antifungal antibiotics produced by *Trichoderma* spp. Soil Biology and Biochemistry, 23: 1011-1020.

Giardina, P., Faraco, V., Pezzella, C., Piscitelli, A., Vanhulle, S. and Sannia, G. 2010. Laccases: a never-ending story. Cellular and Molecular Life Sciences, 67: 369-385.

Glickmann, E. and Dessaux, Y. 1995. A critical examination of the specificity of the Salkowski reagent for indolic compounds produced by phytopathogenic bacteria. Applied and Environmental Microbiology, 61: 793-796.

Gnanamangai, B. M., Ponmurugan, P., Jeeva, S. E., Manjukarunambika, K., Elango, V., Hemalatha, K., Kakati, J. P., Mohanraj, R. and Prathap, S. 2017. Biosynthesised silver and copper nanoformulation as foliar spray to control bird's eye spot disease in tea plantations. IET Nanobiotechnology, 11: 917-928.

Granke, L. L., Quesada-Ocampo, L., Lamour, K. and Hausbeck, M. K. 2012. Advances in research on *Phytophthora capsici* on vegetable crops in the United States. Plant Disease, 96: 1588-1600.

Gravel, V., Antoun, H. and Tweddell, R. J. 2007. Growth stimulation and fruit yield improvement of greenhouse tomato plants by inoculation with *Pseudomonas putida* or *Trichoderma atroviride*: possible role of indole acetic acid (IAA). Soil Biology and Biochemistry, 39: 1968-1977.

Griffiths, D. A. 1970. The fine structure of developing microsclerotia of *Verticillium dahliae* Kleb. Archiv für Mikrobiologie, 74: 207-212.

Grovel, O., Pouchus, Y. F., du Pont, T. R., Montagu, M., Amzil, Z. and Verbist, J.-F. 2002. Ion trap MSn for identification of gliotoxin as the cytotoxic factor of a marine strain of *Aspergillus fumigatus* Fresenius. Journal of Microbiological Methods, 48: 171-179.

Gruber, S. and Zeilinger, S. 2014. The transcription factor Ste12 mediates the regulatory role of the Tmk1 MAP kinase in mycoparasitism and vegetative hyphal fusion in the filamentous fungus *Trichoderma atroviride*. PloS ONE, 9: e111636.

Gu, X., Wang, R., Sun, Q., Wu, B. and Sun, J.-Z. 2020. Four new species of *Trichoderma* in the *Harzianum* clade from northern China. MycoKeys, 73: 109.

Guilger-Casagrande, M. and Lima, R. d. 2019. Synthesis of silver nanoparticles mediated by fungi: a review. Frontiers in Bioengineering and Biotechnology, 7: 287.

Guilger, M., Pasquoto-Stigliani, T., Bilesky-Jose, N., Grillo, R., Abhilash, P. C., Fraceto, L. F. and De Lima, R. 2017. Biogenic silver nanoparticles based on *Trichoderma harzianum*:

synthesis, characterization, toxicity evaluation and biological activity. Scientific Reports, 7: 1-13.

Guo, R., Wang, Z., Zhou, C., Liu, Z., Zhang, P. and Fan, H. 2020. Transcriptomic analysis reveals biocontrol mechanisms of *Trichoderma harzianum* ACCC30371 under eight culture conditions. Journal of Forestry Research, 31: 1863-1873.

Gupta, K., Jana, P. C. and Meikap, A. K. 2010. Optical and electrical transport properties of polyaniline–silver nanocomposite. Synthetic Metals, 160: 1566-1573.

Gupta, R. K., Kumar, V., Gundampati, R. K., Malviya, M., Hasan, S. H. and Jagannadham, M. V. 2017. Biosynthesis of silver nanoparticles from the novel strain of *Streptomyces* Sp. BHUMBU-80 with highly efficient electroanalytical detection of hydrogen peroxide and antibacterial activity. Journal of Environmental Chemical Engineering, 5: 5624-5635.

Halifu, S., Deng, X., Song, X. and Song, R. 2019. Effects of two *Trichoderma* strains on plant growth, rhizosphere soil nutrients, and fungal community of *Pinus sylvestris* var. *mongolica* annual seedlings. Forests, 10: 758.

Halifu, S., Deng, X., Song, X., Song, R. and Liang, X. 2020. Inhibitory mechanism of *Trichoderma virens* ZT05 on *Rhizoctonia solani*. Plants, 9: 912.

Hall, T. A. 1999. BioEdit: a user-friendly biological sequence alignment editor and analysis program for Windows 95/98/NT. Nucleic Acids Symposium Series, 41: 95-98.

Harman, G. E. 2006. Overview of mechanisms and uses of *Trichoderma* spp. Phytopathology, 96: 190-194.

Harman, G. E., Howell, C. R., Viterbo, A., Chet, I. and Lorito, M. 2004. *Trichoderma* species— opportunistic, avirulent plant symbionts. Nature Reviews Microbiology, 2: 43-56.

Hartman, G. L. and Wang, T. C. 1992. *Phytophthora* blight of pepper: screening for disease resistance. International Journal of Pest Management, 38: 319-322.

Hausbeck, M. K. and Lamour, K. H. 2004. *Phytophthora capsici* on vegetable crops: research progress and management challenges. Plant Disease, 88: 1292-1303.

He, D., Zhan, J. and Xie, L. 2016. Problems, challenges and future of plant disease management: from an ecological point of view. Journal of Integrative Agriculture, 15: 705-715.

Hebbar, K. P. and Lumsden, R. D. 1999. Biological control of seedling diseases. In Biopesticides: Use and Delivery, 103-116: Springer.

Hirpara, D. G. and Gajera, H. 2020. Green synthesis and antifungal mechanism of silver nanoparticles derived from chitin-induced exometabolites of *Trichoderma interfusant*. Applied Organometallic Chemistry, 34: e5407.

Holt, R. D. and Hochberg, M. E. 1997. When is biological control evolutionarily stable (or is it)? Ecology, 78: 1673-1683.

Howell, C. R. 1998. The role of antibiosis in biocontrol. In *Trichoderma* and *Gliocladium*, ed. G.E. In: Harman, Kubicek, C.P. (Eds.), 173e184.: Taylor and Francis, London.

Howell, C. R., Stipanovic, R. D. and Lumsden, R. D. 1993. Antibiotic production by strains of *Gliocladium virens* and its relation to the biocontrol of cotton seedling diseases. Biocontrol Science and Technology, 3: 435-441.

Hoyos-Carvajal, L., Orduz, S. and Bissett, J. 2009. Growth stimulation in bean (*Phaseolus vulgaris* L.) by *Trichoderma*. Biological Control, 51: 409-416.

Hu, D., Yu, S., Yu, D., Liu, N., Tang, Y., Fan, Y., Wang, C. and Wu, A. 2019. Biogenic *Trichoderma harzianum*-derived selenium nanoparticles with control functionalities originating from diverse recognition metabolites against phytopathogens and mycotoxins. Food Control, 106: 106748.

Hu, M., Li, Q. L., Yang, Y.-B., Liu, K., Miao, C.P., Zhao, L. X. and Ding, Z. T. 2017. Koninginins RS from the endophytic fungus *Trichoderma koningiopsis*. Natural Product Research, 31: 835-839.

Hu, X., Bai, Y., Chen, T., Hu, D., Yang, J. and Xu, X. 2013. An optimized method for in vitro production of *Verticillium dahliae* microsclerotia. European Journal of Plant Pathology, 136: 225-229.

Hua, L., Zeng, H., He, L., Jiang, Q., Ye, P., Liu, Y., Sun, X. and Zhang, M. 2021. Gliotoxin Is an Important Secondary Metabolite Involved in Suppression of *Sclerotium Rolfsii* of *Trichoderma virens* T23. Phytopathology, 111: 1720-1725.

Hussain, S. A., Noorani, R. and Qureshi, I. H. 1975. Isolation and characterization of gliotoxin, ergosterol, palmitic acid and mannitol–metabolic products of *Trichoderma hamatum* Bainier. Pakistan Journal of Scientific and Industrial Research, 18: 221-223.

Hyakumachi, M. 1994. Plant-growth-promoting fungi from turfgrass rhizosphere with potential for disease suppression. Soil Microorganisms, 44: 53-68.

Hyakumachi, M., Nishimura, M., Arakawa, T., Asano, S., Yoshida, S., Tsushima, S. and Takahashi, H. 2012. *Bacillus thuringiensis* suppresses bacterial wilt disease caused by *Ralstonia solanacearum* with systemic induction of defense-related gene expression in tomato. Microbes and Environments, 28: 128-134.

Ingle, A., Gade, A., Pierrat, S., Sonnichsen, C. and Rai, M. 2008. Mycosynthesis of silver nanoparticles using the fungus *Fusarium acuminatum* and its activity against some human pathogenic bacteria. Current Nanoscience, 4: 141-144.

Innocenti, G., Montanari, M., Righini, H. and Roberti, R. 2019. Trichoderma species associated with green mould disease of *Pleurotus ostreatus* and their sensitivity to prochloraz. Plant Pathology, 68: 392-398.

Iravani, S., Korbekandi, H., Mirmohammadi, S. V. and Zolfaghari, B. 2014. Synthesis of silver nanoparticles: chemical, physical and biological methods. Research in Pharmaceutical Sciences, 9: 385-406.

Jabnoun-Khiareddine, H., Daami-Remadi, M., Ayed, F. and El Mahjoub, M. 2009. Biological control of tomato *Verticillium* wilt by using indigenous *Trichoderma* spp. The African Journal of Plant Science and Biotechnology, 3: 26-36.

Jain, N., Bhargava, A., Majumdar, S., Tarafdar, J. C. and Panwar, J. 2011. Extracellular biosynthesis and characterization of silver nanoparticles using *Aspergillus flavus* NJP08: a mechanism perspective. Nanoscale, 3: 635-641.

Jaklitsch, W. M. 2009. European species of *Hypocrea* Part I. The green-spored species. Studies in Mycology, 63: 1-91.

Jaklitsch, W. M. 2011. European species of *Hypocrea* part II: species with hyaline ascospores. Fungal Diversity, 48: 1-250.

Jaklitsch, W. M., Kubicek, C. P. and Druzhinina, I. S. 2008. Three European species of *Hypocrea* with reddish brown stromata and green ascospores. Mycologia 100: 796-815.

Jaklitsch, W. M., Stadler, M. and Voglmayr, H. 2012. Blue pigment in *Hypocrea caerulescens* sp. nov. and two additional new species in sect. *Trichoderma*. Mycologia, 104: 925-941.

Jaklitsch, W. M. and Voglmayr, H. 2011. *Nectria eustromatica* sp. nov., an exceptional species with a hypocreaceous stroma. Mycologia, 103: 209-218.

Jaklitsch, W. M. and Voglmayr, H. 2012. *Hypocrea britdaniae* and *H. foliicola*: two remarkable new European species. Mycologia, 104: 1213-1221.

Jaklitsch, W. M. and Voglmayr, H. 2013. New combinations in *Trichoderma* (Hypocreaceae, Hypocreales). Mycotaxon, 126: 143-156.

Jaklitsch, W. M. and Voglmayr, H. 2015. Biodiversity of *Trichoderma* (Hypocreaceae) in Southern Europe and Macaronesia. Studies in Mycology, 80: 1-87.

Jeevan, P., Ramya, K. and Rena, A. E. 2012. Extracellular biosynthesis of silver nanoparticles by culture supernatant of *Pseudomonas aeruginosa*. Indian Journal of Biotechnology, 11: 72-76.

Jeleń, H., Błaszczyk, L., Chełkowski, J., Rogowicz, K. and Strakowska, J. 2014. Formation of 6-n-pentyl-2H-pyran-2-one (6-PAP) and other volatiles by different *Trichoderma* species. Mycological Progress, 13: 589-600.

Ji, S., Liu, Z., Liu, B. and Wang, Y. 2019. Comparative analysis of biocontrol agent *Trichoderma asperellum* ACCC30536 transcriptome during its interaction with *Populus davidiana× P. alba* var. *pyramidalis*. Microbiological Research, 227: 126294.

Jiang, H., Zhang, L., Zhang, J., Ojaghian, M. R. and Hyde, K. D. 2016a. Antagonistic interaction between *Trichoderma asperellum* and *Phytophthora capsici* in *in vitro*. Journal of Zhejiang University Science B, 17: 271-281.

Jiang, Y., Wang, J. L., Chen, J., Mao, L. J., Feng, X. X., Zhang, C. L. and Lin, F. C. 2016b. *Trichoderma* biodiversity of agricultural fields in east China reveals a gradient distribution of species. PLoS ONE, 11: e0160613.

Jones, R. W. and Pettit, R. E. 1987. Variation sensitivity among anastomosis groups of *Rhizoctonia solani* to the antibiotic gliotoxin. Plant Disease, 71: 34-36.

Joshi, S. M., De Britto, S., Jogaiah, S. and Ito, S.I. 2019. Mycogenic selenium nanoparticles as potential new generation broad spectrum antifungal molecules. Biomolecules, 9: 419.

Kamala, T., Devi, S. I., Sharma, K. C. and Kennedy, K. 2015. Phylogeny and taxonomical investigation of *Trichoderma* spp. from Indian region of Indo-Burma biodiversity hot spot region with special reference to Manipur. BioMed Research International, 2015: 285261.

Katoh, K. and Standley, D. M. 2013. MAFFT multiple sequence alignment software version 7: improvements in performance and usability. Molecular Biology and Evolution, 30: 772-780.

Kaur, P. 2018. Biosynthesis of nanoparticles using eco-friendly factories and their role in plant pathogenicity: a review. Biotechnology Research and Innovation, 2: 63-73.

Khan, R. A. A., Najeeb, S., Hussain, S., Xie, B. and Li, Y. 2020. Bioactive secondary metabolites from *Trichoderma* spp. against phytopathogenic fungi. Microorganisms, 8: 817.

Kim, C. S., Shirouzu, T., Nakagiri, A., Sotome, K. and Maekawa, N. 2013. *Trichoderma eijii* and *T. pseudolacteum*, two new species from Japan. Mycological Progress, 12: 739-753.

Kim, D., Langmead, B. and Salzberg, S. L. 2015. HISAT: a fast spliced aligner with low memory requirements. Nature Methods, 12: 357-360.

Kim, S.-H., Lee, H.-S., Ryu, D.-S., Choi, S.-J. and Lee, D.-S. 2011. Antibacterial activity of silver-nanoparticles against *Staphylococcus aureus* and *Escherichia coli*. Microbiology and Biotechnology Letters, 39: 77-85.

Kloepper, J. W. and Schroth, M. N. 1981. Development of a powder formulation of rhizobacteria for inoculation of potato seed pieces. Phytopathology, 71: 590-592.

Köhl, J., Kolnaar, R. and Ravensberg, W. J. 2019. Mode of action of microbial biological control agents against plant diseases: relevance beyond efficacy. Frontiers in Plant Science, 10: 845.

Kraus, G. F., Druzhinina, I., Gams, W., Bissett, J., Zafari, D., Szakacs, G., Koptchinski, A., Prillinger, H., Zare, R. and Kubicek, C. P. 2004. *Trichoderma brevicompactum* sp. nov. Mycologia, 96: 1059-1073.

Kubicek, C. P., Bissett, J., Druzhinina, I., Kullnig-Gradinger, C. and Szakacs, G. 2003. Genetic and metabolic diversity of *Trichoderma*: a case study on South-East Asian isolates. Fungal Genetics and Biology, 38: 310-319.

Kubicek, C. P., Herrera-Estrella, A., Seidl-Seiboth, V., Martinez, D. A., Druzhinina, I. S., Thon, M., Zeilinger, S., Casas-Flores, S., Horwitz, B. A. and Mukherjee, P. K. 2011. Comparative genome sequence analysis underscores mycoparasitism as the ancestral life style of *Trichoderma*. Genome Biology, 12: 1-15.

Kullnig-Gradinger, C. M., Szakacs, G. and Kubicek, C. P. 2002. Phylogeny and evolution of the genus *Trichoderma*: a multigene approach. Mycological Research, 106: 757-767.

Kumar, C. G. and Mamidyala, S. K. 2011. Extracellular synthesis of silver nanoparticles using culture supernatant of *Pseudomonas aeruginosa*. Colloids and Surfaces B: Biointerfaces, 84: 462-466.

Kumari, M., Giri, V. P., Pandey, S., Kumar, M., Katiyar, R., Nautiyal, C. S. and Mishra, A. 2019. An insight into the mechanism of antifungal activity of biogenic nanoparticles than their chemical counterparts. Pesticide Biochemistry and Physiology, 157: 45-52.

Kwon-Chung, K. J. and Sugui, J. A. 2009. What do we know about the role of gliotoxin in the pathobiology of *Aspergillus fumigatus*? Medical Mycology, 47: S97-S103.

Lam, S. T. and Gaffney, T. D. 1993. Biological activities of bacteria used in plant pathogen control. In Biotechnology in plant disease control., ed. I Chet, 291-320. New York: John Wiley.

Lamsal, K., Kim, S. W., Jung, J. H., Kim, Y. S., Kim, K. S. and Lee, Y. S. 2011. Application of silver nanoparticles for the control of *Colletotrichum* species in *in vitro* and pepper anthracnose disease in field. Mycobiology, 39: 194-199.

Lan, X., Zhang, J., Zong, Z., Ma, Q. and Wang, Y. 2017. Evaluation of the biocontrol potential of *Purpureocillium lilacinum* QLP12 against *Verticillium dahliae* in eggplant. Biomed Research International, 2017: 4101357.

Langmead, B., Trapnell, C., Pop, M. and Salzberg, S. L. 2009. Ultrafast and memory-efficient alignment of short DNA sequences to the human genome. Genome Biology, 10: 1-10.

Larkin, R. P., Ristaino, J. B. and Campbell, C. L. 1995. Detection and quantification of *Phytophthora capsici* in soil. Phytopathology, 85: 1057-1063.

Lee, B. K., Kim, B. S., Chang, S. W. and Hwang, B. K. 2001. Aggressiveness to pumpkin cultivars of isolates of *Phytophthora capsici* from pumpkin and pepper. Plant Disease, 85: 497-500.

Lewis, J. A., Roberts, D. P. and Hollenbeck, M. D. 1991. Induction of cytoplasmic leakage from *Rhizoctonia solani* hyphae by *Gliocladium virens* and partial characterization of a leakage factor. Biocontrol Science and Technology, 1: 21-29.

Li, C. X., Liu, S. Y., Sivasithamparam, K. and Barbetti, M. J. 2009. New sources of resistance to Sclerotinia stem rot caused by *Sclerotinia sclerotiorum* in Chinese and Australian *Brassica napus* and *B. juncea* germplasm screened under Western Australian conditions. Australasian Plant Pathology, 38: 149-152.

Li, X.-L., Ojaghian, M. R., Zhang, J.-Z. and Zhu, S.-J. 2017. A new species of *Scopulariopsis* and its synergistic effect on pathogenicity of *Verticillium dahliae* on cotton plants. Microbiological Research, 201: 12-20.

Lieckfeldt, E., Kuhls, K. and Muthumeenakshi, S. 2002. Molecular taxonomy of *Trichoderma* and *Gliocladium* and their teleomorphs. In *Trichoderma* and *Gliocladium*:basic biology, taxonomy and genetics, ed. C. P. and Harman In: Kubicek, G. E. (eds.). , 35-53: Taylor & Francis Ltd.

Limón, M. C., Pintor-Toro, J. A. and Benítez, T. 1999. Increased antifungal activity of *Trichoderma harzianum* transformants that overexpress a 33-kDa chitinase. Phytopathology, 89: 254-261.

Lin, X. and Heitman, J. 2005. Chlamydospore formation during hyphal growth in *Cryptococcus neoformans*. Eukaryotic Cell, 4: 1746-1754.

Liu, P. g. and Yang, Q. 2005. Identification of genes with a biocontrol function in *Trichoderma harzianum* mycelium using the expressed sequence tag approach. Research in Microbiology, 156: 416-423.

Livak, K. J. and Schmittgen, T. D. 2001. Analysis of relative gene expression data using real-time quantitative PCR and the 2(-Delta Delta C(T)) Method. Methods, 25: 402-408.

Loo, Y. Y., Rukayadi, Y., Nor-Khaizura, M.-A.-R., Kuan, C. H., Chieng, B. W., Nishibuchi, M. and Radu, S. 2018. In vitro antimicrobial activity of green synthesized silver nanoparticles against selected gram-negative foodborne pathogens. Frontiers in Microbiology, 9: 1555.

López, A. C., Alvarenga, A. E., Zapata, P. D., Luna, M. F. and Villalba, L. L. 2019. *Trichoderma* spp. from Misiones, Argentina: effective fungi to promote plant growth of the regional crop Ilex paraguariensis St. Hil. Mycology, 10: 210-221.

Lorito, M., Farkas, V., Rebuffat, S., Bodo, B. and Kubicek, C. P. 1996. Cell wall synthesis is a major target of mycoparasitic antagonism by *Trichoderma harzianum*. Journal of Bacteriology, 178: 6382-6385.

Lumsden, R. D., Locke, J. C., Adkins, S. T., Walter, J. and Ridout, C. J. 1992. Isolation and localization of the antibiotics gliotoxin produced by *Gliocladium virens* from alginate prill in soil and soilless media. Phytopathology, 82: 230e235.

Ma, H., Feng, X., Chen, Y., Chen, C. and Zhou, M. 2009. Occurrence and characterization of dimethachlon insensitivity in *Sclerotinia sclerotiorum* in Jiangsu Province of China. Plant Disease, 93: 36-42.

Malinich, E. A., Wang, K., Mukherjee, P. K., Kolomiets, M. and Kenerley, C. M. 2019. Differential expression analysis of *Trichoderma virens* RNA reveals a dynamic transcriptome during colonization of *Zea mays* roots. BMC Genomics, 20: 1-19.

Maliszewska, I., Aniszkiewicz, L. and Sadowski, Z. 2009. Biological synthesis of gold nanostructures using the extract of *Trichoderma koningii*. Acta Physica Polonica A, 116: 163-165.

Manikandaselvi, S., Sathya, V., Vadivel, V., Sampath, N. and Brindha, P. 2020. Evaluation of bio control potential of AgNPs synthesized from *Trichoderma viride*. Advances in Natural Sciences: Nanoscience and Nanotechnology, 11: 035004.

Marco, J. L. and Felix, C. R. 2007. Purification and characterization of a beta-Glucanase produced by *Trichoderma harzianum* showing biocontrol potential. Brazilian Archives of Biology and Technology, 50: 21-29.

Marques, E., Martins, I. and Mello, S. C. M. 2018. Antifungal potential of crude extracts of *Trichoderma* spp. Biota Neotro,p 18: e20170418.

Mathre, D., Cook, R. and Callan, N. W. 1999. From discovery to use: traversing the world of commercializing biocontrol agents for plant disease control. Plant Disease, 83: 972-983.

McDonald, B. A. and Linde, C. 2002. Pathogen population genetics, evolutionary potential, and durable resistance. Annual Review of Phytopathology, 40: 349-379.

McLean, K., Swaminathan, J., Frampton, C., Hunt, J., Ridgway, H. and Stewart, A. 2005. Effect of formulation on the rhizosphere competence and biocontrol ability of *Trichoderma atroviride* C52. Plant Pathology, 54: 212-218.

Mei, J., Qian, L., Disi, J. O., Yang, X., Li, Q., Li, J., Frauen, M., Cai, D. and Qian, W. 2011. Identification of resistant sources against *Sclerotinia sclerotiorum* in *Brassica* species with emphasis on *B. oleracea*. Euphytica, 177: 393-399.

Menzies, J. D. and Griebel, G. E. 1967. Survival and saprophytic growth of *Verticillium dahliae* in uncropped soil. Phytopathology, 57: 703-709.

Migheli, Q., González-Candelas, L., Dealessi, L., Camponogara, A. and Ramón-Vidal, D. 1998. Transformants of *Trichoderma longibrachiatum* overexpressing the β-1, 4-endoglucanase gene egl1 show enhanced biocontrol of *Pythium ultimum* on cucumber. Phytopathology, 88: 673-677.

Mihajlović, M., Rekanović, E., Hrustić, J., Grahovac, M. and Tanović, B. 2017. Methods for management of soilborne plant pathogens. Pesticidi I Fitomedicina, 32: 9-24.

Milagres, A. M. F., Machuca, A. and Napoleao, D. 1999. Detection of siderophore production from several fungi and bacteria by a modification of chrome azurol S (CAS) agar plate assay. Journal of Microbiological Methods, 37: 1-6.

Mirmajlessi, S. M., MÄND, M., Najdabbasi, N., Larena, I. and Loit, E. 2016. Screening of native *Trichoderma harzianum* isolates for their ability to control *Verticillium* wilt of strawberry. Zemdirbyste, 103: 397-404.

Mishra, S. and Singh, H. 2015. Biosynthesized silver nanoparticles as a nanoweapon against phytopathogens: exploring their scope and potential in agriculture. Applied Microbiology and Biotechnology, 99: 1097-1107.

Modrzewska, M., Błaszczyk, L., Stępień, Ł., Urbaniak, M., Waśkiewicz, A., Yoshinari, T. and Bryła, M. 2022. *Trichoderma* versus *Fusarium*–Inhibition of Pathogen Growth and Mycotoxin Biosynthesis. Molecules, 27: 8146.

Mokhtar, M. M. and El-Mougy, N. S. 2014. Bio-compost application for controlling soil-borne plant pathogens–a review. International Journal of Engineering and Innovative Technology, 4: 61-68.

Morán-Diez, M. E., Carrero-Carrón, I., Rubio, M. B., Jiménez-Díaz, R. M., Monte, E. and Hermosa, R. 2019. Transcriptomic analysis of *Trichoderma atroviride* overgrowing plant-wilting *Verticillium dahliae* reveals the role of a new M14 metallocarboxypeptidase CPA1 in biocontrol. Frontiers in Microbiology, 10: 1120.

Mukherjee, M., Mukherjee, P. K., Horwitz, B. A., Zachow, C., Berg, G. and Zeilinger, S. 2012a. Trichoderma–plant–pathogen interactions: advances in genetics of biological control. Indian Journal of Microbiology, 52: 522-529.

Mukherjee, P., Roy, M., Mandal, B., Dey, G., Mukherjee, P., Ghatak, J., Tyagi, A. and Kale, S. 2008. Green synthesis of highly stabilized nanocrystalline silver particles by a non-pathogenic and agriculturally important fungus *T. asperellum*. Nanotechnology, 19: 075103.

Mukherjee, P. K., Buensanteai, N., Moran-Diez, M. E., Druzhinina, I. S. and Kenerley, C. M. 2012b. Functional analysis of non-ribosomal peptide synthetases (NRPSs) in *Trichoderma*

*virens* reveals a polyketide synthase (PKS)/NRPS hybrid enzyme involved in the induced systemic resistance response in maize. Microbiology, 158: 155-165.

Mukherjee, P. K., Horwitz, B. A., Singh, U. S., Mukherjee, M. and Schmoll, M. 2013. *Trichoderma*: Biology and Applications. 234-289, UK: CABI.

Mukherjee, P. K., Mendoza-Mendoza, A., Zeilinger, S. and Horwitz, B. A. 2022. Mycoparasitism as a mechanism of *Trichoderma*-mediated suppression of plant diseases. Fungal Biology Reviews, 39: 15-33.

Nandini, B., Hariprasad, P., Prakash, H. S., Shetty, H. S. and Geetha, N. 2017. Trichogenic-selenium nanoparticles enhance disease suppressive ability of *Trichoderma* against downy mildew disease caused by *Sclerospora graminicola* in pearl millet. Scientific Reports, 7: 1-11.

Nassr, S. and Barakat, R. 2013. Effect of factors on conidium germination of *Botrytis cinerea* in vitro. International Journal of Plant and Soil Science, 2: 41-54.

Naziya, B., Murali, M. and Amruthesh, K. N. 2019. Plant growth-promoting fungi (PGPF) instigate plant growth and induce disease resistance in *Capsicum annuum* L. upon infection with *Colletotrichum capsici* (Syd.) Butler & Bisby. Biomolecules, 10: 41.

Nega, A. 2014. Review on concepts in biological control of plant pathogens. Journal of Biology, Agriculture and Healthcare, 4: 33-54.

Nelson, P. E. and Wilhelm, S. 1958. Thermal death range of *Verticillium albo-atrum*. Phytopathology, 48: 613-616.

Ni, Y., Guo, Y., Wang, J., Xia, R., Wang, X., Ash, G. and Li, J. 2014. Responses of physiological indexes and leaf epicuticular waxes of *Brassica napus* to *Sclerotinia sclerotiorum* infection. Plant Pathology, 63: 174-184.

Nieto-Jacobo, M. F., Steyaert, J. M., Salazar-Badillo, F. B., Nguyen, D. V., Rostás, M., Braithwaite, M., De Souza, J. T., Jimenez-Bremont, J. F., Ohkura, M. and Stewart, A. 2017. Environmental growth conditions of *Trichoderma* spp. affects indole acetic acid derivatives, volatile organic compounds, and plant growth promotion. Frontiers in Plant Science, 8: 102.

Niide, O., Suzuki, Y., Yoshimaru, T., Inoue, T., Takayama, T. and Ra, C. 2006. Fungal metabolite gliotoxin blocks mast cell activation by a calcium-and superoxide-dependent

mechanism: implications for immunosuppressive activities. Clinical Immunology, 118: 108-116.

Nirengerg, H. I. 1976. Untersuchungen uber die morpholoigische und biologische Differnzierung in der Fusarium-Sektion Liseola. Mitt. Biol. Bundesanst. Land-u. Forstwirtsch. Berlin-Dahlem, 169: 1-32.

Noshad, A., Iqbal, M., Folkers, L., Hetherington, C., Khan, A., Numan, M. and Ullah, S. 2019. Antibacterial effect of silver nanoparticles (AgNPs) synthesized from *Trichoderma harzianum* against *Clavibacter michiganensis*. Journal of Nano Research, 58: 10-19.

Ojaghian, S. 2020. A new record of *Sclerotinia sclerotiorum* infecting potato plants in China. Journal of Plant Pathology, 102: 1273-1273.

Oskiera, M., Szczech, M. and Bartoszewski, G. 2015. Molecular identification of *Trichoderma* strains collected to develop plant growth-promoting and biocontrol agents. Journal of Horticultural Research, 23: 75-86.

Osorio-Hernández, E., Hernández-Castillo, F. D., Gallegos-Morales, G., Rodríguez-Herrera, R. and Castillo-Reyes, F. 2011. In-vitro behavior of *Trichoderma* spp. against *Phytophthora capsici* Leonian. African Journal of Agricultural Research, 6: 4594-4600.

Othman, A. M., Elsayed, M. A., Elshafei, A. M. and Hassan, M. M. 2017. Application of response surface methodology to optimize the extracellular fungal mediated nanosilver green synthesis. Journal of Genetic Engineering and Biotechnology, 15: 497-504.

Overvoorde, P., Fukaki, H. and Beeckman, T. 2010. Auxin control of root development. Cold Spring Harbor Perspectives in Biology, 2: a001537.

Pal, K. K. and Gardener, B. M. 2006. Biological control of plant pathogens. The Plant Health Instructor, 2: 1117-1142.

Palmgren, M. G., Edenbrandt, A. K., Vedel, S. E., Andersen, M. M., Landes, X., Østerberg, J. T., Falhof, J., Olsen, L. I., Christensen, S. B. and Sandøe, P. 2015. Are we ready for back-to-nature crop breeding. Trends in Plant Science, 20: 155-164.

Parra, G. and Ristaino, J. B. 2001. Resistance to mefenoxam and metalaxyl among field isolates of *Phytophthora capsici* causing *Phytophthora* blight of bell pepper. Plant Disease, 85: 1069-1075.

Patouillard, N. 1895. Enumeration des champignons recoltes par le rr. pp. Farges et Soulie dans le Thibet oriental & le Su-Tchuen, Bulletin de la Société mycologique de France, 11: 196-199

Pawlak, K. and Kołodziejczak, M. 2020. The role of agriculture in ensuring food security in developing countries: Considerations in the context of the problem of sustainable food production. Sustainability, 12: 5488.

Pedrero-Méndez, A., Insuasti, H. C., Neagu, T., Illescas, M., Rubio, M. B., Monte, E. and Hermosa, R. 2021. Why is the correct selection of *Trichoderma* strains important? The case of wheat endophytic strains of *T. harzianum* and *T. simmonsii*. Journal of Fungi, 7: 1087.

Pozo, M. J., Baek, J., Garcıa, J. M. and Kenerley, C. M. 2004. Functional analysis of tvsp1, a serine protease-encoding gene in the biocontrol agent *Trichoderma virens*. Fungal Genetics and Biology, 41: 336-348.

Prabhu, S. and Poulose, E. K. 2012. Silver nanoparticles: mechanism of antimicrobial action, synthesis, medical applications, and toxicity effects. International Nano Letters, 2: 1-10.

Purdy, L. H. 1979. *Sclerotinia sclerotiorum*: history, diseases and symptomatology, host range, geographic distribution, and impact. Phytopathology, 69: 875-880.

Qiao, M., Du, X., Zhang, Z., Xu, J. and Yu, Z. 2018. Three new species of soil-inhabiting *Trichoderma* from southwest China. MycoKeys, 63: 345-359.

Quesada-Ocampo, L., Fulbright, D. W. and Hausbeck, M. K. 2009. Susceptibility of Fraser fir to *Phytophthora capsici*. Plant Disease, 93: 135-141.

Rai, M., Kon, K., Ingle, A., Duran, N., Galdiero, S. and Galdiero, M. 2014. Broad-spectrum bioactivities of silver nanoparticles: the emerging trends and future prospects. Applied Microbiology and Biotechnology, 98: 1951-1961.

Rai, M., Yadav, A. and Gade, A. 2009. Silver nanoparticles as a new generation of antimicrobials. Biotechnology Advances, 27: 76-83.

Raja, H. A., Miller, A. N., Pearce, C. J. and Oberlies, N. H. 2017. Fungal identification using molecular tools: a primer for the natural products research community. Journal of Natural Products, 80: 756-770.

Raja, M., Sharma, R. K., Jambhulkar, P., Sharma, K. R. and Sharma, P. 2021. Biosynthesis of silver nanoparticles from *Trichoderma harzianum* Th3 and its efficacy against root rot complex pathogen in groundnut. Materials Today: Proceedings, 43: 3140-3143.

Ramírez-Delgado, E., Luna-Ruíz, J. J., Moreno-Rico, O., Quiroz-Velásquez, J. D. C. and Hernández-Mendoza, J. L. 2018. Effect of *Trichoderma* on growth and sporangia production of *Phytophthora capsici*. Journal of Agricultural Science, 10: 8-15.

Reghmit, A., Benzina-tihar, F., López Escudero, F. J., Halouane-Sahir, F., Oukali, Z., Bensmail, S. and Ghozali, N. 2021. *Trichoderma* spp. isolates from the rhizosphere of healthy olive trees in northern Algeria and their biocontrol potentials against the olive wilt pathogen, *Verticillium dahliae*. Organic Agriculture, 11: 639-657.

Rehrig, W. Z., Ashrafi, H., Hill, T., Prince, J. and Van Deynze, A. 2014. CaDMR1 cosegregates with QTL Pc5. 1 for resistance to *Phytophthora capsici* in pepper (*Capsicum annuum*). The Plant Genome, 7: 1-12.

Reino, J. L., Guerrero, R. F., Hernández-Galán, R. and Collado, I. G. 2008. Secondary metabolites from species of the biocontrol agent *Trichoderma*. Phytochemistry Reviews, 7: 89-123.

Reithner, B., Ibarra-Laclette, E., Mach, R. L. and Herrera-Estrella, A. 2011. Identification of mycoparasitism-related genes in *Trichoderma atroviride*. Applied and Environmental Microbiology, 77: 4361-4370.

Rifai, M. A. 1969. A revision of the genus *Trichoderma*. Mycological papers, 116: 1-56.

Ristaino, J. B. 1990. Intraspecific variation among isolates of *Phytophthora capsici* from pepper and cucurbit fields in North Carolina. Phytopathology, 80: 1253-1259.

Roberts, D. P. and Lumsden, R. D. 1990. Effect of extracellular metabolites from *Gliocladium virens* on germination of sporangia and mycelial growth of *Pythium ultimum*. Phytopathology, 80: 461-465.

Roberts, P. D., Gevens, A. J., McGovern, R. J. and Kucharek, T. A. 2008. Vegetable diseases caused by *Phytophthora capsici* in Florida. University of Florida, Extension Digital Information Source SP159. In Vegetable diseases caused by *Phytophthora capsici* in Florida. University of Florida, Extension Digital Information Source SP159.

Ronquist, F., Teslenko, M., Van Der Mark, P., Ayres, D. L., Darling, A., Höhna, S., Larget, B., Liu, L., Suchard, M. A. and Huelsenbeck, J. P. 2012. MrBayes 3.2: efficient Bayesian phylogenetic inference and model choice across a large model space. Systematic Biology, 61: 539-542.

Rudakiya, D. M. and Pawar, K. 2017. Bactericidal potential of silver nanoparticles synthesized using cell-free extract of *Comamonas acidovorans*: *in vitro* and *in silico* approaches. 3 Biotechnology, 7: 1-12.

Saklani, V., Suman, J. V. K. and Jain, K. 2012. Microbial synthesis of silver nanoparticles: a review. Journal of Biotechnology and Biomaterials, 13: 2718-2725.

Salem, S. S. and Fouda, A. 2021. Green synthesis of metallic nanoparticles and their prospective biotechnological applications: an overview. Biological Trace Element Research, 199: 344-370.

Samuels, G. J. 2006. *Trichoderma*: systematics, the sexual state, and ecology. Phytopathology, 96: 195-206.

Samuels, G. J., Dodd, S. L., Gams, W., Castlebury, L. A. and Petrini, O. 2002. *Trichoderma* species associated with the green mold epidemic of commercially grown *Agaricus bisporus*. Mycologia, 94: 146-170.

Samuels, G. J., Lieckfeldt, E. and Nirenberg, H. I. 1999. *Trichoderma asperellum*, a new species with warted conidia, and redescription of *T. viride*. Sydowia-Horn, 51: 71-88.

Saravanakumar, K. and Wang, M. H. 2020. Isolation and molecular identification of *Trichoderma* species from wetland soil and their antagonistic activity against phytopathogens. Physiological and Molecular Plant Pathology, 109: 101458.

Sastry, M., Ahmad, A., Khan, M. I. and Kumar, R. 2003. Biosynthesis of metal nanoparticles using fungi and actinomycete. Current Science, 85: 162-170.

Savazzini, F., Longa, C. M. O. and Pertot, I. 2009. Impact of the biocontrol agent *Trichoderma atroviride* SC1 on soil microbial communities of a vineyard in northern Italy. Soil Biology and Biochemistry, 41: 1457-1465.

Scharf, D. H., Brakhage, A. A. and Mukherjee, P. K. 2016. Gliotoxin–bane or boon? Environmental Microbiology, 18: 1096-1109.

Schmoll, M., Seiboth, B., Druzhinina, I. and Kubicek, C., P 2014. 10 Genomics analysis of biocontrol species and industrial enzyme producers from the genus *Trichoderma*. Fungal Genomics, 13: 233-264.

Schoch, C. L., Seifert, K. A., Huhndorf, S., Robert, V., Spouge, J. L., Levesque, C. A., Chen, W. and Consortium, F. B. 2012. Nuclear ribosomal internal transcribed spacer (ITS) region as

a universal DNA barcode marker for Fungi. Proceedings of the National Academy of Sciences, 109: 6241-6246.

Schuster, A. and Schmoll, M. 2010. Biology and biotechnology of *Trichoderma*. Applied Microbiology and Biotechnology, 87: 787-799.

Schwyn, B. and Neilands, J. B. 1987. Universal chemical assay for the detection and determination of siderophores. Analytical Biochemistry, 160: 47-56.

Segarra, G., Aviles, M., Casanova, E., Borrero, C. and Trillas, I. 2013. Effectiveness of biological control of *Phytophthora capsici* in pepper by *Trichoderma asperellum* strain T34. Phytopathologia Mediterranea, 52: 77-83.

Segarra, G., Casanova, E., Avilés, M. and Trillas, I. 2010. *Trichoderma asperellum* strain T34 controls *Fusarium* wilt disease in tomato plants in soilless culture through competition for iron. Microbial Ecology, 59: 141-149.

Seidl, V., Song, L., Lindquist, E., Gruber, S., Koptchinskiy, A., Zeilinger, S., Schmoll, M., Martínez, P., Sun, J. and Grigoriev, I. 2009. Transcriptomic response of the mycoparasitic fungus *Trichoderma atroviride* to the presence of a fungal prey. BMC Genomics, 10: 1-13.

Shah, S., Nasreen, S. and Sheikh, P. A. 2012. Cultural and morphological characterization of *Trichoderma* spp. associated with green mold disease of *Pleurotus* spp. in Kashmir. Research Journal of Microbiology, 7: 139–144.

Shameli, K., Bin Ahmad, M., Jazayeri, S. D., Sedaghat, S., Shabanzadeh, P., Jahangirian, H., Mahdavi, M. and Abdollahi, Y. 2012. Synthesis and characterization of polyethylene glycol mediated silver nanoparticles by the green method. International Journal of Molecular Sciences, 13: 6639-6650.

Shentu, X.-P., Liu, W.-P., Zhan, X.-H., Xu, Y.-P., Xu, J.-F., Yu, X.-P. and Zhang, C. X. 2014a. Transcriptome sequencing and gene expression analysis of *Trichoderma brevicompactum* under different culture conditions. PloS ONE, 9: e94203.

Shentu, X., Zhan, X., Ma, Z., Yu, X. and Zhang, C. 2014b. Antifungal activity of metabolites of the endophytic fungus *Trichoderma brevicompactum* from garlic. Brazilian Journal of Microbiology, 45: 248-254.

Shi, Y., Xie, X., Song, J., Jin, Z., Chai, A., Li, S. and Li, B. 2016. First report of *Sclerotinia* rot on *Andrographis paniculata* in China. Canadian Journal of Plant Pathology, 38: 522-526.

Shobha, B., Lakshmeesha, T. R., Ansari, M. A., Almatroudi, A., Alzohairy, M. A., Basavaraju, S., Alurappa, R., Niranjana, S. R. and Chowdappa, S. 2020. Mycosynthesis of ZnO Nanoparticles Using *Trichoderma* spp. Isolated from Rhizosphere Soils and Its Synergistic Antibacterial Effect against *Xanthomonas oryzae* pv. *oryzae*. Journal of Fungi, 6: 181.

Sid Ahmed, A., Pérez-Sánchez, C., Egea, C. and Candela, M. E. 1999. Evaluation of *Trichoderma harzianum* for controlling root rot caused by *Phytophthora capsici* in pepper plants. Plant Pathology, 48: 58-65.

Silvestro, D. and Michalak, I. 2012. raxmlGUI: a graphical front-end for RAxML. Organisms Diversity and Evolution, 12: 335-337.

Singh, A., Shahid, M., Srivastava, M., Pandey, S., Sharma, A. and Kumar, V. 2014. Optimal physical parameters for growth of *Trichoderma* species at varying pH, temperature and agitation. Virology Mycology, 3: 1-7.

Singh, S., Dureja, P., Tanwar, R. S. and Singh, A. 2005. Production and antifungal activity of secondary metabolites of *Trichoderma virens*. Pesticide Research Journal, 17: 26-29.

Singh, S., Sharma, V., Sharma, S., Kumar, S. and Tiwari, M. 2006. Molecular characterization of *Trichoderma* taxa causing green mould disease in edible mushrooms. Current Science, 90: 427-431.

Skoneczny, D., Oskiera, M., Szczech, M. and Bartoszewski, G. 2015. Genetic diversity of *Trichoderma atroviride* strains collected in Poland and identification of loci useful in detection of within-species diversity. Folia Microbiologica, 60: 297-307.

Song, R., Li, J., Xie, C., Jian, W. and Yang, X. 2020. An overview of the molecular genetics of plant resistance to the *Verticillium* wilt pathogen *Verticillium dahliae*. International Journal of Molecular Sciences, 21: 1120.

Sood, M., Kapoor, D., Kumar, V., Sheteiwy, M. S., Ramakrishnan, M., Landi, M., Araniti, F. and Sharma, A. 2020. *Trichoderma*: The "secrets" of a multitalented biocontrol agent. Plants, 9: 762.

Soylu, S., Yigitbas, H., Soylu, E. M. and Kurt, Ş. 2007. Antifungal effects of essential oils from oregano and fennel on *Sclerotinia sclerotiorum*. Journal of Applied Microbiology, 103: 1021-1030.

Srivastava, M., Shahid, M., Pandey, S., Kuma, V., Singh, A., Trived, S. and Srivastava, Y. K. 2015. Trichoderma: A scientific approach against soil borne pathogens. African Journal of Microbiology Research, 9: 2377-2384.

Srivastava, M. P., Gupta, S. and Sharm, Y. K. 2018. Detection of siderophore production from different cultural variables by CAS-agar plate assay. Asian Journal of Pharmacy and Pharmacology, 4: 66-69.

Steindorff, A. S., do Nascimento Silva, R., Coelho, A. S. G., Nagata, T., Noronha, E. F. and Ulhoa, C. J. 2012. *Trichoderma harzianum* expressed sequence tags for identification of genes with putative roles in mycoparasitism against *Fusarium solani*. Biological Control, 61: 134-140.

Steindorff, A. S., Ramada, M. H. S., Coelho, A. S. G., Miller, R. N. G., Pappas, G. J., Ulhoa, C. J. and Noronha, E. F. 2014. Identification of mycoparasitism-related genes against the phytopathogen *Sclerotinia sclerotiorum* through transcriptome and expression profile analysis in *Trichoderma harzianum*. BMC Genomics, 15: 1-14.

Stewart, A. and Hill, R. 2014. Applications of *Trichoderma* in plant growth promotion. In Biotechnology and biology of *Trichoderma*, 415-428. The Netherlands: Elsevier: Amsterdam.

Steyaert, J. M., Ridgway, H. J., Elad, Y. and Stewart, A. 2003. Genetic basis of mycoparasitism: a mechanism of biological control by species of *Trichoderma*. New Zealand Journal of Crop and Horticultural Science, 31: 281-291.

Sun, X. T., Lu, X. Y., Zhang, J.-Z. and Zhu, S. 2016. Identification of pathotype of *Verticillium dahliae* isolates on cotton in Zhejiang Province and phenotypic analysis on inhibitory effect by high temperature. Journal of Zhejiang University (Agriculture and Life Sciences), 42: 671-678.

Sun, Z., Sun, M. and Li, S. 2015. Identification of mycoparasitism-related genes in *Clonostachys rosea* 67-1 active against *Sclerotinia sclerotiorum*. Scientific Reports, 5: 18169.

Sundaravadivelan, C. and Padmanabhan, M. N. 2014. Effect of mycosynthesized silver nanoparticles from filtrate of *Trichoderma harzianum* against larvae and pupa of dengue vector *Aedes aegypti* L. Environmental Science and Pollution Research, 21: 4624-4633.

Svahn, K. S., Göransson, U., El-Seedi, H., Bohlin, L., Larsson, D. J., Olsen, B. and Chryssanthou, E. 2012. Antimicrobial activity of filamentous fungi isolated from highly antibiotic-contaminated river sediment. Infection Ecology and Epidemiology, 2: 11591.

Tančić-Živanov, S., Medić-Pap, S., Danojević, D. and Prvulović, D. 2020. Effect of *Trichoderma* spp. on growth promotion and antioxidative activity of pepper seedlings. Brazilian Archives of Biology and Technology, 63: e20180659.

Thorvaldsdóttir, H., Robinson, J. T. and Mesirov, J. P. 2013. Integrative Genomics Viewer (IGV): high-performance genomics data visualization and exploration. Briefings in Bioinformatics, 14: 178-192.

Tjamos, E. C. and Fravel, D. R. 1995. Detrimental effects of sublethal heating and *Talaromyces flavus* on microsclerotia of *Verticillium dahliae*. Phytopathology, 85: 388-392.

Tomah, A. A., Abd Alamer, I. S., Li, B. and Zhang, J.-Z. 2020. A new species of *Trichoderma* and gliotoxin role: A new observation in enhancing biocontrol potential of *T. virens* against *Phytophthora capsici* on chili pepper. Biological Control, 145: 104261.

Trapnell, C., Roberts, A., Goff, L., Pertea, G., Kim, D., Kelley, D. R., Pimentel, H., Salzberg, S. L., Rinn, J. L. and Pachter, L. 2012. Differential gene and transcript expression analysis of RNA-seq experiments with TopHat and Cufflinks. Nature Protocols, 7: 562-578.

Tripathi, R. M., Gupta, R. K., Shrivastav, A., Singh, M. P., Shrivastav, B. R. and Singh, P. 2013. *Trichoderma koningii* assisted biogenic synthesis of silver nanoparticles and evaluation of their antibacterial activity. Advances in Natural Sciences: Nanoscience and Nanotechnology, 4: 035005.

Tronsmo, A. 1991. Biological and integrated controls of *Botrytis cinerea* on apple with *Trichoderma harzianum*. Biological Control, 1: 59-62.

Tyśkiewicz, R., Nowak, A., Ozimek, E. and Jaroszuk-Ściseł, J. 2022. *Trichoderma*: The current status of its application in agriculture for the biocontrol of fungal phytopathogens and stimulation of plant growth. International Journal of Molecular Sciences, 23: 2329.

Ukkund, S. J., Ashraf, M., Udupa, A. B., Gangadharan, M., Pattiyeri, A., Marigowda, Y. K., Patil, R. and Puthiyllam, P. 2019. Synthesis and characterization of silver nanoparticles from *Fuzarium Oxysporum* and investigation of their antibacterial activity. Materials Today: Proceedings, 9: 506-514.

Vahabi, K. and Dorcheh, S. K. 2014. Biosynthesis of silver nano-particles by *Trichoderma* and its medical applications. In Biotechnology and biology of *Trichoderma*, ed. Elsevier: London Editor. 2014, UK., 393-404: Elsevier.

Vahabi, K., Mansoori, G. A. and Karimi, S. 2011. Biosynthesis of silver nanoparticles by fungus *Trichoderma reesei* (a route for large-scale production of AgNPs). Insciences Journal, 1: 65-79.

Vargas, W. A., Mukherjee, P. K., Laughlin, D., Wiest, A., Moran-Diez, M. E. and Kenerley, C. M. 2014. Role of gliotoxin in the symbiotic and pathogenic interactions of *Trichoderma virens*. Microbiology, 160: 2319-2330.

Vey, A., Hoagland, R. E. and Butt, T. M. 2001. Toxic metabolites of fungal biocontrol agents. Fungi as biocontrol agents: Progress, Problems and Potential, 1: 311-346.

Vieira, P. M., Coelho, A. S.; Steindorff, A. S., de siqueira, S. J. L., Silva, R. N. and Ulhoa, C. J. 2013. Identification of differentially expressed genes from *Trichoderma harzianum* during growth on cell wall *Fusarium solani* as tool for biotechnological application. MBC Genomics, 14: 177

Villaverde, J. J., Sevilla-Morán, B., López-Goti, C., Alonso-Prados, J. L. and Sandín-España, P. 2018. Considerations of nano-QSAR/QSPR models for nanopesticide risk assessment within the European legislative framework. Science of the Total Environment, 634: 1530-1539.

Vinale, F., Ghisalberti, E., Sivasithamparam, K., Marra, R., Ritieni, A., Ferracane, R., Woo, S. and Lorito, M. 2009. Factors affecting the production of *Trichoderma harzianum* secondary metabolites during the interaction with different plant pathogens. Letters in Applied Microbiology, 48: 705-711.

Vinale, F., Marra, R., Scala, F., Ghisalberti, E., Lorito, M. and Sivasithamparam, K. 2006. Major secondary metabolites produced by two commercial *Trichoderma* strains active against different phytopathogens. Letters in Applied Microbiology, 43: 143-148.

Vinale, F., Sivasithamparam, K., Ghisalberti, E. L., Marra, R., Woo, S. L. and Lorito, M. 2008. Trichoderma–plant–pathogen interactions. Soil Biology and Biochemistry, 40: 1-10.

Vinale, F., Strakowska, J., Mazzei, P., Piccolo, A., Marra, R., Lombardi, N., Manganiello, G., Pascale, A., Woo, S. L. and Lorito, M. 2016. Cremenolide, a new antifungal, 10-member

lactone from *Trichoderma cremeum* with plant growth promotion activity. Natural Product Research, 30: 2575-2581.

Vizcaíno, J. A., Redondo, J., Suárez, M. B., Cardoza, R. E., Hermosa, R., González, F. J., Rey, M. and Monte, E. 2007. Generation, annotation, and analysis of ESTs from four different *Trichoderma* strains grown under conditions related to biocontrol. Applied Microbiology and Biotechnology, 75: 853-862.

Wang, H., Xu, Z., Gao, L. and Hao, B. 2009. A fungal phylogeny based on 82 complete genomes using the composition vector method. BMC Evolutionary Biology, 9: 1-13.

Wang, Z., Ma, L.Y., Cao, J., Li, Y.L., Ding, L.N., Zhu, K.M., Yang, Y.H. and Tan, X.L. 2019. Recent advances in mechanisms of plant defense to *Sclerotinia sclerotiorum*. Frontiers in Plant Science, 10: 1314.

Weindling, R. and Emerson, O. H. 1936. The isolation of a toxic substance from the culture filtrates of *Trichoderma*. Phytopathology, 26: 1068-1070.

Wheeler, M. H., Tolmsoff, W. J., Bell, A. and Mollenhauer, H. H. 1978. Ultrastructural and chemical distinction of melanins formed by *Verticillium dahliae* from (+)-scytalone, 1, 8-dihydroxynaphthalene, catechol, and L-3, 4-dihydroxyphenylalanine. Canadian Journal of Microbiology, 24: 289-297.

White, T. J., Bruns, T., Lee, S. and Taylor, J. 1990. Amplification and direct sequencing of fungal ribosomal RNA genes for phylogenetics. PCR protocols: a guide to methods and applications. MycoKeys, 18: 315-322.

Wilhelm, S. 1955. Longevity of the *Verticillium* wilt fungus in the laboratory and field. Phytopathology, 45: 180-181.

Xiao-Yan, S., Qing-Tao, S., Shu-Tao, X., Xiu-Lan, C., Cai-Yun, S. and Yu-Zhong, Z. 2006. Broad-spectrum antimicrobial activity and high stability of Trichokonins from *Trichoderma koningii* SMF2 against plant pathogens. FEMS Microbiology Letters, 260: 119-125.

Xiaojun, C., Wongkaew, S., Jie, Y., Xuehui, Y., Haiyong, H., Shiping, W., Qigqun, T., Lishuang, W., Athinuwat, D. and Buensanteai, N. 2014. *In vitro* inhibition of pathogenic *Verticillium dahliae*, causal agent of potato wilt disease in China by *Trichoderma* isolates. African Journal of Biotechnology, 13: 3402-3412.

Xilin, Z., Xuemei, S. and Gufeng, Z. 2003. Preliminary Report on the Monitoring of the Resistance of *Sclerotinia Libertiana* to Carbendazim and its Integrated Management. Pesticide Science and Administration, 6: 18-22.

Xiong, J., Xie, L. and Ojaghian, S. 2021. First record of white rot on *Ipomoea batatas* caused by *Sclerotinia sclerotiorum* in China. Archives of Phytopathology and Plant Protection, 54: 354-358.

Yamanaka, M., Hara, K. and Kudo, J. 2005. Bactericidal actions of a silver ion solution on *Escherichia coli,* studied by energy-filtering transmission electron microscopy and proteomic analysis. Applied and Environmental Microbiology, 71: 7589-7593.

Yan, L. Y., Kang, Y. P., Lei, Y., Huang, J. Q., Wan, L. Y. and Liao, B. S. 2014. First report of *Sclerotinia sclerotiorum* causing sclerotinia blight on peanut (*Arachis hypogaea*) in Northeastern China. Plant Disease, 98: 156-156.

Yu, Z. F., Qiao, M., Zhang, Y. and Zhang, K.-Q. 2007. Two new species of *Trichoderma* from Yunnan, China. Antonie van Leeuwenhoek, 92: 101-108.

Yun, C. and Daohuai, D. 1988. *Phytophthora capsici* as the main cause of *Capsicum* plant wilt in Beijing region. Acta Phytopathologica Sinica (China), 1: 7-12.

Zhang, F., Zhu, Z., Yang, X., Ran, W. and Shen, Q. 2013. *Trichoderma harzianum* T-E5 significantly affects cucumber root exudates and fungal community in the cucumber rhizosphere. Applied Soil Ecology, 72: 41-48.

Zhang, G. Z., Yang, H. T., Zhang, X., Zhou, F., Wu, X., Xie, X., Zhao, X. and Zhou, H. 2022. Five new species of *Trichoderma* from moist soils in China. MycoKeys, 87: 133-157.

Zhang, J. and Li, M. 2009. A new species of Bipolaris from the halophyte *Sesuvium portulacastrum* in Guangdong Province, China. Mycotaxon, 109: 289-300.

Zhang, W., Zhang, L. and Sun, Y. 2015. Size-controlled green synthesis of silver nanoparticles assisted by L-cysteine. Frontiers of Chemical Science and Engineering, 9: 494-500.

Zhao, L., Wang, Y. and Kong, S. 2020. Effects of *Trichoderma asperellum* and its siderophores on endogenous auxin in *Arabidopsis thaliana* under iron-deficiency stress. International Microbiology, 23: 501-509.

Zhu, W., Liu, X., Chen, M., Tao, N., Tendu, A. and Yang, Q. 2021. A New MiRNA MiRm0002 in Eggplant Participates in the Regulation of Defense Responses to *Verticillium* Wilt. Plants, 10: 2274.

Zhu, Z. X., Xu, H.X., Zhuang, W.Y. and Li, Y. 2017. Two new green-spored species of *Trichoderma* (Sordariomycetes, Ascomycota) and their phylogenetic positions. MycoKeys, 26: 61.

Zhu, Z. X. and Zhuang, W. Y. 2015. Three new species of *Trichoderma* with hyaline ascospores from China. Mycologia, 107: 328-345.

# Supplementary

**Supplementary Table 4-1.** Gene ontology classification of DEGs

| 6d-3d | | | | | |
|---|---|---|---|---|---|
| **Ontology** | **Term_name** | **Up_Count** | **Up_Percent** | **Down_Count** | **Down_Percent** |
| cellular_component | extracellular region | 34 | 2.84 | 62 | 5.21 |
| cellular_component | cell | 3 | 0.25 | 2 | 0.17 |
| cellular_component | nucleoid | 1 | 0.08 | 2 | 0.17 |
| cellular_component | membrane | 132 | 11.03 | 107 | 8.98 |
| cellular_component | cell junction | 1 | 0.08 | 6 | 0.5 |
| cellular_component | membrane-enclosed lumen | 8 | 0.67 | 17 | 1.43 |
| cellular_component | protein-containing complex | 55 | 4.59 | 103 | 8.65 |
| cellular_component | organelle | 233 | 19.47 | 238 | 19.98 |
| cellular_component | other organism part | 1 | 0.08 | 2 | 0.17 |
| cellular_component | extracellular region part | 7 | 0.58 | 15 | 1.26 |
| cellular_component | organelle part | 137 | 11.45 | 160 | 13.43 |
| cellular_component | membrane part | 172 | 14.37 | 163 | 13.69 |
| cellular_component | synapse part | 3 | 0.25 | 5 | 0.42 |
| cellular_component | cell part | 384 | 32.08 | 452 | 37.95 |
| cellular_component | synapse | 0 | 0 | 2 | 0.17 |
| cellular_component | supramolecular complex | 2 | 0.17 | 13 | 1.09 |
| Total | | 1173 | 97.99 | 1349 | 113.27 |
| biological_process | reproduction | 9 | 0.75 | 0 | 0 |
| biological_process | cell killing | 2 | 0.17 | 0 | 0 |
| biological_process | immune system process | 2 | 0.17 | 4 | 0.34 |
| biological_process | behavior | 1 | 0.08 | 2 | 0.17 |
| biological_process | metabolic process | 280 | 23.39 | 439 | 36.86 |
| biological_process | cell proliferation | 1 | 0.08 | 0 | 0 |
| biological_process | carbohydrate utilization | 0 | 0 | 1 | 0.08 |
| biological_process | cellular process | 334 | 27.9 | 459 | 38.54 |
| biological_process | nitrogen utilization | 1 | 0.08 | 0 | 0 |
| biological_process | reproductive process | 24 | 2.01 | 11 | 0.92 |
| biological_process | biological adhesion | 1 | 0.08 | 0 | 0 |
| biological_process | signaling | 3 | 0.25 | 2 | 0.17 |
| biological_process | multicellular organismal process | 13 | 1.09 | 12 | 1.01 |
| biological_process | developmental process | 32 | 2.67 | 25 | 2.1 |
| biological_process | growth | 12 | 1 | 3 | 0.25 |
| biological_process | locomotion | 3 | 0.25 | 4 | 0.34 |
| biological_process | rhythmic process | 1 | 0.08 | 2 | 0.17 |
| biological_process | response to stimulus | 67 | 5.6 | 46 | 3.86 |

| biological_process | localization | 104 | 8.69 | 109 | 9.15 |
|---|---|---|---|---|---|
| biological_process | multi-organism process | 30 | 2.51 | 38 | 3.19 |
| biological_process | biological regulation | 128 | 10.69 | 90 | 7.56 |
| biological_process | cellular component organization or biogenesis | 73 | 6.1 | 82 | 6.88 |
| biological_process | cell aggregation | 2 | 0.17 | 1 | 0.08 |
| biological_process | detoxification | 4 | 0.33 | 10 | 0.84 |
| Total | | 1127 | 94.14 | 1340 | 112.51 |
| molecular_function | catalytic activity | 368 | 30.74 | 560 | 47.02 |
| molecular_function | structural molecule activity | 7 | 0.58 | 67 | 5.63 |
| molecular_function | transporter activity | 74 | 6.18 | 68 | 5.71 |
| molecular_function | binding | 331 | 27.65 | 384 | 32.24 |
| molecular_function | antioxidant activity | 4 | 0.33 | 7 | 0.59 |
| molecular_function | translation regulator activity | 0 | 0 | 1 | 0.08 |
| molecular_function | nutrient reservoir activity | 1 | 0.08 | 1 | 0.08 |
| molecular_function | molecular transducer activity | 5 | 0.42 | 1 | 0.08 |
| molecular_function | toxin activity | 2 | 0.17 | 2 | 0.17 |
| molecular_function | molecular function regulator | 15 | 1.25 | 13 | 1.09 |
| molecular_function | molecular carrier activity | 0 | 0 | 1 | 0.08 |
| molecular_function | transcription regulator activity | 44 | 3.68 | 15 | 1.26 |
| Total | | 851 | 71.08 | 1120 | 94.03 |
| **9d-3d** | | | | | |
| **Ontology** | **Term_name** | **Up_Count** | **Up_Percent** | **Down_Count** | **Down_Percent** |
| cellular_component | extracellular region | 56 | 3.19 | 127 | 6.47 |
| cellular_component | cell | 4 | 0.23 | 3 | 0.15 |
| cellular_component | nucleoid | 1 | 0.06 | 4 | 0.2 |
| cellular_component | membrane | 184 | 10.47 | 199 | 10.14 |
| cellular_component | cell junction | 7 | 0.4 | 8 | 0.41 |
| cellular_component | membrane-enclosed lumen | 7 | 0.4 | 42 | 2.14 |
| cellular_component | protein-containing complex | 119 | 6.77 | 221 | 11.26 |
| cellular_component | organelle | 394 | 22.41 | 453 | 23.08 |
| cellular_component | other organism part | 1 | 0.06 | 2 | 0.1 |
| cellular_component | extracellular region part | 13 | 0.74 | 27 | 1.38 |
| cellular_component | organelle part | 232 | 13.2 | 306 | 15.59 |
| cellular_component | membrane part | 237 | 13.48 | 283 | 14.42 |
| cellular_component | synapse part | 8 | 0.46 | 6 | 0.31 |
| cellular_component | cell part | 611 | 34.76 | 836 | 42.59 |
| cellular_component | synapse | 5 | 0.28 | 4 | 0.2 |
| cellular_component | supramolecular complex | 3 | 0.17 | 20 | 1.02 |
| Total | | 1882 | 107.08 | 2541 | 129.46 |
| biological_process | reproduction | 12 | 0.68 | 4 | 0.2 |
| biological_process | cell killing | 3 | 0.17 | 0 | 0 |
| biological_process | immune system process | 3 | 0.17 | 9 | 0.46 |

| biological_process | behavior | 4 | 0.23 | 1 | 0.05 |
|---|---|---|---|---|---|
| biological_process | metabolic process | 449 | 25.54 | 738 | 37.6 |
| biological_process | cell proliferation | 2 | 0.11 | 0 | 0 |
| biological_process | carbohydrate utilization | 0 | 0 | 1 | 0.05 |
| biological_process | cellular process | 534 | 30.38 | 780 | 39.74 |
| biological_process | nitrogen utilization | 2 | 0.11 | 0 | 0 |
| biological_process | reproductive process | 43 | 2.45 | 24 | 1.22 |
| biological_process | biological adhesion | 5 | 0.28 | 0 | 0 |
| biological_process | signaling | 3 | 0.17 | 2 | 0.1 |
| biological_process | multicellular organismal process | 18 | 1.02 | 16 | 0.82 |
| biological_process | developmental process | 55 | 3.13 | 39 | 1.99 |
| biological_process | growth | 18 | 1.02 | 6 | 0.31 |
| biological_process | locomotion | 4 | 0.23 | 5 | 0.25 |
| biological_process | rhythmic process | 1 | 0.06 | 1 | 0.05 |
| biological_process | response to stimulus | 108 | 6.14 | 88 | 4.48 |
| biological_process | localization | 157 | 8.93 | 193 | 9.83 |
| biological_process | multi-organism process | 47 | 2.67 | 62 | 3.16 |
| biological_process | biological regulation | 239 | 13.59 | 168 | 8.56 |
| biological_process | cellular component organization or biogenesis | 126 | 7.17 | 143 | 7.28 |
| biological_process | cell aggregation | 3 | 0.17 | 1 | 0.05 |
| biological_process | detoxification | 6 | 0.34 | 19 | 0.97 |
| Total | | 1842 | 104.76 | 2300 | 117.17 |
| molecular_function | catalytic activity | 502 | 28.56 | 918 | 46.77 |
| molecular_function | structural molecule activity | 9 | 0.51 | 90 | 4.58 |
| molecular_function | transporter activity | 98 | 5.57 | 122 | 6.21 |
| molecular_function | binding | 504 | 28.67 | 664 | 33.83 |
| molecular_function | antioxidant activity | 8 | 0.46 | 13 | 0.66 |
| molecular_function | protein tag | 0 | 0 | 3 | 0.15 |
| molecular_function | translation regulator activity | 0 | 0 | 1 | 0.05 |
| molecular_function | nutrient reservoir activity | 0 | 0 | 3 | 0.15 |
| molecular_function | molecular transducer activity | 6 | 0.34 | 4 | 0.2 |
| molecular_function | toxin activity | 3 | 0.17 | 4 | 0.2 |
| molecular_function | molecular function regulator | 25 | 1.42 | 23 | 1.17 |
| molecular_function | molecular carrier activity | 1 | 0.06 | 1 | 0.05 |
| molecular_function | transcription regulator activity | 90 | 5.12 | 22 | 1.12 |
| Total | | 1246 | 70.88 | 1868 | 95.14 |
| 12d-3d | | | | | |
| Ontology | Term_name | Up_Count | Up_Percent | Down_Count | Down_Percent |
| cellular_component | extracellular region | 43 | 2.22 | 108 | 5.27 |
| cellular_component | cell | 5 | 0.26 | 4 | 0.2 |
| cellular_component | nucleoid | 0 | 0 | 6 | 0.29 |
| cellular_component | membrane | 201 | 10.38 | 208 | 10.15 |

| cellular_component | cell junction | 5 | 0.26 | 9 | 0.44 |
|---|---|---|---|---|---|
| cellular_component | membrane-enclosed lumen | 12 | 0.62 | 45 | 2.2 |
| cellular_component | protein-containing complex | 225 | 11.62 | 213 | 10.39 |
| cellular_component | organelle | 549 | 28.36 | 471 | 22.98 |
| cellular_component | other organism part | 1 | 0.05 | 2 | 0.1 |
| cellular_component | extracellular region part | 11 | 0.57 | 22 | 1.07 |
| cellular_component | organelle part | 351 | 18.13 | 321 | 15.66 |
| cellular_component | membrane part | 249 | 12.86 | 285 | 13.9 |
| cellular_component | synapse part | 5 | 0.26 | 7 | 0.34 |
| cellular_component | cell part | 807 | 41.68 | 845 | 41.22 |
| cellular_component | synapse | 3 | 0.15 | 5 | 0.24 |
| cellular_component | supramolecular complex | 5 | 0.26 | 21 | 1.02 |
| Total | | 2472 | 127.68 | 2572 | 125.47 |
| biological_process | reproduction | 10 | 0.52 | 3 | 0.15 |
| biological_process | cell killing | 2 | 0.1 | 0 | 0 |
| biological_process | immune system process | 6 | 0.31 | 9 | 0.44 |
| biological_process | behavior | 3 | 0.15 | 2 | 0.1 |
| biological_process | metabolic process | 555 | 28.67 | 748 | 36.49 |
| biological_process | cell proliferation | 6 | 0.31 | 0 | 0 |
| biological_process | carbohydrate utilization | 0 | 0 | 1 | 0.05 |
| biological_process | cellular process | 681 | 35.18 | 786 | 38.34 |
| biological_process | nitrogen utilization | 3 | 0.15 | 0 | 0 |
| biological_process | reproductive process | 55 | 2.84 | 29 | 1.41 |
| biological_process | biological adhesion | 5 | 0.26 | 2 | 0.1 |
| biological_process | signaling | 8 | 0.41 | 1 | 0.05 |
| biological_process | multicellular organismal process | 20 | 1.03 | 17 | 0.83 |
| biological_process | developmental process | 62 | 3.2 | 34 | 1.66 |
| biological_process | growth | 23 | 1.19 | 9 | 0.44 |
| biological_process | locomotion | 4 | 0.21 | 4 | 0.2 |
| biological_process | rhythmic process | 1 | 0.05 | 2 | 0.1 |
| biological_process | response to stimulus | 145 | 7.49 | 95 | 4.63 |
| biological_process | localization | 176 | 9.09 | 208 | 10.15 |
| biological_process | multi-organism process | 53 | 2.74 | 61 | 2.98 |
| biological_process | biological regulation | 337 | 17.41 | 185 | 9.02 |
| biological_process | cellular component organization or biogenesis | 181 | 9.35 | 156 | 7.61 |
| biological_process | cell aggregation | 3 | 0.15 | 1 | 0.05 |
| biological_process | detoxification | 5 | 0.26 | 19 | 0.93 |
| Total | | 2344 | 121.07 | 2372 | 115.73 |
| molecular_function | catalytic activity | 527 | 27.22 | 923 | 45.02 |
| molecular_function | structural molecule activity | 10 | 0.52 | 87 | 4.24 |
| molecular_function | transporter activity | 98 | 5.06 | 126 | 6.15 |
| molecular_function | binding | 591 | 30.53 | 660 | 32.2 |

| molecular_function | antioxidant activity | 8 | 0.41 | 18 | 0.88 |
|---|---|---|---|---|---|
| molecular_function | protein tag | 0 | 0 | 4 | 0.2 |
| molecular_function | translation regulator activity | 1 | 0.05 | 1 | 0.05 |
| molecular_function | nutrient reservoir activity | 2 | 0.1 | 1 | 0.05 |
| molecular_function | molecular transducer activity | 8 | 0.41 | 3 | 0.15 |
| molecular_function | toxin activity | 2 | 0.1 | 2 | 0.1 |
| molecular_function | molecular function regulator | 46 | 2.38 | 23 | 1.12 |
| molecular_function | molecular carrier activity | 1 | 0.05 | 1 | 0.05 |
| molecular_function | transcription regulator activity | 127 | 6.56 | 25 | 1.22 |
| Total | | 1421 | 73.39 | 1874 | 91.43 |

| 15d-3d | | | | | |
|---|---|---|---|---|---|
| **Ontology** | **Term_name** | **Up_Count** | **Up_Percent** | **Down_Count** | **Down_Percent** |
| cellular_component | extracellular region | 41 | 2.14 | 147 | 6.95 |
| cellular_component | cell | 2 | 0.1 | 3 | 0.14 |
| cellular_component | nucleoid | 0 | 0 | 2 | 0.09 |
| cellular_component | membrane | 189 | 9.87 | 214 | 10.12 |
| cellular_component | cell junction | 2 | 0.1 | 9 | 0.43 |
| cellular_component | membrane-enclosed lumen | 11 | 0.57 | 32 | 1.51 |
| cellular_component | protein-containing complex | 178 | 9.3 | 176 | 8.33 |
| cellular_component | organelle | 471 | 24.61 | 460 | 21.76 |
| cellular_component | other organism part | 1 | 0.05 | 1 | 0.05 |
| cellular_component | extracellular region part | 5 | 0.26 | 26 | 1.23 |
| cellular_component | organelle part | 289 | 15.1 | 292 | 13.81 |
| cellular_component | membrane part | 236 | 12.33 | 274 | 12.96 |
| cellular_component | synapse part | 4 | 0.21 | 9 | 0.43 |
| cellular_component | cell part | 706 | 36.89 | 814 | 38.51 |
| cellular_component | synapse | 3 | 0.16 | 3 | 0.14 |
| cellular_component | supramolecular complex | 3 | 0.16 | 19 | 0.9 |
| Total | | 2141 | 111.85 | 2481 | 117.36 |
| biological_process | reproduction | 10 | 0.52 | 6 | 0.28 |
| biological_process | cell killing | 2 | 0.1 | 0 | 0 |
| biological_process | immune system process | 5 | 0.26 | 7 | 0.33 |
| biological_process | behavior | 2 | 0.1 | 2 | 0.09 |
| biological_process | metabolic process | 499 | 26.07 | 708 | 33.49 |
| biological_process | cell proliferation | 2 | 0.1 | 1 | 0.05 |
| biological_process | carbohydrate utilization | 0 | 0 | 1 | 0.05 |
| biological_process | cellular process | 602 | 31.45 | 766 | 36.23 |
| biological_process | nitrogen utilization | 4 | 0.21 | 0 | 0 |
| biological_process | reproductive process | 48 | 2.51 | 31 | 1.47 |
| biological_process | biological adhesion | 3 | 0.16 | 0 | 0 |
| biological_process | signaling | 6 | 0.31 | 3 | 0.14 |
| biological_process | multicellular organismal process | 15 | 0.78 | 16 | 0.76 |

| biological_process | developmental process | 54 | 2.82 | 49 | 2.32 |
|---|---|---|---|---|---|
| biological_process | growth | 20 | 1.04 | 10 | 0.47 |
| biological_process | locomotion | 5 | 0.26 | 4 | 0.19 |
| biological_process | rhythmic process | 0 | 0 | 3 | 0.14 |
| biological_process | response to stimulus | 139 | 7.26 | 109 | 5.16 |
| biological_process | localization | 165 | 8.62 | 183 | 8.66 |
| biological_process | multi-organism process | 52 | 2.72 | 67 | 3.17 |
| biological_process | biological regulation | 282 | 14.73 | 195 | 9.22 |
| biological_process | cellular component organization or biogenesis | 141 | 7.37 | 162 | 7.66 |
| biological_process | cell aggregation | 5 | 0.26 | 1 | 0.05 |
| biological_process | detoxification | 7 | 0.37 | 20 | 0.95 |
| Total | | 2068 | 108.02 | 2344 | 110.88 |
| molecular_function | catalytic activity | 524 | 27.38 | 923 | 43.66 |
| molecular_function | structural molecule activity | 9 | 0.47 | 85 | 4.02 |
| molecular_function | transporter activity | 102 | 5.33 | 103 | 4.87 |
| molecular_function | binding | 566 | 29.57 | 653 | 30.89 |
| molecular_function | antioxidant activity | 9 | 0.47 | 23 | 1.09 |
| molecular_function | protein tag | 0 | 0 | 4 | 0.19 |
| molecular_function | translation regulator activity | 1 | 0.05 | 0 | 0 |
| molecular_function | nutrient reservoir activity | 2 | 0.1 | 2 | 0.09 |
| molecular_function | molecular transducer activity | 10 | 0.52 | 4 | 0.19 |
| molecular_function | toxin activity | 3 | 0.16 | 3 | 0.14 |
| molecular_function | molecular function regulator | 28 | 1.46 | 25 | 1.18 |
| molecular_function | molecular carrier activity | 1 | 0.05 | 2 | 0.09 |
| molecular_function | transcription regulator activity | 120 | 6.27 | 27 | 1.28 |
| Total | | 1375 | 71.83 | 1854 | 87.69 |

**Supplementary Figure 4-1.** Visualization of the DEGs by volcano plot.
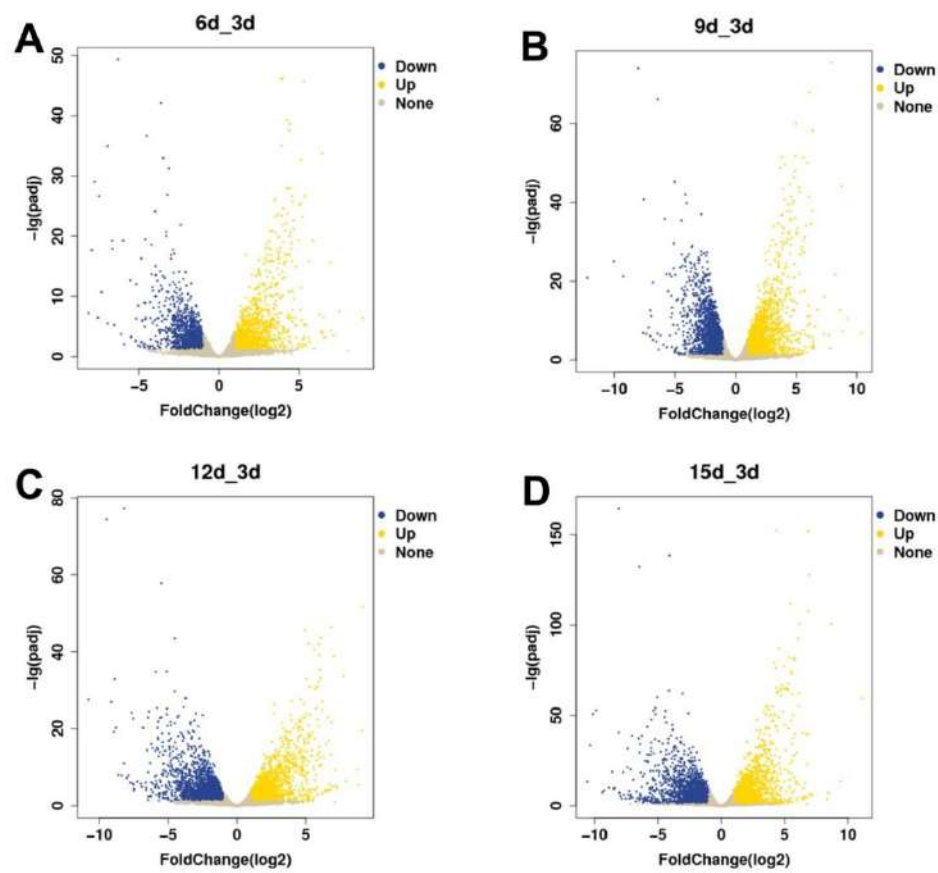
## List of Publications

**Tomah, A.A.**; Abd Alamer, I.S.; Li, B.; Zhang, J.-Z. A new species of *Trichoderma* and gliotoxin role: A new observation in enhancing biocontrol potential of *T. virens* against *Phytophthora capsici* on chili pepper. Biological Control, 2020, **145**, 104261.

**Tomah, A.A.**; Abd Alamer, I.S.; Li, B.; Zhang, J.-Z. Mycosynthesis of silver nanoparticles using screened *Trichoderma* isolates and their antifungal activity against *Sclerotinia sclerotiorum*. Nanomaterials, 2020, **10**, 1955.

Alamer, I.S.A.; **Tomah, A.A.**; Li, B.; Zhang, J.Z. Isolation, identification and characterization of rhizobacteria strains for biological control of bacterial wilt (Ralstonia solanacearum) of eggplant in China. Agriculture, 2020, **10**, 37.

**Tomah, A.A.**; Abd Alamer, I.S.; Ahmed, T.; Li, B.; Zhang, J.-Z. Trichoderma: a safer synthesis for nanoparticles, Advantages and prospective applications (submitted).

Alamer, I.S.A.; **Tomah, A.A.**; Li, B.; Zhang, J.Z. Biosynthesis of silver chloride nanoparticles by rhizospheric bacteria and their antibacterial activity against Phytopathogenic bacterium *Ralstonia solanacearum*. Molecules, 2022; 27(1), 224.

**Tomah, A.A.**; Abd Alamer, I.S.; Li, B.; Zhang, J.-Z. Identification of *Trichoderma virens* genes responsible for microsclerotia degrading and control on *Verticillium* wilt disease in eggplant. (Under review).